

**Università di Bologna**

---

**Corso di Dottorato in Ingegneria Agraria**

**Meccanica Agraria – AGR/09**

**ANALYSIS OF RECIPROCATING SINGLE  
BLADE CUTTER BARS**

*Tesi di Dottorato di:*

Cesare Maglioni

*Coordinatore e Relatore:*

Prof. Ing. Adriano Guarnieri

*Correlatore:*

Ing. Giovanni Molari

---

**XIX Ciclo**



**Università di Bologna**

---

**Corso di Dottorato in Ingegneria Agraria**

**Meccanica Agraria – AGR/09**

**ANALYSIS OF RECIPROCATING SINGLE  
BLADE CUTTER BARS**

*Tesi di Dottorato di:*

Cesare Maglioni

*Coordinatore e Relatore:*

Prof. Ing. Adriano Guarnieri

*Correlatore:*

Ing. Giovanni Molari

---

**XIX Ciclo**



*Keywords:*

Cutter Bar, Crank – Conrod Mechanism,  
Cutting Resistance, Non – Circular Gear,  
Torque Balancing



*The real dynamic problem begins where there are  
less invariants than degrees of freedom*  
[Poincaré, introduction to *Méthodes nouvelles de  
la mécanique céleste*, 1892]



### Acknowledgements:

Thank to my family and friends, for support and life. Thank to Prof. Adriano Guarnieri and Ing. Giovanni Molari, from the Department of Agricultural Engineering and Economics, University of Bologna, and to Prof. John Fielke and Ing. Jack Desboilles, from the Agricultural Machinery Research and Design Centre, University of South Australia, for the opportunities. Thank also to Lotti (Faenza - Italy) and Fama Pruning System (Mantova - Italy) companies, for the supply of equipment and drawings.



# INDEX

---



INDEX.....	11
I INTRODUCTION .....	15
I.1 SYSTEM DESCRIPTION.....	17
I.2 AIM AND PROCEEDING.....	19
II MODELS .....	23
II.1 INTRODUCTION.....	25
II.2 CUTTING RESISTANCE.....	25
II.2.1 Model development.....	26
II.2.2 Model benefits and limits.....	34
II.3 CUTTER BAR.....	35
II.3.1 Crank-conrod mechanism kinematics and dynamics.....	36
II.3.2 Counterbar equilibrium.....	40
II.3.3 Equation of motion.....	42
II.4 ON THE BALANCING OF CRANK – CONROD MECHANISMS.....	47
II.5 DISSIPATIVE AND RESISTANCE POWERS MEASUREMENT.....	50
III SENSITIVITY ANALYSIS.....	53
III.1 INTRODUCTION.....	55
III.2 SENSITIVITY ANALYSIS RESULTS.....	56
III.2.1 Rotational speed trend in time.....	56
III.2.2 Driving torque trend in time.....	61
III.2.3 Other functions trend in time.....	66
IV ALTERNATIVE SOLUTION.....	69
IV.1 INTRODUCTION.....	71
IV.2 ADDITIVE SHAFT WITH NON CIRCULAR GEARING.....	73
IV.2.1 Arrangement description and gear ratio calculation.....	74
IV.2.2 Generation of variable radius pitch lines.....	78
IV.2.3 Other constraints.....	79

IV.3	SOLUTION APPLICATION IN VOID WORKING CONDITIONS.....	81
IV.3.1	Gear profiles and discussion .....	82
IV.3.2	Benefits in void and standard working conditions.....	85
V	CONCLUSIONS .....	89
APPENDIX A .....		93
A.1	MAPLE CODE FOR SOLVING THE EQUATION OF MOTION.....	95
APPENDIX B .....		99
B.1	MAPLE CODE FOR THE SENSITIVITY ANALYSIS ON THE PARAMETER “D” .....	101
B.2	MAPLE CODE FOR THE SENSITIVITY ANALYSIS ON THE PARAMETER “P” .....	102
B.3	MAPLE CODE FOR THE SENSITIVITY ANALYSIS ON THE PARAMETER “FS”.....	104
B.4	MAPLE CODE FOR THE SENSITIVITY ANALYSIS ON THE PARAMETER “N” .....	105
B.5	MAPLE CODE FOR THE SENSITIVITY ANALYSIS ON THE PARAMETER “L” .....	106
APPENDIX C .....		109
C.1	MAPLE CODE FOR THE APPLICATION OF NON CIRCULAR GEARING .....	111
C.2	MAPLE CODE FOR THE NON CIRCULAR GEARING SENSITIVITY ANALYSIS.....	113
REFERENCES.....		117

# I

# INTRODUCTION

---



## Introduction

### *I.1 SYSTEM BRIEF DESCRIPTION*

The first mechanical cutting bar was created in the USA in 1822 by Bailey [54]. In the following years the system was implemented using harvester based principles, and only reached Europe approximately in the mid 19th century for forage and grass cutting [44].

The standard type cutter bar (or sickle bar) consists essentially of three basic component parts: the carrying frame, supporting all the other parts, the cutting systems, a double or single reciprocating multi-teeth blade, and the drive system that transfers the power from a dedicated engine, or from the tractor Power Take Off, directly to the blade [53].

The simplest cutting system consists of a single movable reciprocating cutting tool, which leads its cutting work in conjunction with a stationary counterbar that usually acts as carrying frame too (Figure I. 1). The cutting tool is typically a high quality steel bar on which are riveted the knives (or teeth), which are standardized trapezoidal tempered steel plates, while the counterbar is a steel bar on which are screwed the fingers. The latter have cut-outs in which knives hide at instantaneous extreme positions or through which they pass and also act as guard against impact with rocks and soil unevenness. The greased tight contact between the two members is guaranteed by clips fixed with screws to the counterbar, serving as guide and easily replaceable when worn-out [8].

With the forward motion of the system, plants, stalk and shrub to be cut are trapped cyclically in little bundle between knives and fingers and, since the cutting action is carried only by the knife thanks to the opposite support carried by the finger, the cut occurs in *shear mode* (Figure I. 1). Sometimes the counterbar is provided with countercutting edges, the ledger plates, which are riveted to the fingers and involve a cutting action from both sides of stalk bundles [8, 23 and 44].

Recently, following this improvement and alternatively to the single movable blade, double blade cutter bars have been introduced. With this type of cutting system the stationary counterbar disappear, leaving its place to a second, same kind and counter-phase movable cutting tool (Figure I. 1). The resultant cutting action occurs again in shear mode, because the two blades carry the cutting and counter action each other reciprocally, but the guard action fails [23, 56].

In both cases, the moving blade is equipped with many teeth, to allow a shorter blade stroke with a large overall cutting front, while each tooth have cutting edges on both oblique sides, to allow the cutting action both on forward and return paths.

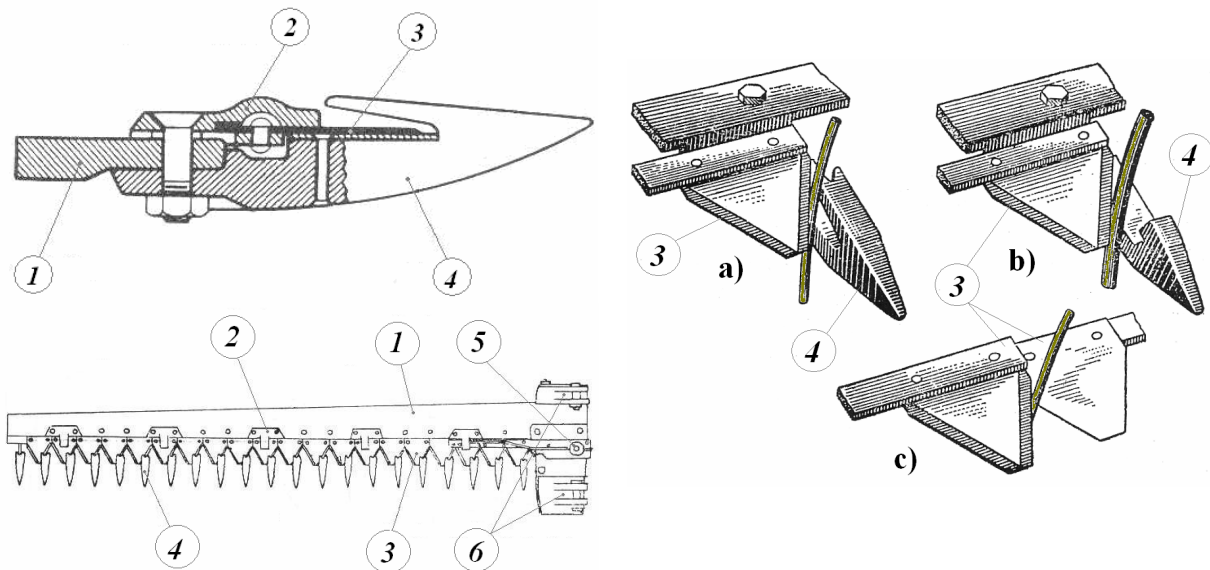


**Figure I. 1 – Single blade cutter bar and its transversal section, on the left, and working principia for different type of single (a and b) and double (c) blade cutter bars, on the right: counterbar (1), clips (2), blade knives (3), fingers (4), conrod small end (5) and link for the tractor frame (6).**

The drive system must convert the rotary motion of the PTO, or the rotary motion of a dedicated engine, in a reciprocating motion useful for the blade. As underlined later on (see Paragraph II.3.3), this conversion has a strong influence on the overall equilibrium of the cutter bar, and hence it affects some of the main working properties like the allowed blade speed, the feed rate and the power request [29, 45 and 58].

Nowadays this task it is commonly carried out by means of an eccentric crank-connecting rod planar mechanism, but even hydraulic transmissions and other different spatial, planar or pendular mechanisms have been used over the years [5, 30], with the main purpose of a balance improving and vibration reduction of the whole system [23, 53]. Anyway, in spite of the high influence upon the working properties and the increased utilization of cutting bars even for pruning [16, 27] the crank-conrod mechanism remains the most commonly adopted drive system. What is more, this mechanism has never been substantially modified because of its simplicity and economic construction [37, 45].

Cutter bars are typically used in simple agricultural machineries, like mowers for grass and weed cutting, and constitute the standard cutting apparatus in combine harvesters, for forage and hay harvesting [2, 23]. Recently, these cutting systems have been introduced even for fruit trees and vineyards trimming, pruning, thinning and leaves removal, commonly with a planar crank mechanism of motion and with the aid of simple supporting structures allowing them to be directly linked to the tractor [16, 24, 27, 43 and 48], Figure I. 2. Anyway, standard cutter bars are generally recognized not to be suitable for this task, having an upper cutting limit of 20 – 25 mm in diameter [28].

## Introduction

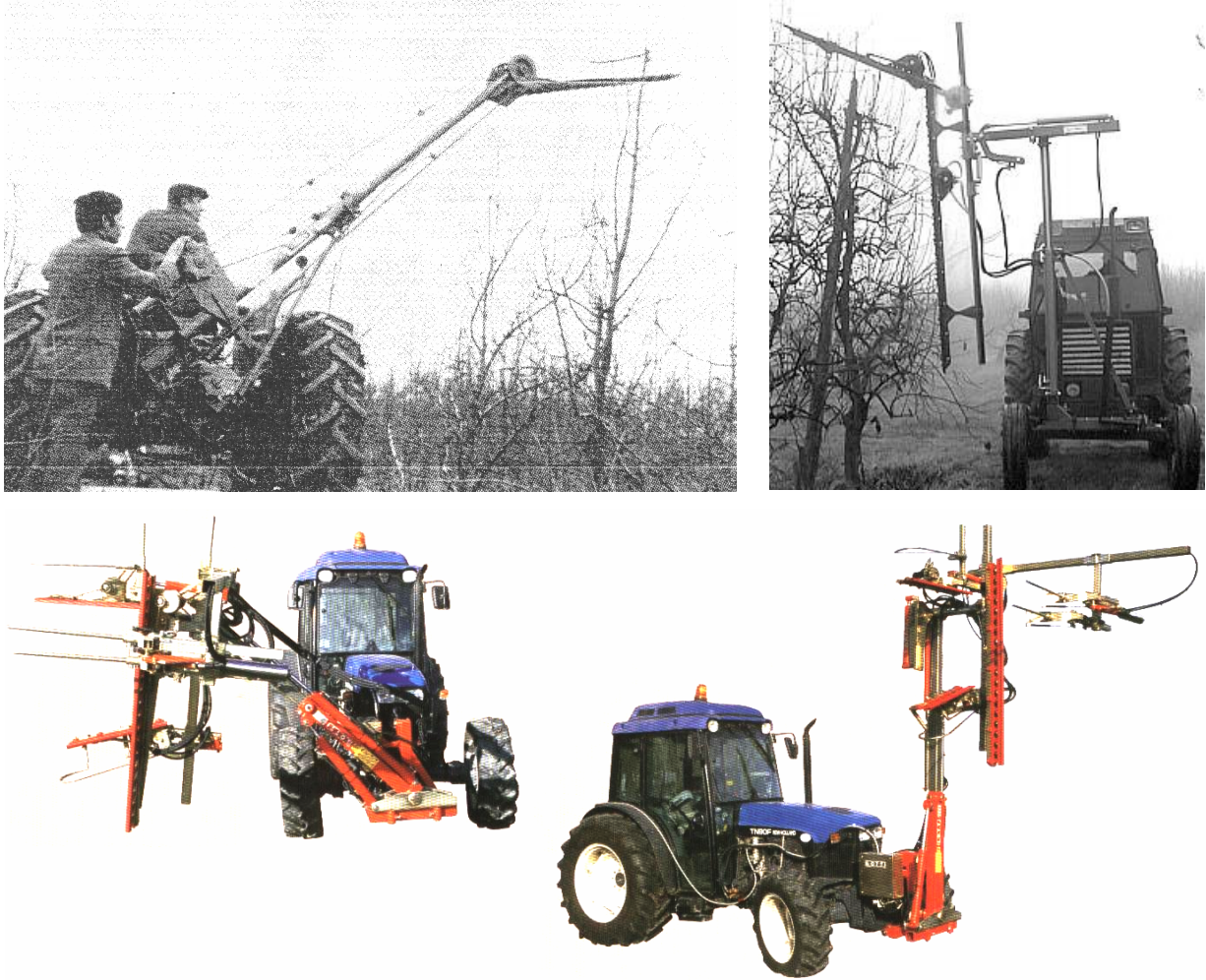


**Figure I. 2 – Less (up) and more recent (down) examples of use of standard cutter bar for pruning trees and vineyards trimming and thinning, with a classical cantilever applications.**

### *I.2 AIM AND PROCEEDING*

The main problem regarding this cutting system is the vibration phenomena that arises during the work, particularly for the single blade type and when the cutter bar is constrained to the main structure by only one of the two lateral ends (overhanging cutter bar), typically for weeds cutting purposes. For high rotational speed the order of magnitude for this effect can overcome 200 mm, hence it can be considered as large oscillation, while when the cutter bar is constrained by both the two ends, for low rotational speeds or in case of double blade cutter bar, the effect is still present but with a lower magnitude [23, 30, 53 and 54].

These vibrations affect negatively both cutting quality and working safety in a significant way, while the bar should “float” easily over the ground, without bouncing [53]. The situation gets worse when pruning trees and vineyards. Indeed, the increased and more discontinuous cutting resistance carried by tree branches and shrubs requires a larger amount of power and the bar

has to be stronger and stiffer. Hence, the already existing vibratory phenomena increases, thus considerably diminishing both cutting quality and safety [42].

In an attempt to avoid these problems, and hence reduce the oscillating deflection of the cutter bar tip, the manufacturers usually tend to use longer conrods [8], to limit the total cutting width or even suggest the use of double blade mechanisms [23, 56], generally reducing the versatility of the system, increasing its cost, wear, tear and the chances of jamming and breaking [5, 38 and 53]. Besides, to evaluate the real extent of these problems the system dynamics have to be analyzed in detail and the cutting resistance mathematically estimated in order to obtain a quantitative description of the system behaviour in the specific case trees pruning, since the working conditions are totally different from the standard ones.

Early studies on the cutter bar regarded the cutting area optimization under different tool configurations and the evaluation of the cutting speed influence in relation to geometric parameters, with different levels of approximation [10, 30, 32, 51 and 53]. These researches, involving only kinematic analysis, regarded cutting action optimization for grasses and forages, so they are not suitable in the case of larger shrubs [24, 28 and 30]. In this latter situation, indeed, factors prevailed like counterbar configuration, the actual deflection and resistance of the shrub under cutting [5, 51] and dynamic factors like instantaneous cutting force, torque or motion shape over time become significant.

Later studies evaluated the cutting force for different configurations of the blade and counterbar [29, 58] and cutting efficiency in function of several geometric tool parameters [40]. Dynamic analysis has been also carried out [2, 32] and, in addition, some empirical models for cutting resistance have been developed using energetic criteria [11, 53] or experimental data obtained in static cutting conditions [14, 31, 52 and 58].

Anyway, even if there have been many attempts, none of them have worked so well that it can be said the mentioned vibratory phenomena have been solved. The cutter bar system remains still far from ideal in its basic design [15], the disequilibrium problem remains generally unsolved, its causes is not analyzed nor solution is theoretically proposed.

Nevertheless, clashing with the old axiom that there is nothing new under the sun [30], several aspects have still to be clarified, especially regarding the dynamic behaviour of the whole system under these new working conditions. These include, firstly, the influence of inertia forces and motion irregularity on the mechanism disequilibrium. Also, it would be useful to determine the effect of the shrub on the mentioned motion irregularity as well as the correlation between the cutter bar geometric, kinematic and dynamic parameters and the motion law of the driving mechanism, so that to characterize the disequilibrium in terms of these parameters.

## Introduction

Finally, the disequilibrium source would have to be directly investigated, rather than try to find a palliative solution to improve the cutter bar balancing and efficiency.

In order to investigate these aspects, with the main purpose of understanding the disequilibrium sources and hence to develop a suitable solution, only the more common and problematic cutter bar type will be taken under consideration here below: this is the single blade type, with a planar slider-crank mechanism of motion, since it is the most commonly used in pruning trees where the cutting resistance is higher and the vibration level as well. The developed analysis and the proposed alternative solution could be then reviewed and extended, with the right modifications, even for double blade cutter bars.

The aim of this thesis is not only the construction of a single blade cutter bar complete mathematical model, in the case of a crank-conrod mechanism drive system and for the particular working condition of branches cutting, but also to investigate directly and in the widest way the disequilibrium source, together with carry the proposal of an alternative solution against the vibratory problems.

In Chapter II this task is started with the development of a new and simplified mathematical (dynamic) model for the cutting resistance. Successively, the dynamic model of the whole cutter bar, that is the sum of its equilibrium equations and its equation of motion, is worked out. Chapter II ends with some consideration on the balancing enhancement and on the energy requirements in standard working conditions.

The developed model is then numerically integrated, to gain the mechanism motion law and all the mathematical functions that defines the system disequilibrium and affect its balancing. This outcomes allow, in Chapter III, the optimization of the system in relation to the material being cut and in relation to the geometric and dynamic characteristics of the cutter bar itself, by means of a sensitivity analysis based on the influencing parameters involved in the system dynamics. This analysis yields to important information which are useful not only for the understanding of the unbalancing sources, but also for a general system improvement.

Chapter IV regards the development of an alternative solution, using a modified crank – conrod drive system. This alternative solution, proposed for the system optimization in relation to the highlighted disequilibrium phenomena, is based always on the flywheel principia but uses even a pair of non circular gears. The application of this new solution is firstly designed for the present arrangement and, secondly, numerically simulated in a way that allows understanding the benefits carried to the system even in standard working conditions.

Chapter V finally reports the thesis conclusions, overlooking the whole research from the beginning to its temporary end.



# II

# MODELS

---



### II.1 INTRODUCTION

*Nella modellazione del sistema dinamico, in taluni casi è sufficiente uno schema a corpi rigidi tra loro genericamente interconnessi, mentre per altri è necessario considerare la deformabilità distribuita dei vari elementi [...] è necessaria inoltre la conoscenza dei diversi campi di forze a cui i vari elementi sono soggetti nella loro forma più completa, poiché tali campi influenzano in maniera determinante il comportamento del sistema stesso [13].*

*When modelling the dynamical system, sometimes it is adequate to assume a scheme with generically interconnected rigid bodies, while in other cases it is necessary to take under consideration the distributed deformability of each part [...] it is necessary as well the complete knowledge of the diverse force fields under which each part is subjected, because these fields influence decisively the behaviour of the whole system itself [free translation from the original version].*

In this chapter, the dynamic behaviour of reciprocating single blade cutter bar with slider-crank mechanism of motion will be taken under consideration. Thereby, the description of the equilibrium for each component of the system will be carried out, beginning from the kinematic analysis of the drive system through the highlight of each acting force field (both external and internal). These force fields are generic functions of the unique DOF that will be than assumed. Wherethrough making clear these dependences, it will be possible to describe the whole equilibrium in function of the solely assumed DOF and hence to deduce the drive system single DOF equation of motion (Paragraph II.3.3).

The equation of motion will be subsequently integrated, resulting in the *mechanism's motion law* which constitutes, together with the equilibrium equations, the system mathematical model.

Before all, anyway, the external force field carried by the material being cut, namely the cutting resistance, has to be defined from a mathematical standpoint.

### II.2 CUTTING RESISTANCE

The cutting action is carried out by means of the reciprocating rectilinear motion of the blade in conjunction with the rectilinear forward motion of the carrying machine (i.e. the tractor), so that each knife follows the same sinusoidal path, which is the basis for the definition of the cutting pattern, Figure II. 1 [10, 30].

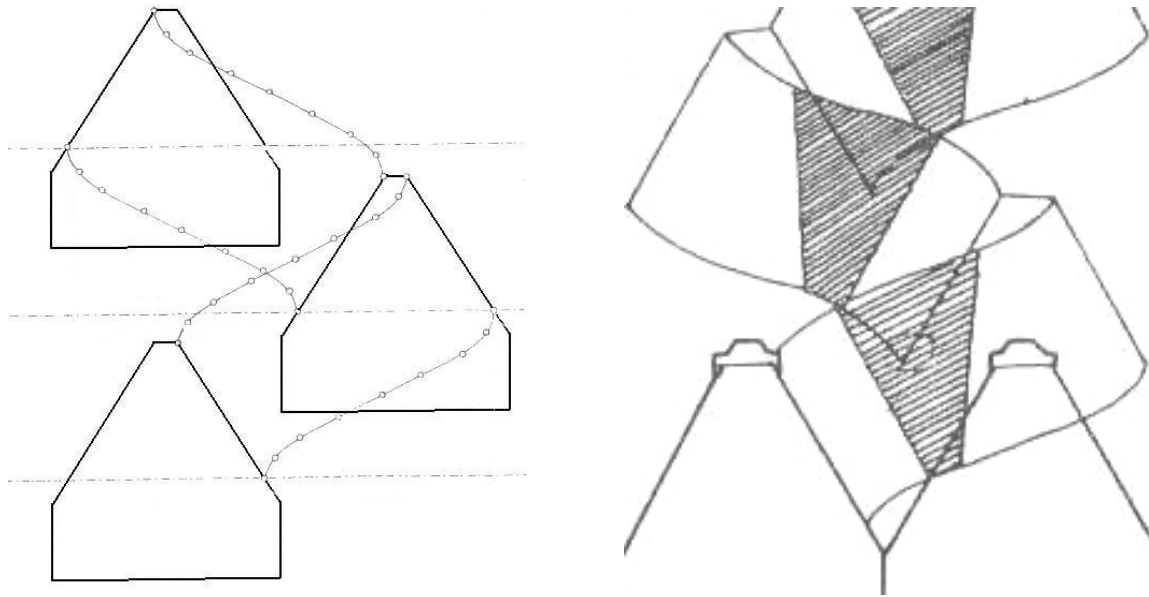


**Figure II. 1 – Teeth cutting pattern (on the left) and effective cutting area (on the right).**

In the past many studies clarified several aspects about this sort of operation. Initially, researches has mainly involved kinematic and geometric analysis of the tool pattern for forage and grass cutting, with the purpose of maximize the cutting area covered by the blade and optimize its speed (i.e. the blade average speed).

Afterwards, dynamic analysis and experimental tests have evaluated the average (or sometimes the instantaneous) value of the minimum knife cutting force required to carry out the cutting action, on the basis of the knife geometry and the cut configuration [7]. Various and similar expressions have been then formulated, with the purpose of understanding the cutting resistance trend as a function of the knife displacement inside the plant. These models take under consideration several factors, like the knife edge shape (edge bevel angle), plant characteristics (material Poisson's ratio, bulk, compressive or elasticity modulus), a not well specified value for the initial material compressive strength and internal friction.

Finally, the cutting force shape in function of the knife displacement has been experimentally described only in the case of *static cutting* (i.e. cutting performed slowly) [14].

### II.2.1 Model development

With nothing to steal from these basilar analysis, and without the willingness of a more complete and in-depth description of the knife cutting action<sup>1</sup>, for the purpose of the

<sup>1</sup> For this purpose see: Y. Hirai, E. Inoue, K. Mori: "Reaction Force Of Wheat Stalks During The Reel Operation Of A Combine Harvester", Proceedings of the International Conference on Crop Harvesting and Processing, 9-11 February 2003 (Louisville, Kentucky USA), ASAE Publication Number 701P1103e, Graeme Quick ed., 2003.

## Models

subsequent equilibrium analysis a different kind of cutting resistance model could be more useful.

In the context of a dynamical analysis it could be useful to have a simplified model allowing the description of the cutting resistance instantaneous dependence not only upon the displacement of the knife, but even upon its speed, which is not uniform and is one of the most important parameters during the cutting path. Moreover, because of what will be mentioned below, in the case here studied it is impossible to exactly know the instantaneous displacement of the knife *inside* the plant, while more useful it would be to have a model based on the absolute (kinematically predictable) displacement of the knife. Finally, the mentioned dependence of the model upon geometrical factors could be a strong limitation in applying the cutting resistance model as a reference for different cases. For this purpose it could be easier and reasonable to have a simplified model that neglect this dependence and hence could be used for different knife geometries.

Calling with  $R$  the *instantaneous cutting resistance* carried by the plant, hereafter has been explained a short and qualitatively description of the cutting action to develop a simplified dynamic model for this force field. To this end, the whole action is hence subdivided in four main stages and the knife is assumed to feed in the solely direction of its reciprocating motion<sup>2</sup> [5, 7, 52, 53].

In the first stage the shrubs, moving frontally and perpendicularly to the blade, are subdivided in little bundles by the fingers, until the knives finished their forward and return stroke. Therefore, the effective cutting action lasts for a portion much shorter than the entire stroke of the knife, since the dimension occupied by the fingers cannot be covered with shrubs, and even since the cut cannot begin until the shrubs reach the countercutting support and the consequent opening force, carried along the fibres by the knife, overcomes the material shear strength.

So, being  $x_1$  the blade displacement and calling with  $x_{0A}$  the mean value of  $x$  for which the plant reaches the countercutting support, for  $x < x_{0A}$  no cutting is possible, and  $R$  is due only to the stalks bending and to their bending stiffness, value that is negligible in comparison to the overall cutting force in the case of a counterblade is present [53]:

$$R = kx_1 \approx 0 \quad \text{for } x_1 < x_{0A}, \text{ stage 0} \quad (\text{II.1})$$

---

<sup>2</sup> This is an approximation. Actually, the generic knife presses the shrubs with a certain force perpendicularly to the knife edge itself, and simultaneously travels toward a certain direction  $s$ , following the sinusoidal path as specified above. Because of this movement, the stalks slide across the knife edge and, considering the friction between the knife edge and the material, the direction of motion of the knife relatively to the stalk can be deduced by the path  $s$  adding, or subtracting, depending on the specific position, the angle of friction.

The value of  $x_{0A}$ , which depends on the quantity of shrubs under cutting, can be estimated statistically and in function of geometric parameters.

Successively, reached by both the knife and the countercutting edge, the bundles are squeezed in between, and a certain amount of stalk slides on the knife edge. Anyhow, at this early stage (A) the effective cutting action didn't take already place since the knife force is not high enough to carry out the cutting action. Hence, the generic bundle of biological material is compressed and the resistance  $R$  is due only to the compressive strength of the plant  $R_C$

$$R = R_C(\text{material}) \quad \text{for } x_{0A} \leq x_1 < x_{AB}, \text{ stage A} \quad (\text{II.2})$$

that depends intrinsically upon the material being cut and will represent the starting value of the cutting resistance in function of the blade displacement.

In correspondence to point  $x_{AB}$ , the knife cutting force reaches the minimum value needed to begin the cut, and the shrubs stop their sliding movement relatively to the knife because of the pressure and the friction. Here, the opening force carried by the knife in the direction of the plant fibres overcomes the shear strength of the biological material, keeping on even the compressive action. Hence, during this stage (B) the cutting action coexists with the compressive one and the total needed cutting force rises both because of the increase in shrubs quantity and in the value of the shear strength:

$$R = R_T(\text{material, shrubs q.ty}) \quad \text{for } x_1 \geq x_{AB}, \text{ stage B and C} \quad (\text{II.3})$$

At point  $x_{BC}$  the maximum value of the necessary cutting force  $R_T$  is reached, and the material under cutting is structurally destroyed. From this point onwards there is no more compressive action and the value of  $R$  decreases, due both to the settlement in the biological structure and the decrease in shrubs quantity.

Figure II. 2 represents some examples of cutting force trend in function of the knife displacement, in the case of a single shrub and when cut is performed slowly (static cutting). Obviously, when there are more shrubs under the same knife edge, which is a standard circumstance in working conditions, the total cutting force raises and the corresponding cutting diagram is different. In this case for each shrub it could be assumed a diagram similar to the above one, with a force peak translated on the abscissa because of the difference in their position inside the space between knife and finger. Finally, for more knife edges working simultaneously, like in practice, the total force shape could be very different, since the shrubs randomly fit the spaces between knives and fingers. Raising the quantity of shrubs being cut, the case approximates again to the situation of a uniform distribution of material, like for forages, and the cutting force becomes proportional to the cutting area again [31].

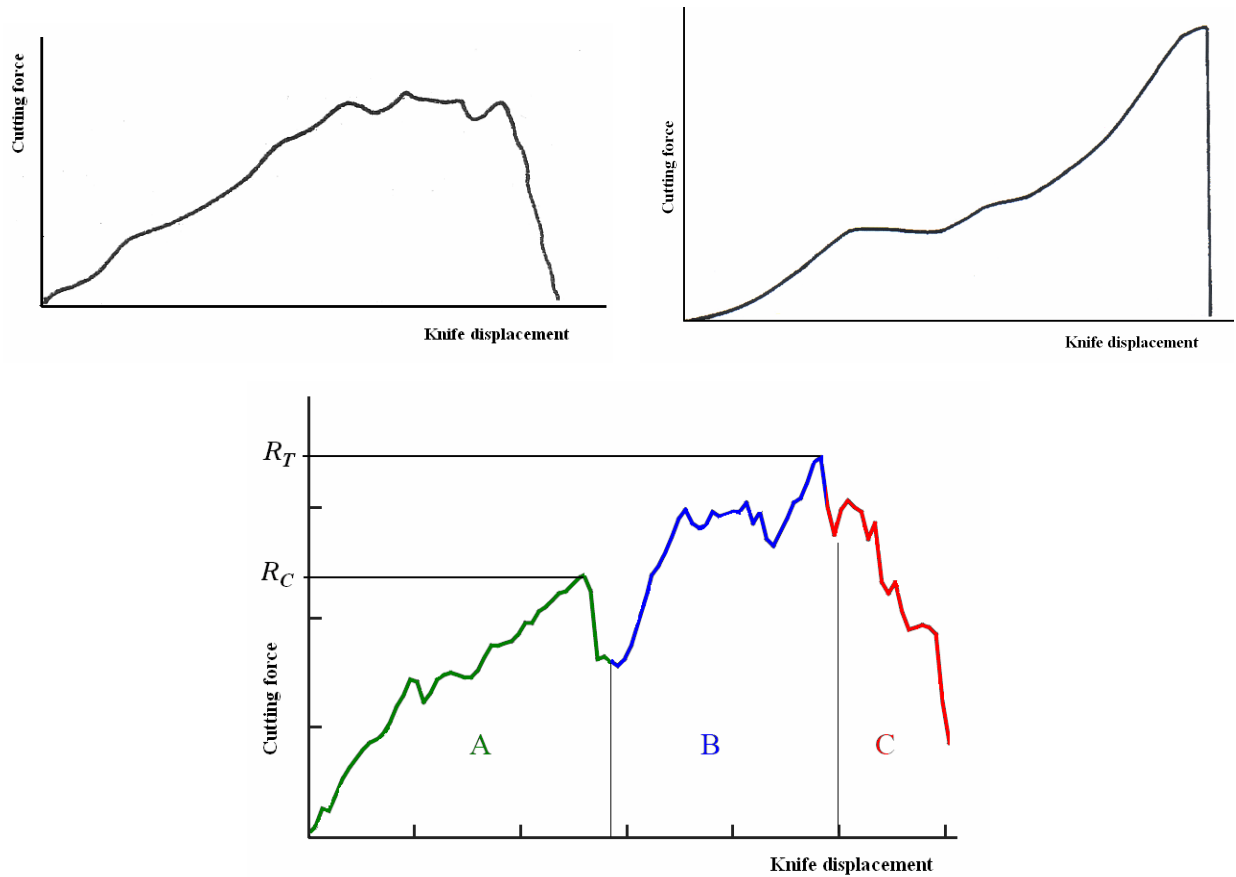


**Figure II. 2 – Examples of cutting force/displacement diagram for different fibrous materials, obtained experimentally with a static cut of a single shrub.**

Taking into account the description made above, the conventional simplified model for the trend of  $R(x_1)$  is built beginning from the analysis carried out by Kepner, [31], The Author analyses a generic double blade cutting bar and the *instantaneous* cutting force<sup>3</sup> generated. This force is calculated neglecting friction and inertia forces, and so it corresponds to our definition of the *cutting resistance*  $R^4$ . Considering a single pair of knife edges, Kepner highlight how this force is basically proportional to the infinitesimal area  $dA$  being cut by the two knife edges<sup>5</sup> in their reciprocal approaching  $dx_k + dx_p$  (Figure II. 3):

$$R = \frac{E \cdot dA}{dx_k + dx_p} \tag{II.4}$$

where  $k$  and  $p$  mean respectively knife and plate (the second movable knife). In the case of a single blade cutter bar it is:

<sup>3</sup> The Author uses the expression “averaged cutting force exerted during any increment of time” because he develops the analysis on the basis of little and not infinitesimal increments of displacement  $x_1$ . Passing to infinitesimal quantity, the notion “averaged” loses its meaning and the force function is translated into the present one.

<sup>4</sup> For this assertion see equation II.28 at page 38. Neglecting inertia and friction forces the knife active cutting force becomes equal to the plant passive cutting resistance.

<sup>5</sup> And measured in the plane of motion of the knife edge itself.

$$dx_p = 0, \quad dx_k = dx_1 \quad \Rightarrow \quad R = E \cdot \frac{dA}{dx_1} \quad (\text{II.5})$$

where  $dA$  is the area actually mowed by the knife during its infinitesimal displacement  $dx_1$  and  $E$  represents the specific energy required for the cut, measured in  $\text{J/m}^2$ . This specific energy is a solely function of the material being cut and it is calculated integrating the cutting force during the whole knife stroke, so it takes into account both the compression energy and the energy effectively used in the cut [46].

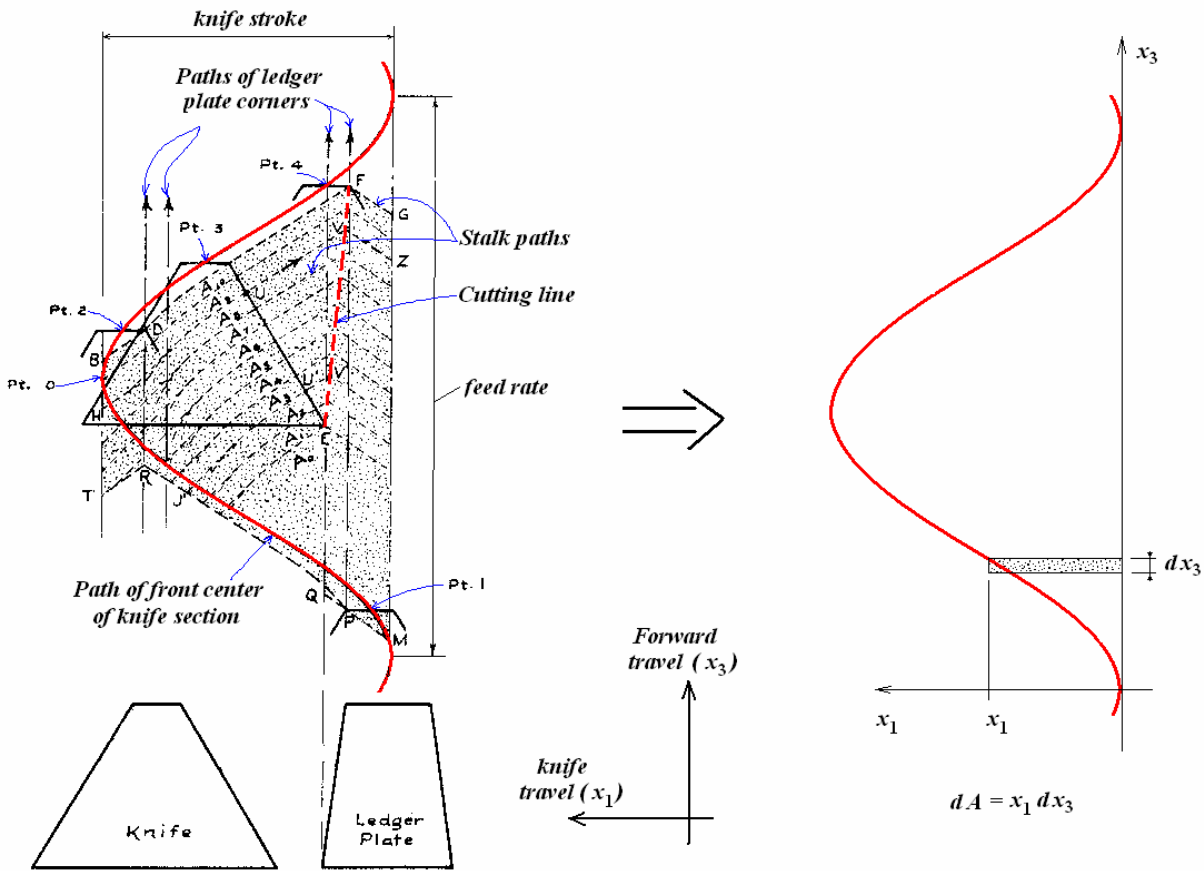


Figure II. 3 – Single blade cutting diagram for the right edge of a knife tooth, [31]. The real cutting area is dotted in grey, while the continuous red curve represents the tooth path. It could be observed the tiny approximation that has been made by neglecting the fingers dimensions. On the right the cutting area calculation scheme is represented.

During the work the area covered by the knife movement is a little different from the area effectively mowed, because of the knives and fingers dimensions themselves. This difference is negligible for single blade systems [31] (Figure II. 3), hence the value of  $R$  can be obtained by matching these areas and calculating  $dA$  as the covered area:

$$dA = z \cdot x_1 \cdot dx_3 = z \cdot x_1 \cdot \frac{dx_3}{dt} \cdot \frac{dt}{d\vartheta} \cdot d\vartheta = zx_1 \frac{\dot{x}_3}{\dot{\vartheta}} d\vartheta \quad (\text{II.6})$$

## Models

where  $z$  is the total knives number<sup>6</sup>,  $\dot{x}_3$  is the forward speed of the tractor carrying the cutting system (supposed to be uniform and in the  $x_3$  direction) in  $\text{m s}^{-1}$ ,  $x_1$  is the blade displacement in m,  $\dot{\vartheta}$  is the crank rotational speed in  $\text{rad s}^{-1}$  and  $d\vartheta$  is the crank infinitesimal rotational displacement in rad. From II.5 and II.6, the cutting resistance is:

$$R = E \cdot \frac{dA}{dx_1} = E \cdot \frac{dA}{d\vartheta} \cdot \frac{d\vartheta}{dt} \cdot \frac{dt}{dx_1} = Ez\dot{x}_3 \frac{x_1}{\dot{x}_1} \quad (\text{II.7})$$

where  $\dot{x}_1$  is the instantaneous blade speed in  $\text{m s}^{-1}$ . This equation is in good agreement even with the results of other Authors [22], where  $R$  results to be inversely proportional to the first power of the cutting speed.

Finally, Introducing the statistical coefficient  $p = p_1 \cdot p_2$  (%), which takes into consideration the random filling of the cutting area ( $p_1$ ) and the number of teeth simultaneously in action ( $p_2$ ), for the forward (increasing value for  $x_1$ ) and return stroke (decreasing value for  $x_1$ ), respectively, it gives:

$$R = \frac{1}{\dot{x}_1} p z E \dot{x}_3 \begin{cases} x_1(\vartheta) \\ c - x_1(\vartheta) \end{cases} = \frac{1}{\dot{x}_1} D(\vartheta) \quad (\text{II.8})$$

whose direction is always opposed to the blade speed:

$$\bar{R} = -R \text{sgn}(\dot{x}_1) \quad (\text{II.9})$$

and where  $c$  is the blade overall stroke in m:

$$c = e / \tan(\beta_0) - e / \tan(\beta_1) \quad (\text{II.10})$$

with  $e$  the mechanism eccentricity (m) while  $\beta_0$  and  $\beta_1$  are the conrod angle calculated respectively at the outer and inner dead centre positions of the mechanism ( $\text{rad}$ )<sup>7</sup>.

This model represents a first approximation of the cutting resistance, where the shrubs are cut instantaneously at the first contact with the knife: it doesn't take into account what above described, that is the cut can occur only along the line  $EF$  (Figure II. 3), locus where knife and finger meet. Hence the obtained trend, as it is in (II.8), should be limited to a certain window in respect to the overall blade stroke [31, 51].

For this purpose it could be assumed that the calculated trend remains valid between the coordinates  $x_E$  and  $x_F$  (m) that characterize the beginning and the end of the line  $EF$  on the  $x_1$  direction, while the force is null elsewhere:

<sup>6</sup> The number of knives and not the number of knife edges (the twice) because the edges belonging to the same knife never work at the same time.

<sup>7</sup> For their calculation see next Paragraph

$$\left\{ \begin{array}{l} R = 0 \\ R = \frac{1}{\dot{x}_1} pzE\dot{x}_3 \begin{cases} x_1(\vartheta) \\ c - x_1(\vartheta) \end{cases} = \frac{1}{\dot{x}_1} D(\vartheta) \end{array} \right. \quad \begin{array}{l} \text{for } x_1 < x_E \text{ and } x_1 > x_F \\ \text{for } x_E \leq x_1 \leq x_F \end{array} \quad (\text{II.11})$$

Calculating these two coordinates, it could be observed that for shrubs with a certain thickness, but not for forages as it was in [31], the line  $EF$  doesn't coincide with the finger edge anymore, as far as the quantity of shrubs under cutting increases. Simplifying the problem, this observation could be neglected and the finger edge could be taken as the definition of the line  $EF$ : calling with  $2r$  the overall stroke (m), with  $F_E$  ed  $F_F$  respectively the bottom and head finger width (m) and with  $K_E$  e  $K_F$  respectively the bottom and head knife width (m), it is:

$$\begin{aligned} x_E &= 2r - K_E/2 - F_E/2 \\ x_F &= 2r - K_F/2 - F_F/2 \end{aligned} \quad (\text{II.12})$$

that has to be considered only for the cutting (forward) stroke of each knife edge: for example, during the forward stroke of the left hand edge (left hand cutting stroke), the right hand edge doesn't cut anything while it accumulates material for the subsequent returning stroke (right hand cutting stroke), and vice versa. Hence, assuming conventionally the positive forces consistent with the positive knife speed (increasing blade displacement) it becomes:

$$\left\{ \begin{array}{l} R = \frac{x_1(\vartheta)}{\dot{x}_1} pzE\dot{x}_3 > 0 \\ R = \frac{c - x_1(\vartheta)}{\dot{x}_1} pzE\dot{x}_3 < 0 \\ R = 0 \end{array} \right. \quad \begin{array}{l} \text{for } x_E \leq x_1 \leq x_F \quad \text{and} \quad \dot{x}_1 > 0 \text{ (} x_1 \text{ increase)} \\ \text{for } x_E \leq x_1 \leq x_F \quad \text{and} \quad \dot{x}_1 < 0 \text{ (} x_1 \text{ decrease)} \\ \text{elsewhere} \end{array} \quad (\text{II.13})$$

For fresh vineyard wood it can be estimated  $E = 3 \cdot 10^2 \text{ J/m}^2$  (see [46]<sup>8</sup>) while the two statistical rates may be assumed to be  $p_1 = 33\%$  and  $p_2 = 50\%$  for an averaged situation. The resulting trend of the cutting resistance  $R$ , which is then assumed for the subsequent analysis, is calculated and shown in Figure II. 4 for different values of the total filling rate  $p$ , while in

<sup>8</sup> In the ASAE book the quantity  $E$  is named as  $ENCSAE$ , the specific cutting energy per unit field area (the area being cut) and it is measured in  $\text{KJ/m}^2$ . Its value is calculated as:

$$ENCSAE = ENCSA \cdot AESF/1000 \quad (\text{II.13b})$$

where  $ENCSA$  is the specific cutting energy per unit cut solids area (the area of solid material), measured in  $\text{J/mm}^2$ , while  $AESF$  is the total solids base area per unit field area of all plants, in  $\text{mm}^2/\text{m}^2$ . For the case of vineyard wood, the specific values of these parameters are not reported in the book, but they can be estimated within the uncertainty that these values experimentally have, that is  $E = 0.1 \div 0.4 \text{ kJ/m}^2$ . Being prudent, a value a bit greater than the average one may be assumed, and so  $E = 0.3 \cdot 10^3 \text{ J/m}^2$ .

## Models

Figure II. 5 it has been calculated for different values of the average running speed  $\omega$ . In line with other Authors [30, 52] and with practice, it can be seen that  $R$  decreases with increasing average running speed.

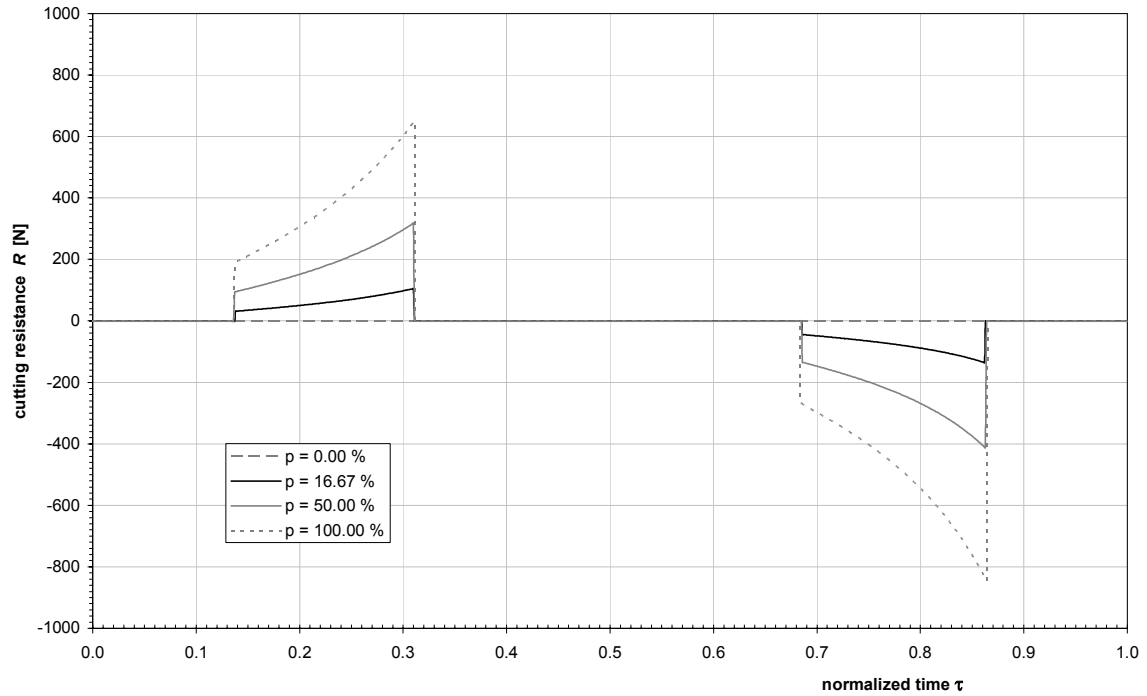


Figure II. 4 – Cutting resistance as a function of normalized and dimensionless time  $\hat{t} = 9/2\pi$ , for different values of filling percentage  $p$ . For the definition of  $\hat{t}$  see Paragraph III.2, page 56.

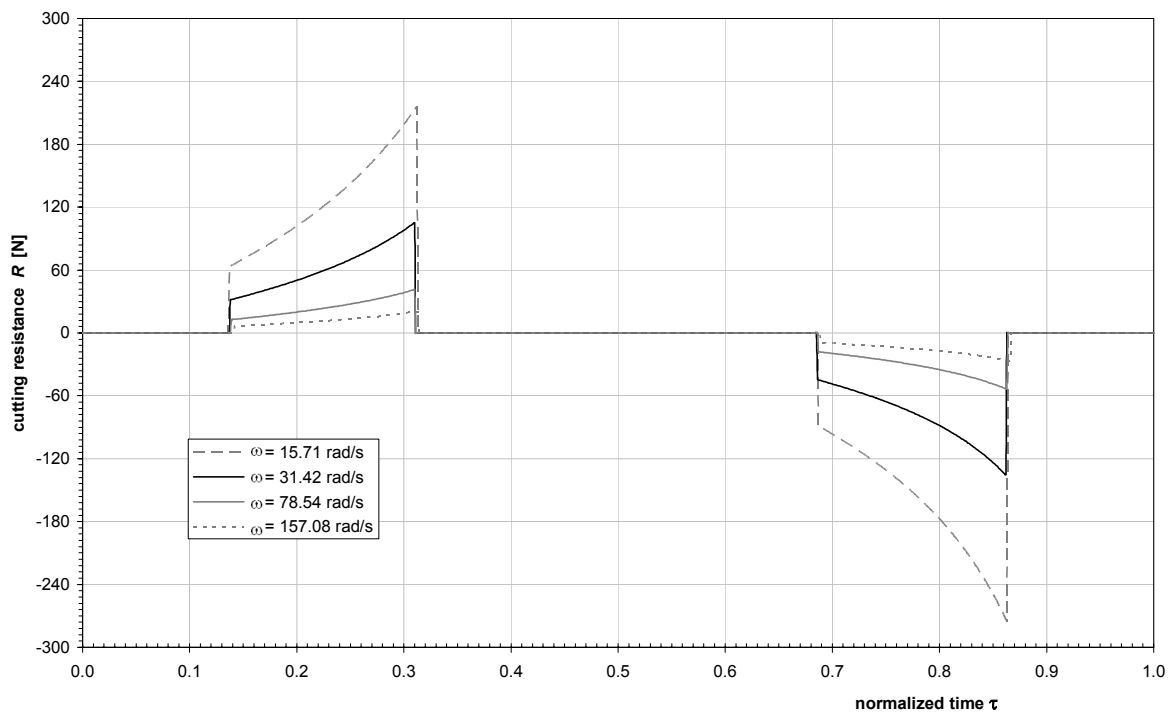


Figure II. 5 – Cutting resistance as a function of normalized time, for different values of the average running speed  $\omega$ .

### II.2.2 Model benefits and limits

The model obtained for the plant cutting resistance has the main benefit to be analytically simple and to be based on some of the blade kinematic and geometrical parameters ( $z$ ,  $\dot{x}_3$ ,  $x_1$  and  $\dot{x}_1$ ). These dependences amplify the model possibility of application, allowing it to be well adapted for different kind of cutting bars.

The developed model is fundamentally a kinematic model of cutting, while from the plant point of view it depends solely on the plant energetic parameter  $E$ . This is a great simplification from a biological standpoint but carries an advantage in terms of computation, benefit that will be discussed successively in Paragraph II.5.

It has to be remembered, anyway, that what above developed is only a qualitative model for the plant cutting resistance. This model is useful for the subsequent calculation and it would be helpful even for a comparison between the results of different cutting bars. Anyway it cannot be used for a comparison with experimental data not only because of the approximations introduced, but also because in practice there are several variables bringing their influence on the real trend of this force [7, 52].

For instance, the stochastic variability of  $E$  within the same kind of plant and even within the same shrub during the cut can just introduce a not negligible discrepancy with the model. This energetic coefficient, that is calculated integrating the force itself during the cutting path, cannot highlight the differences within the path due to the compression or the fibres structure destruction. To allow these aspects to be taken into account, the instantaneous value of the specific energy  $E(t)$  has to be considered instead of the averaged one, evaluating the dependence of  $E$  upon the coordinate  $x_1$  and so raising the complexity of the model. As a matter of fact, while cutting plants which have a specific fibrous structural resistance, the value of the work involved depends on the direction of cutting and not only on the magnitude of the cross section surface. It depends, also, on the positioning of the knife relatively to the stalk.

Moreover, the plant resistance is not uniform even in relation to the quantity of biological material that is instantaneously cut. The stochastic parameter  $p$  has been hence introduced and assumed constant to avoid this variability.

In conclusion, the cutting resistance has an extremely variable trend in practice, due to the instantaneous values of  $E$  and  $p$ . Their constancy is an approximation, which have been made for simplicity purposes.

### II.3 CUTTER BAR

Figure II. 6 shows a typical single blade cutter bar. The carrying frame, integral with the toothed counterbar, is fixed on the tractor chassis and acts as a guide for the motion of a reciprocating steel plate on which the tempered steel trapezoidal teeth are bolted or welded. The counterbar teeth help to divide the shrub into sheaves to facilitate the cut, and act as a counterpart to the cutting action of the blade teeth. The drive system, an eccentric crank-conrod mechanism, is connected to a hydraulic motor that takes power from the tractor hydraulic circuit [30].

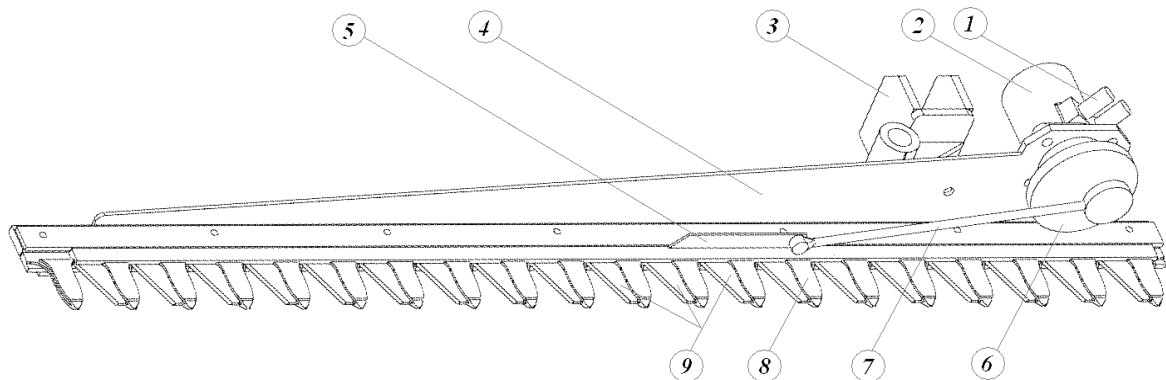


**Figure II. 6 – Reciprocating single blade cutter bar: hydraulic connection (1), hydraulic motor (2), dap-joint for the tractor chassis (3), counterbar (4), blade (5), crank disc (6), connecting rod (7), counterbar teeth (8), blade teeth (9).**

In the following subparagraphs the kinematic and dynamic analysis of this mechanical system are carried out, considering separately the drive system and the counterbar, together with the development of the mechanism equation of motion by means the application of an energetic criteria.

The crank – conrod drive system is well known from an engineering point of view, and also clearly and completely explained in many mechanical engineering books, both practically and mathematically. Anyway it could be stated that, in practice, its application is mainly analyzed making some approximations, like the uniformity of the crank rotational speed and, sometimes, the negligibility of the mechanism eccentricity [1, 25]. These assumptions, that are clearly rightful and explainable in common cases like internal combustion engines or automatic machineries, cannot be made here. This is because they refer to parameters which have to be deeply analyzed and their influence has to be clarified before any assumption is made.

Hence it has been found helpful to report in this thesis a complete analysis of the mechanism which doesn't make any preliminary assumption, nor approximation. However, the chance to assume any approximation remains up till the sensibility analysis will be carried out in the next Chapter.

The mathematical model of the system is developed assuming the crank angular position  $\vartheta$  (rad) as the unique DOF, measured from the outer dead center position and considering the general case of a non – uniform rotational crank speed ( $\dot{\vartheta} \neq \text{constant}$ ). Considering each member as infinitely rigid, the kinematic single DOF equations of the mechanism as well as the equations of equilibrium for each component can be written.

The reference frame is assumed as originating from the conrod motion plane, at the crank rotational axis projection. The  $X_1$  axis coincides with the blade direction of motion, moving positive on the inward stroke, the  $X_3$  axis coincides with the crank rotational axis in the tractor direction of travel, and the  $X_2$  axis is consequently determined.

### II.3.1 Crank-conrod mechanism kinematics and dynamics

The mechanism kinematics is now analyzed. The blade displacement is identified with the conrod small end displacement  $x_1(\vartheta)$  (m), and it can be written as (Figure II. 7):

$$x_1 = (r + l) \cdot \cos \beta_0 - l \cdot \sqrt{1 - (\lambda \sin \vartheta^* + \lambda')^2} - r \cdot \cos \vartheta^* = x_1(\vartheta) \quad (\text{II.14})$$

where  $\vartheta^* = (\vartheta - \beta_0)$  is the crank angular position, measured from the horizontal  $X_1$  negative position of the crank itself, and  $\beta$  (rad) is the conrod angle. The  $\beta_0$  and  $\beta_1$  values, respectively the conrod angle at the outer and inner dead centre positions, are determined geometrically from:

$$(l + r) \cdot \sin \beta_0 = h - h' = e \quad (\text{II.15})$$

$$(l - r) \cdot \sin \beta_1 = e \quad (\text{II.16})$$

and:

$r$  = crank radius (m)

$l$  = conrod length (m)

$\lambda$  =  $r/l$ , stroke – conrod ratio

$\lambda'$  =  $e/l$ , eccentricity ratio

$e$  =  $h - h'$ , mechanism eccentricity (m)

$h$  = distance, in the  $X_2$  direction, between the cutting line and crank rotational axis (m)

$h'$  = distance, in the  $X_2$  direction, between the cutting line and conrod small end (m)

$\vartheta^*$  =  $(\vartheta - \beta_0)$ , crank angular position measured from the horizontal  $X_1$  negative direction (rad)

The blade linear speed  $\dot{x}_1$  ( $\text{m s}^{-1}$ ) and acceleration  $\ddot{x}_1$  ( $\text{m s}^{-2}$ ) are, consequently:

$$\dot{x}_1 = \dot{\vartheta} \cdot r \cdot (\sin \vartheta^* + \lambda/2 \sin 2\vartheta^* + \lambda' \cos \vartheta^*) = r f'(\vartheta) \dot{\vartheta} \quad (\text{II.17})$$

## Models

$$\begin{aligned} \ddot{x}_1 &= \dot{\vartheta}^2 \cdot r \cdot (\cos \vartheta^* + \lambda \cos 2\vartheta^* - \lambda' \sin \vartheta^*) + \ddot{\vartheta} \cdot r \cdot (\sin \vartheta^* + \lambda/2 \sin 2\vartheta^* + \lambda' \cos \vartheta^*) = \\ &= rf(\vartheta)\ddot{\vartheta} + rf'(\vartheta)\dot{\vartheta}^2 \end{aligned} \quad (\text{II.18})$$

where  $\dot{\vartheta}$  and  $\ddot{\vartheta}$  are respectively the crank rotational speed (rad s<sup>-1</sup>) and acceleration (rad s<sup>-2</sup>), while:

$$f(\vartheta) = \sin \vartheta^* + \lambda/2 \sin 2\vartheta^* + \lambda' \cos \vartheta^* \quad (\text{II.19})$$

and

$$f'(\vartheta) = \frac{df(\vartheta)}{d\vartheta} \quad (\text{II.20})$$

are functions defined only for clearness purpose.

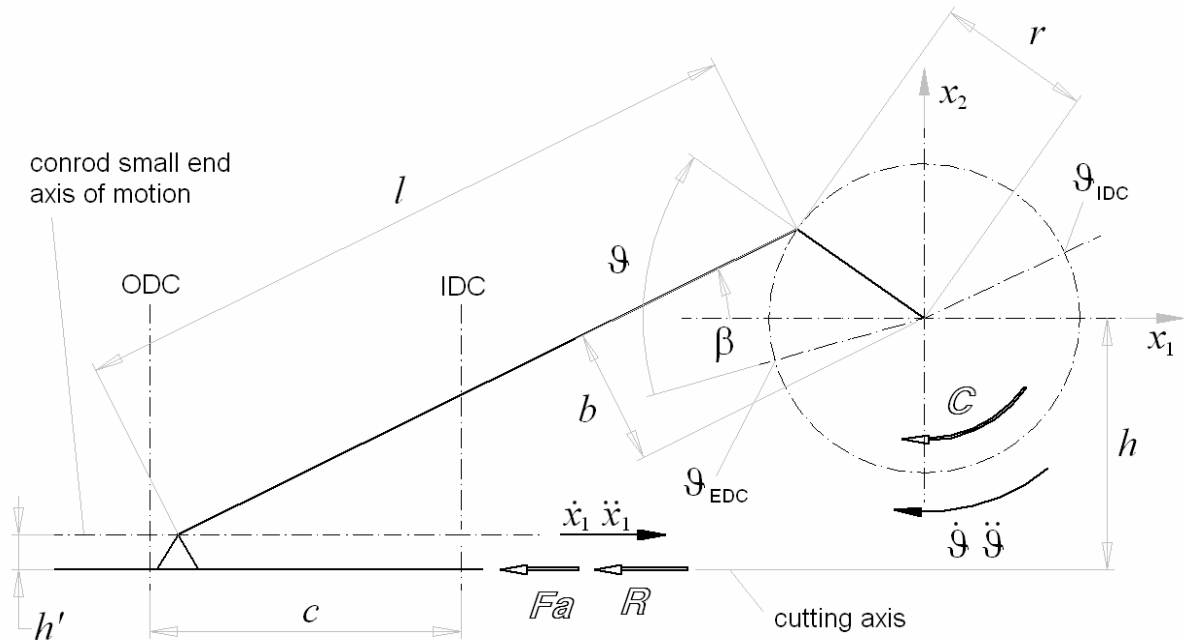


**Figure II. 7 – Mechanism diagram. ODC and IDC represent respectively the outer and the inner dead centre positions.**

The expression for the blade linear acceleration is the sum of two terms. If the crank rotational speed was supposed to be constant  $\dot{\vartheta} = \omega$ , the second of these terms would be null because of  $\ddot{\vartheta} = 0$  and the analysis would consequently be greatly simplified. Anyway this particular circumstance could not be assumed here, the motion irregularity being still unknown. The consequences of this consideration will be shown in the next Chapter.

To study the dynamic equilibrium, the mechanism has been split into its basic components. The blade mass  $m_b$  (kg) has been concentrated on its centre of gravity  $G_b$ , while the conrod inertia has been reduced to an equivalent system having a rotational mass integral with the crank  $m_{c1}$  (kg) and a translational mass integral with the blade  $m_{c2}$  (kg) [3]:

$$\begin{cases} m_{c1} + m_{c2} = m_c \\ -m_{c1} \cdot l_{c1} + m_{c2} \cdot l_{c2} = 0 \end{cases} \quad (\text{II.21})$$

respectively at the distance  $l_{c1}$  (m) and  $l_{c2}$  (m) from the conrod centre of gravity. Hence the total translational mass  $m_T$  (kg) is the sum of  $m_{c2}$  and the blade mass  $m_b$ :

$$m_T = m_b + m_{c2} \quad (\text{II.22})$$

while the rotational bodies total inertia momentum is

$$J_T = J_m + J_d + m_{b1} r^2 \quad (\text{II.23})$$

where  $J_m$  (kg m<sup>2</sup>) and  $J_d$  (kg m<sup>2</sup>) are respectively the motor and crank disc inertia momentums.

Neglecting the system weight<sup>9</sup> and considering all the kinematic pairs but the sliding one (blade – counterbar) as ideal, the input variables are the driving torque  $C(t)$  (Nm), applied to the disc rotational axis, the friction force  $F_a$  (N) between the blade and counterbar and the cutting resistance  $R$  (N), both applied on the blade opposite to its speed direction.

Based on the d'Alembert principle, the rotational equilibrium around the  $X_3$  axis is:

$$C(t) - F_c \cdot b = J_T \ddot{\vartheta} \quad (\text{II.24})$$

where  $F_c$  (N) is the axial force on the conrod and  $b = b(\vartheta)$  (m) is the minimum instantaneous distance between the conrod axis and crank rotational centre, measured on the  $X_1X_2$  plane:

$$b(\vartheta) = r \cdot \sin(\vartheta^* + \beta) = r \cdot \left( \sin \vartheta^* \cdot \sqrt{1 - (\lambda \sin \vartheta^* + \lambda')^2} + \cos \vartheta^* \cdot (\lambda \sin \vartheta^* + \lambda') \right) \quad (\text{II.25})$$

So, having the most general trend for the driving torque  $C(t)$  and the resistance torque  $F_c \cdot b(\vartheta)$ , it is not possible to exclude a priori the existence of the rotational acceleration  $\ddot{\vartheta}$ . Its trend will be drawn by the equation of motion analysis.

Dividing  $F_c$  into its  $X_1$  and  $X_2$  components results that:

$$F_{c1} = F_c \cdot \cos \beta = F_c \cdot \sqrt{1 - (\lambda \sin \vartheta^* + \lambda')^2} \quad (\text{II.26})$$

$$F_{c2} = F_c \cdot \sin \beta = F_c \cdot (\lambda \sin \vartheta^* + \lambda') \quad (\text{II.27})$$

So, the blade translational equilibrium in  $X_1$  direction is (Figure II. 8):

$$F_{c1} - m_T \cdot \ddot{x}_1 - F_a - R = 0 \quad (\text{II.28})$$

where  $-m_T \cdot \ddot{x}_1$  is the inertia force of the translational bodies applied to the blade centre of gravity  $G_b$  and opposite to the blade acceleration direction.

<sup>9</sup> The system weight force changes in direction with the working layout of the cutter bar (horizontal, vertical or more generally oblique layout). This force has been neglected because its value is considerably lower than the values of the other forces involved in the analysis. Moreover its value is constant and, as it is well known from the mechanics of vibrations [13], a constant force implies only a translation in the equilibrium point displacement, while the dynamic behavior in the neighbourhood of this point remains the same. Hence, this neglect allow to consider any working layout of the cutter bar and conduct a more general analysis.

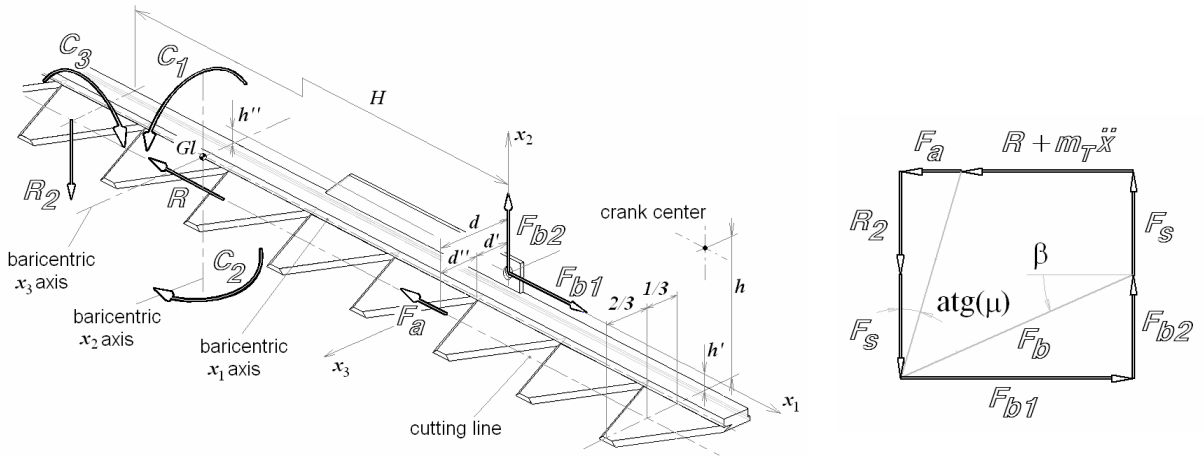


**Figure II. 8 – Particular of the blade with forces and torques, on the left, and blade equilibrium diagram, on the right.**

The translational equilibrium along the  $X_2$  axis is:

$$R_2 + F_s = F_{c2} + F_s \quad (\text{II.29})$$

where  $R_2$  (N) is the counterbar reaction in the  $X_2$  direction, while the clamping force  $F_s$  (N) of the counterbar on the blade appear on both sides of the equation since it is auto-equilibrated. Hence the friction force  $F_a$  due to the total force in the  $X_2$  direction is:

$$F_a = \mu(F_{c2} + F_s) \quad (\text{II.30})$$

with  $\mu$  being the friction coefficient. Using equation (II.28) this becomes:

$$F_a = \frac{\mu((R + m_T \cdot \ddot{x}_1) \cdot \tan \beta + F_s)}{1 - \mu \cdot \tan \beta} \quad (\text{II.31})$$

where

$$\tan \beta = (\lambda' + \lambda \sin \vartheta^*) / \sqrt{1 - (\lambda' + \lambda \sin \vartheta^*)^2} = g(\vartheta) \quad (\text{II.32})$$

Finally, the hypothesis of an ideal cutting line is assumed, so that the cutting resistance  $R$  is idealized to lie on it. This line is parallel to the  $X_1$  axis and is assumed to be placed on the bottom surface of the blade teeth, at a distance of  $2/3$  of the total teeth height from the teeth tip. The friction force  $F_a$  has ideally the same action line, while the counterbar reaction  $R_2$  belongs to the vertical plane through this line and the  $X_2$  axis, in the middle of the blade (Figure II. 8).

Analyzing the blade rotational equilibrium, and considering the vertical and horizontal offsets of the conrod small end from the defined cutting line, it is possible to identify three disequilibrium torques (Figure II. 9):

$$C_3 = F_{c1} \cdot h' - m_T \cdot \ddot{x}_1 \cdot (h' - h'') - F_{c2} \cdot H \quad (\text{II.33})$$

$$C_1 = F_{c2} \cdot d \quad (\text{II.34})$$

$$C_2 = F_{c1} \cdot d - m_T \cdot \ddot{x}_1 \cdot d'' \quad (\text{II.35})$$

Where it is:

$H$  = distance, in the  $X_1$  direction, between the middle of the blade and the conrod small end (m)

$h''$  = distance, in the  $X_2$  direction, between the blade centre of gravity and conrod small end (m)

$d$  = distance, in the  $X_3$  direction, between the cutting line and conrod small end (m)

$d''$  = distance, in the  $X_3$  direction, between the cutting line and blade centre of gravity (m)

$C_j$  = generic disequilibrium torque around the  $j$  axis, with  $j = 1, 2, 3$  (N m).

### II.3.2 Counterbar equilibrium

The forces and torques from the blade ( $F_a, F_{c2}, C_1, C_2, C_3$ ), together with the external forces ( $R$ ) and the forces from the crank pin ( $F_{c1}, F_{c2}$ ), are supported by the counterbar carrying frame, fixed to the tractor chassis by means of a dap-joint.

The translational equilibrium of the counterbar carrying frame (Figure II. 9) in the three directions is:

$$\begin{cases} -F_{c1} + V_1 + F_{i1} + F_a + R = 0 \\ R_2 - F_{c2} + V_2 + F_{i2} = 0 \\ F_{i3} + V_3 = 0 \end{cases} \quad (\text{II.36})$$

where  $V_j$  (N) is the generic dap – joint reaction force and  $F_{ij}$  (N) is the counterbar inertia force in the  $j$  direction, with  $j = 1, 2, 3$ . Using equations (II.28, II.29) and observing that there are no external forces in the  $X_2$  and  $X_3$  directions, these equations become:

$$\begin{cases} V_1 + F_{i1} = m_T \cdot \ddot{x}_1 \\ V_2 + F_{i2} = 0 \\ V_3 + F_{i3} = 0 \end{cases} \quad (\text{II.37})$$

Defining the barycentric axis as the  $X_j$  direction through the counterbar centre of gravity, with  $j = 1, 2$  and  $3$ , the rotational equilibrium around the barycentric  $X_3$  axis is:

$$\begin{aligned} C_{i3} + C_{V3} + C_3 + R_2(H + r \cdot \cos \vartheta + l \cdot \cos \beta - a) - V_2 \cdot x_{GS1} + F_{c2} \cdot a + \\ -(R + F_a) \cdot (h' + h'' + x_{GL2} - x_{GS2}) - F_{c1} \cdot (h - h' + h'' - x_{GL2} + x_{GS2}) + V_1 \cdot x_{GS2} = 0 \end{aligned} \quad (\text{II.38})$$

where:

$C_{Vj}$  = generic dap-joint reaction torque around the  $j$  axis, with  $j = 1, 2, 3$  (N m)

## Models

$C_{ij}$  = generic counterbar inertia torque around the  $j$  axis, with  $j = 1, 2, 3$  (N m)

$a$  = distance, in the  $X_1$  direction, between the counterbar centre of gravity and crank rotational axis (m)

$x_{GSj}$  = distance, in the  $j$  direction, between the dap-joint and counterbar centre of gravity (m)

$x_{GLj}$  = distance, in the  $j$  direction, between the dap-joint and blade centre of gravity (m)

Observing that:

$$h' - h = -e = r \cdot \text{sen} \vartheta - l \cdot \text{sen} \beta \quad (\text{II.39})$$

and substituting equations (II.28, II.29, II.33, II.37 and II.39) into (II.38) after few passages it becomes:

$$C_{i3} + C_{V3} + V_1 \cdot x_{GS2} - V_2 \cdot x_{GS1} = J_T \ddot{\vartheta} - C - m_T \ddot{x}_1 \cdot (x_{GL2} - x_{GS2}) = T_3 \quad (\text{II.40})$$

The rotational equilibrium around the barycentric  $X_1$  axis, using equations (II.34) and (II.37), is:

$$C_{i1} + C_{V1} - V_2 \cdot x_{GS3} + V_3 \cdot x_{GS2} = 0 \quad (\text{II.41})$$

Finally, the rotational equilibrium around the barycentric  $X_2$  axis is:

$$C_{i2} + C_{V2} + C_2 - V_3 \cdot x_{GS1} + V_1 \cdot x_{GS3} + F_{b1} \cdot a' - (R + F_a) \cdot (x_{GL3} + d'' - x_{GS3}) = 0 \quad (\text{II.42})$$

where  $a'$  is the distance, in the  $X_3$  direction, between the conrod small end and counterbar centre of gravity. Using equations (II.35, II.37), equation (II.42) becomes:

$$C_{i2} + C_{V2} - V_2 \cdot x_{GS1} + V_1 \cdot x_{GS3} = -m_T \ddot{x}_1 \cdot (x_{GL3} - x_{GS3}) = T_2 \quad (\text{II.43})$$

The set of equations (II.37, II.40, II.41 II.43) describes the system dynamic equilibrium. These equations are statically coupled, since the dap – joint has a finite structural stiffness.

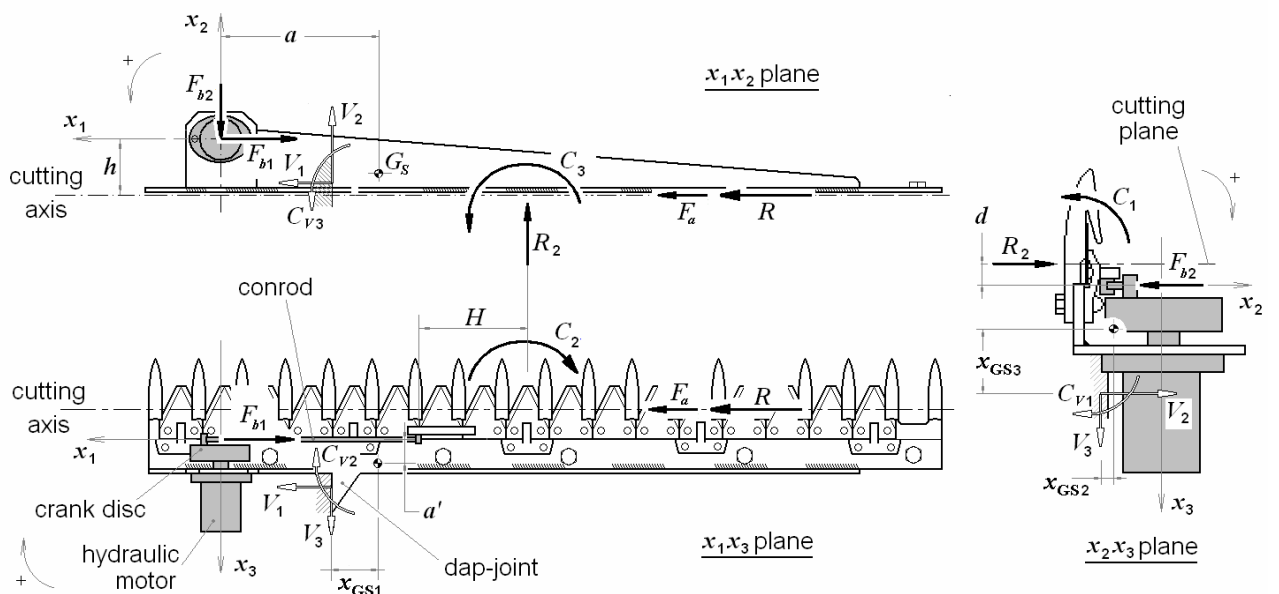


**Figure II. 9 – Cutter bar diagram.**

### II.3.3 Equation of motion

The equilibrium equation (II.24) written in function of the solely DOF  $\vartheta$  and of its derivatives represents the *mechanism's equation of motion*. As well as for the equilibrium equations, this equation is useful to understand the mechanism behavior, but in a different way. Anyway, before proceeding with its development it is necessary to clarify the motion running conditions in which the cutter bar behaves. Moreover, it is necessary a further analysis of each term of the equation itself.

As it could be understood from the above equilibrium analysis, the whole force system involved in the cutter bar analysis is function of the DOF  $\vartheta$  and so it varies with a periodic law. Hence, any external or internal force or torque acting on the cutter bar can be written in terms of  $\vartheta$  and its derivatives. Moreover, in absence of any external not deterministic and not foreseen noise, even the rotational speed and acceleration are periodic functions of the angular displacement  $\vartheta$  and they can be written in terms of it. They oscillate around their average values with period  $T$  whose value is unique and it is due to the motor axis rotation average running speed.

Under these particular circumstances it is said that the mechanical system behaves in a *periodic running condition*, which was expected to be because of the presence of a reciprocating driving mechanism. The not uniform but periodic shape of the rotational speed in time implies obviously the existence of the rotational acceleration  $\ddot{\vartheta}$ , that leads the system to be subjected to continuous transitories, shorter than a singular axis rotation, and never to have an *absolute running condition*.

Hereby, assuming a deterministic model, the crank mechanism motion is periodic, with period  $T = 2\pi/\omega$ , where  $\omega$  is the average value of the rotational speed. Let us analyze any force in

$$C(t) - F_c \cdot b = J_T \ddot{\vartheta} \quad (\text{II.44})$$

to highlight its dependence on the solely DOF and its derivatives, that is the demonstration of a periodic running condition subsistence.

The resistance torque is  $F_c \cdot b(\vartheta)$ , where the dependence of  $b$  on  $\vartheta$  has already been highlighted and  $F_c$  is (II.26, II.28):

$$F_c = (m_T \cdot \ddot{x}_1 + F_a + R) / \sqrt{1 - (\lambda \sin \vartheta^* + \lambda')^2} \quad (\text{II.45})$$

where, as it can be seen from equations (II.8, II.18 and II.31):

$$\ddot{x}_1 = \ddot{x}_1(\vartheta, \dot{\vartheta}, \ddot{\vartheta}) \quad (\text{II.46})$$

## Models

$$F_a = F_a(\ddot{x}_1, R, \beta) = F_a(\vartheta, \dot{\vartheta}, \ddot{\vartheta}) \quad (\text{II.47})$$

$$R = R(\vartheta, \dot{\vartheta}) \quad (\text{II.48})$$

and so even

$$F_c = F_c(\vartheta, \dot{\vartheta}, \ddot{\vartheta}) \quad (\text{II.49})$$

is a periodic function of  $\vartheta$ .

To couch the driving torque as a function of  $\vartheta$  the hydraulic motor functional diagram  $C = C(\dot{\vartheta})$  is used, as well as in the case of absolute running conditions. It has to be observed that these diagrams cannot be used generally under periodic running conditions [25], especially when the oscillation period is shorter than the duration of a single revolution of the axis. This obstacle is overtaken assuming that the driving torque is independent from  $\vartheta$ , as it could be expected using an hydraulic motor, and from  $\ddot{\vartheta}$ . That is, the fluctuation of  $\dot{\vartheta}$  doesn't influence the diagram shape but only modifies the working point coordinates on the diagram itself. The evidence for this assertion can be found observing the functional diagram, where curves within the same family have a similar shape, which doesn't vary with a change in speed. Hence, for small values of rotational speed fluctuation, the motor functional curve can be developed as a Taylor series about the rotational speed average value  $\omega$  [25], neglecting the terms over the first<sup>10</sup>:

$$C \approx \bar{C}(\omega) + \left[ \frac{dC}{d\dot{\vartheta}} \right]_{\omega} (\dot{\vartheta} - \omega) = \bar{C} + k(\dot{\vartheta} - \omega) \quad (\text{II.50})$$

where  $\bar{C}$  (N·m) is the driving torque average value, that is the torque evaluated for the average rotational speed, while  $k$  (kg m<sup>2</sup> s<sup>-1</sup>) is the motor stiffness, in this case meaning hydraulic plant stiffness<sup>11</sup>. Particularly,  $k$  represents the slope of the curve considered in the diagram,

<sup>10</sup> Neglecting higher order terms corresponds to assert the small value of the rotational speed fluctuation.

<sup>11</sup> To define completely equation (II.50) the motor functional diagram is used. Upon it, in case of absolute running conditions, the working point depends solely on the working characteristics of the hydraulic plant that supply the motor. As it could be seen from the diagram showed as an example in the figure below, the nominal value of the driving torque  $C^*$  and the nominal rotational speed  $\omega^*$  (respectively M and min-1 in the functional diagram) are functions of the theoretical pressure difference  $\Delta p$  between the motor intake and outtake and of the theoretical input flow  $Q$ , both plants characteristics. It is:

$$C^* = \Delta p \cdot V \cdot \eta_H \eta_M \quad (\text{II.49a})$$

where  $\eta_H$  and  $\eta_M$  are respectively the hydraulic and mechanical efficiency of the motor, while  $V$  is its cylinder volume at any revolution. The nominal rotational speed is a function of  $V$  and  $Q$ :

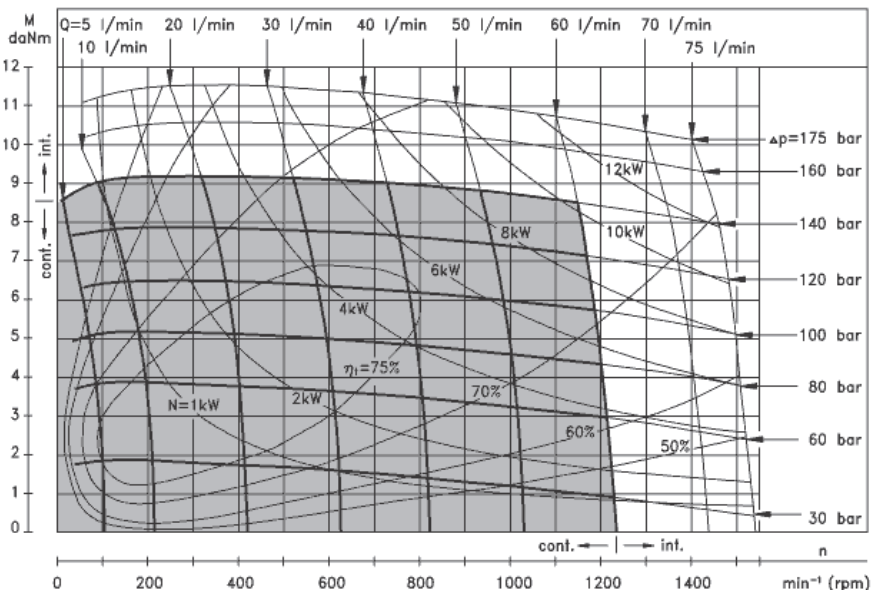
$$\omega^* = \frac{Q}{V} \eta_V \quad (\text{II.49b})$$

where  $\eta_V$  is named volumetric efficiency

calculated in the abscissa point where  $\dot{\vartheta} = \omega$ , and it identifies the motor (hydraulic plant) tendency to maintain a given rotational speed with variations in the resistance torque.

Equation (II.50) asserts that the driving torque is a function of the first derivative of the DOF  $C = C(\dot{\vartheta})$ . Thus, since any terms involved in equation (II.24) is a function of the unique DOF and its derivatives, a periodic running condition subsists.

The equation of motion can be written on the basis of equation (II.24), as it has been said above, that is, following the *forces approach*. Anyway here an *energetic approach* has been



Hence, given the hydraulic plant and the motor, the pressure gap  $\Delta p$  can be varied with the apposite regulation valve at the motor intake, or the input flow  $Q$  can be modified with the tractor gas throttle. Thus it is possible to obtain the wanted values for the torque  $C^*$  and for the rotational speed  $\omega^*$ , accordingly to the above equations, adjusting the working point on the diagram and optimizing the overall motor efficiency  $\eta = \eta_V \eta_H \eta_M$ .

Besides, in case of periodic running conditions the nominal values lose their meaning. The rotational speed is periodically variable, and with it even the driving torque but, anyway, equations (II.49a) and (II.49b) remain valid if the averaged values  $\omega$  and  $\bar{C}(\omega)$  are assumed in the calculus, rather than the nominal ones, as well as the constant  $k$ . Hence in this case, acting on the tractor gas throttle or on the motor intake hydraulic valve, the average rotational speed is modified on the basis of equation (II.49b), but the driving torque trend, and hence its average value and the coefficient  $k$ , depends only upon the resistance and inertia torques, as it is well highlighted by equation (II.24). Therefore, given the quantities  $V$  and  $Q$ , the average rotational speed  $\omega$  is set from equation (II.49b), the average driving torque is equal to the average resistance one, while the coefficient  $k$  is

$$k = \left[ \frac{dC}{d\dot{\vartheta}} \right]_{\omega} = \left[ \frac{d\Delta p}{d\dot{\vartheta}} \right]_{\omega} \cdot V \eta_V \eta_H \eta_M \quad (\text{II.49c})$$

where  $V = \text{constant}$  and where it has been assumed negligible any efficiency variations with small changes in the running speed:

$$\left[ \frac{d\eta_H}{d\dot{\vartheta}} \right] = \left[ \frac{d\eta_M}{d\dot{\vartheta}} \right] = 0 \quad (\text{II.49d})$$

Equation (II.49c) finally highlights that the driving torque oscillation amplitude, anyhow limited for the considered running speed variations, comes only from the variance of the pressure gap  $\Delta p$ . The amplitude of the pressure gap variance, in its turn, depends only upon the plant ability to maintain unaltered its functional characteristics against variations of the externally imposed load. Hence the motor stiffness means here plant stiffness.

## Models

assumed, because it is suitable for some further observations that will be carried subsequently. Hence, the most general motion of the single DOF crank – conrod mechanism can be analyzed using the kinematic energy theorem:

$$W_m + W_r + W_d = \frac{dE}{dt} \quad (\text{II.51})$$

where  $W_m$ ,  $W_r$  and  $W_d$  are respectively the driving, the resistance and the dissipative power, while the term on the right side represents the variation in the kinematic energy of every movable part of the mechanism, rotational and translational.

This equation gives a deeper view on some assertion made above. When the sum of the external force powers is positive, the kinematic energy of the mechanism increases while, on the contrary, when this sum is negative the system reduces its kinematic energy. That is an explanation for the instantaneous variation in the rotational speed  $\dot{\vartheta}$ . Hence, the inertia terms can be thought as an “energy reservoir”: when the system accelerates the inertia terms store the surplus energy in respect to that used in the cutting action and friction overtaking, while when the system decelerates they give it back to make up for the lack of driving power.

On left side of (II.51) it is<sup>12</sup>:

$$W_m = C\dot{\vartheta} = \bar{C}(\omega)\dot{\vartheta} + k(\dot{\vartheta} - \omega)\dot{\vartheta} \quad (\text{II.52})$$

$$W_r = -R\dot{x}_1 = -D(\vartheta) \quad (\text{II.53})$$

$$W_d = -F_a\dot{x}_1 = -r f(\vartheta)\dot{\vartheta} \cdot \frac{\mu((R + m_T \cdot \ddot{x}_1)g(\vartheta) + F_s)}{1 - \mu g(\vartheta)} \quad (\text{II.54})$$

where the negative signs are due to the discordance between the force direction and the blade speed direction (that’s why they are the dissipative and resistance terms), while the kinematic energy variation is:

$$\frac{dE}{dt} = \frac{d}{dt} \left( \frac{1}{2} J_T \dot{\vartheta}^2 + \frac{1}{2} m_T \dot{x}_1^2 \right) = [J_T + m_T r^2 f(\vartheta)^2] \cdot \dot{\vartheta} \ddot{\vartheta} + [m_T r^2 f(\vartheta) f'(\vartheta)] \cdot \dot{\vartheta}^3 \quad (\text{II.55})$$

Substituting the four above equations into equation (II.51) and collecting in respect of  $\vartheta$  and its derivatives, it becomes:

$$\begin{aligned} & \left[ J_T + m_T r^2 \left( 1 + \frac{\mu g(\vartheta)}{1 - \mu g(\vartheta)} \right) f^2(\vartheta) \right] \cdot \dot{\vartheta} \ddot{\vartheta} + \left[ m_T r^2 \left( 1 + \frac{\mu g(\vartheta)}{1 - \mu g(\vartheta)} \right) f(\vartheta) f'(\vartheta) \right] \cdot \dot{\vartheta}^3 - k \cdot \dot{\vartheta}^2 + \\ & + \left( k \omega - \bar{C}(\omega) + r f(\vartheta) F_s \left( \frac{\mu}{1 - \mu g(\vartheta)} \right) \right) \cdot \dot{\vartheta} + \left( 1 + \frac{\mu g(\vartheta)}{1 - \mu g(\vartheta)} \right) \cdot D(\vartheta) = 0 \end{aligned} \quad (\text{II.56})$$

<sup>12</sup> With not ideal constraints the dissipative power cannot be neglected. Here the solely contribution of the friction between the blade and the counterbar is taken into account because it is the most important one.

and so:

$$\begin{aligned}
 & [J_T + A(\vartheta)f^2(\vartheta)] \cdot \left( \frac{d^2\vartheta}{dt^2} \right) \left( \frac{d\vartheta}{dt} \right) + [A(\vartheta)f(\vartheta)f'(\vartheta)] \cdot \left( \frac{d\vartheta}{dt} \right)^3 - k \cdot \left( \frac{d\vartheta}{dt} \right)^2 + B(\vartheta) \cdot \left( \frac{d\vartheta}{dt} \right) + \\
 & + (D(\vartheta)A(\vartheta))/m_T r^2 = 0
 \end{aligned} \quad (II.57)$$

where  $f(\vartheta)$ ,  $f'(\vartheta)$ ,  $g(\vartheta)$  and  $D(\vartheta)$  have already been shown, while  $A(\vartheta)$  and  $B(\vartheta)$  are the following functions of the DOF:

$$A(\vartheta) = m_T r^2 \left( \frac{1}{1 - \mu g(\vartheta)} \right) \quad (II.58)$$

$$B(\vartheta) = k \omega - \bar{C}(\omega) + r \mu f(\vartheta) F_s \left( \frac{1}{1 - \mu g(\vartheta)} \right) \quad (II.59)$$

Obviously equation (II.57) assumes three different forms depending on the value of  $\vartheta$ , since the form of  $D(\vartheta)$  is (II.11, II.13):

$$\begin{cases} D(\vartheta) = 0 & \text{for } \vartheta < \vartheta_E \text{ and } \vartheta > \vartheta_F \\ D(\vartheta) = pzE\ddot{x}_3 \begin{cases} x_1(\vartheta) > 0 & \text{for } \vartheta_E \leq \vartheta \leq \vartheta_F \text{ and } \dot{x}_1 > 0 \text{ (} x_1 \text{ increase)} \\ c - x_1(\vartheta) < 0 & \text{for } \vartheta_E \leq \vartheta \leq \vartheta_F \text{ and } \dot{x}_1 < 0 \text{ (} x_1 \text{ decrease)} \end{cases} \end{cases} \quad (II.60)$$

where  $\vartheta_E$  and  $\vartheta_F$  are respectively the crank angles for which (see equation II.12):

$$x_1(\vartheta) \Big|_{\vartheta=\vartheta_E} = x_E \quad (II.61)$$

$$x_1(\vartheta) \Big|_{\vartheta=\vartheta_F} = x_F \quad (II.62)$$

Equation (II.57) is the equation of motion of the mechanism. It is an ordinary non – homogeneous second order differential equation, strongly non – linear and with  $\vartheta$  dependent coefficients. This kind of differential equation doesn't admit, generally, a closed form solution [1, 13 and 49], but it can be numerically integrated<sup>13</sup> assuming convenient boundary conditions. The solution of equation (II.57) represents the *motion law*  $\vartheta(t)$  of the mechanism.

Using the geometric and inertia characteristics of a common cutter bar sold on the Italian market (type Regina, Lotti srl, Faenza, Italy), and using standard working conditions, the equation of motion (II.57) has been numerically integrated (see Appendix A for the code list). The assumed boundary conditions are the values of the rotational speed for the minimum and maximum value of the integration time, assumed to be equal to the rotational speed average value.

<sup>13</sup> Here, anyway, every term in the equation is periodic. Hence an exact closed form solution can be found reducing the equation itself to an equivalent first order system and subsequently developing it as a Fourier series.

## Models

From the obtained motion law, the time shape of all the  $\vartheta$  dependent functions shown above has been calculated, numerically, as well as the functions  $\dot{\vartheta}(\vartheta)$  and  $\ddot{\vartheta}(\vartheta)$ . Any force and torque in the equilibrium analysis has been then expressed in function of the solely DOF.

### *II.4 ON THE BALANCING OF CRANK – CONROD MECHANISMS*

The minimization of the system disequilibrium could be faced by means of three different approaches.

The first approaching way is optimizing the geometry of the mechanism. Following this approach the system geometry is modified in a way that allows minimizing both forces and torques magnitudes. This geometrical optimization can be carried out on the basis of the mechanism's equilibrium equations. Anyway, this kind of approach has to be seen only as a preliminary design optimization of the system because, as it will be observed, it allows obtaining only a limited level of balancing.

Another way is to optimize the dynamics of the mechanism. Following this approach the system dynamic is modified, in a way that allows minimizing forces and torques magnitudes and dynamic fluctuations. This is the commonly adopted approach for this kind of mechanisms, and implies the use of additional ballasts and inertial bodies in a way that the dynamic of the mechanism is finally changed. This approach can be carried out on the basis of the equations of motion too but, as it is well known, it allows obtaining only a limited level of balancing. Moreover its application introduces a high level of complexity.

The last method to face the disequilibrium is to directly optimize the motion law: following this approach the system's kinematics is modified, in a way that allows minimizing both forces and torques dynamic fluctuations over time. This optimization can be carried out on the solely basis of the mechanism's motion law.

Only the latter approach will be taken into consideration and developed in this thesis, in a separate Chapter, the dynamic balancing being well adopted and deeply analyzed in more specialized texts. Before continuing further, anyway, some considerations on the equilibrium equations could allow a preliminary design optimization of the system, that is following the first approach. This will allow a roughly understanding on which are the dynamic and geometric factors that have more influence on the system disequilibrium, which is important for the analysis conducted in the next chapter.

Analyzing the equilibrium, the unbalancing could be clarified. The forces are not null only for the  $X_1$  translation direction (II.37) and the rotations around the  $X_2$  and  $X_3$  directions (II.43,

II.40).

In the  $X_1$  direction the force produces a disequilibrium, and so a vibrational movement, which is not of major importance for the cutting quality. Moreover, using nominal working parameters which will be explained hereafter, the force has nominal fluctuation amplitude of only about 600 N. With this order of magnitude, and even because the cutter bar could be considered longitudinally infinitely stiff, the disequilibrium could be considered as negligible.

The unbalanced torque around the  $X_2$  direction  $T_2$  has a nominal fluctuation amplitude of slightly less than 10 Nm, which is not a negligible value. Anyway this value can be reduced by means of a change in the cutter bar geometry, making the blade and counterbar centres of gravity coincide in the  $X_3$  direction

$$x_{GL3} \approx x_{GS3} \quad (II.63)$$

The unbalanced torque around the  $X_3$  direction  $T_3$  has the most influence on cutting quality, because it makes the cutter bar move in the plane that is perpendicular to the tractor direction of travel. Moreover its magnitude is the most severe, with nominal fluctuation amplitude of about 24 Nm, which is about 350 kg at the cutter bar end tip (Figure II. 11). This force arise from the sum of three components: the torque caused by the blade translational inertia force  $-m_T \ddot{x}_1(x_{GL2} - x_{GS2})$ , the (crank disc) inertia torque  $-J_T \ddot{\vartheta}$  and the driving torque  $C$ , each one fluctuating as shown in Figure II. 10.

Under nominal working conditions, the first of the three components has the main contribution to the total unbalancing amplitude, with an average value of about 69% of the overall fluctuation. Anyway, as stated before, this value is geometrically avoidable making the blade and counterbar centres of gravity coincide in the  $X_2$  direction.

$$x_{GL2} \approx x_{GS2} \quad (II.64)$$

i.e. having the counterbar centre of gravity practically on the cutting line. This means moving the hydraulic motor closer to the blade, making the mechanism less eccentric as stated by previous Authors [30], or leaving the engine in the same position but adding an equivalent ballast on the opposite side of the blade.

On the other hand the second component of  $T_3$ , the inertia torque, is practically negligible, with an average contribution of less than 0.50% of the overall fluctuation, while the driving torque, which gives 30.50% of the total forcing magnitude, is strongly  $\vartheta$  dependent, highly discontinuous and absolutely not geometrically reducible. This final observation has suggested to analyze directly the motion law  $\vartheta(t)$  in order to understand how to make the driving torque more uniform.

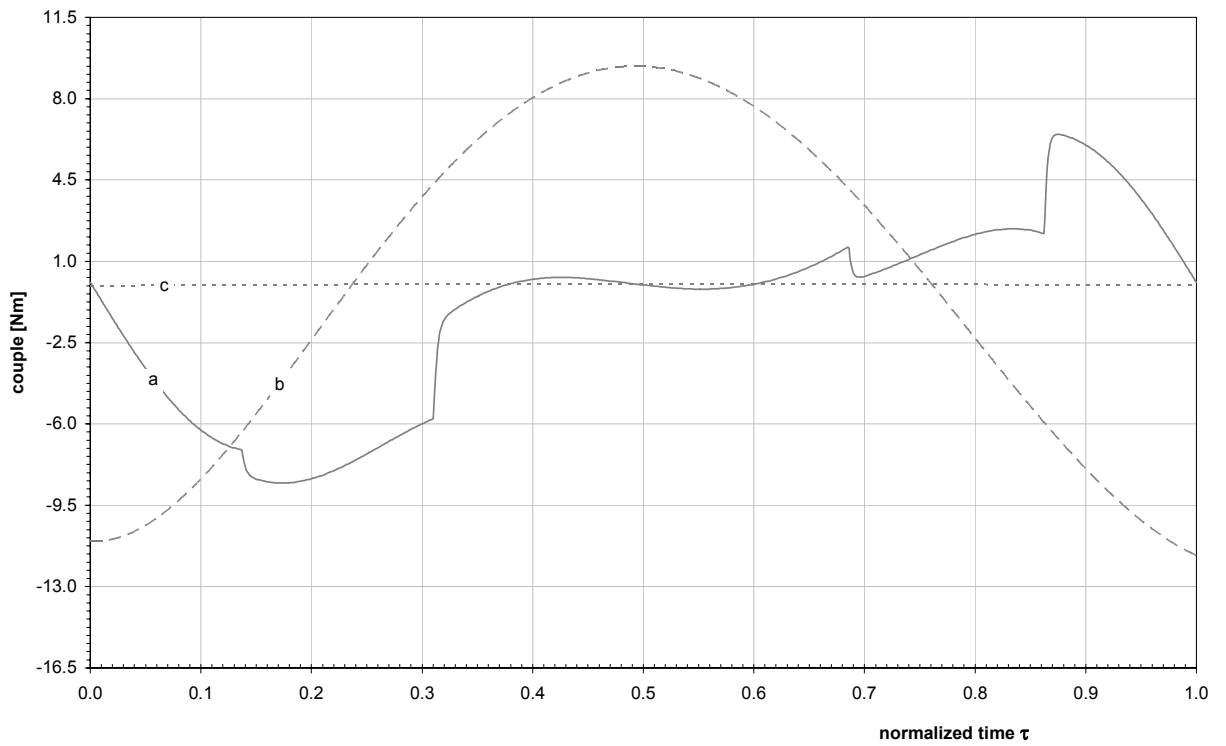


Figure II. 10 – The diagram shows (a) the driving torque, (b) the torque due to blade inertia and (c) the inertia torque due to crank disc as a function of normalized time.

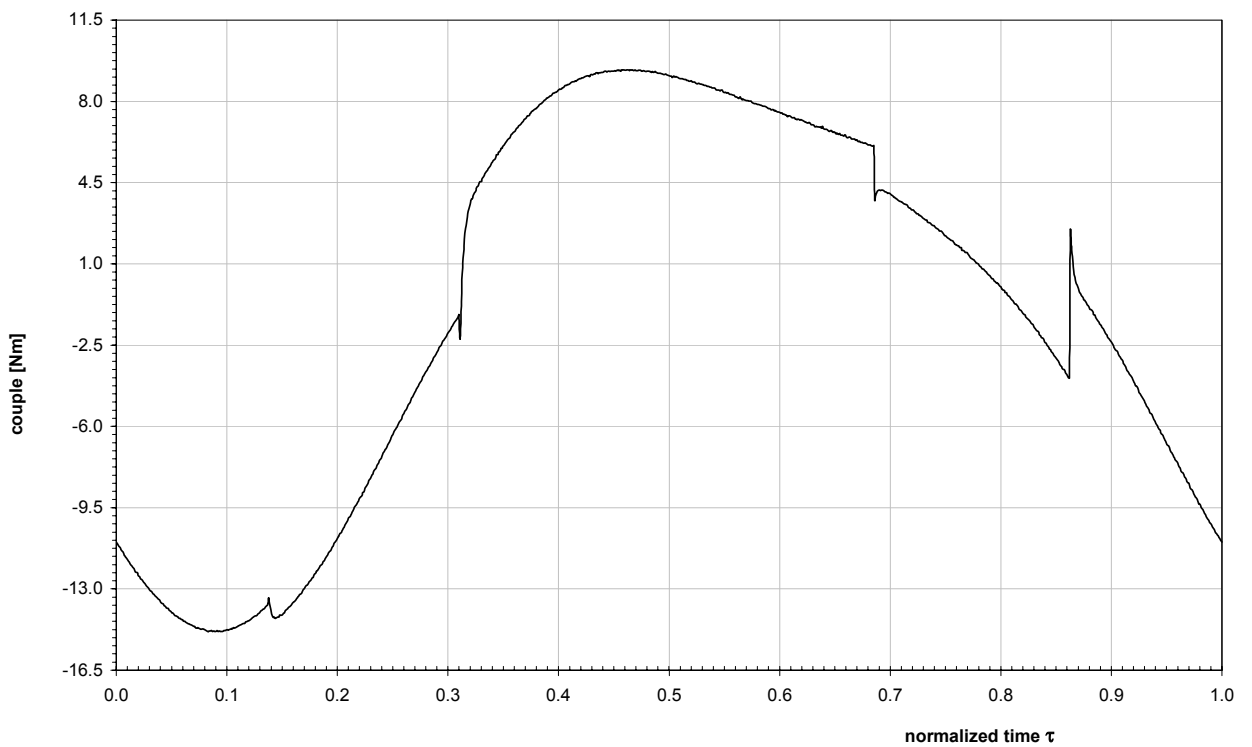


Figure II. 11 – The diagram shows the overall unbalanced torque around the  $X_3$  direction, that is the superposition of the three contribution showed above.

## II.5 DISSIPATIVE AND RESISTANCE POWERS MEASUREMENT

Performing some experimental measures, it is possible to estimate the different influence that friction and cutting force have on the overall energy requirement of the system and, finally, to evaluate the energy quote effectively used for the cutting action.

Multiplying each member of equation (II.51) for  $dt$  and integrating over a whole crank cycle the total kinematic energy variation has to be null, because of the subsistence of a periodic running condition with angular period  $2\pi$ , precisely. Hence it is:

$$\int_t^{t+T} (W_m + W_r + W_d) dt = T \cdot (\overline{W}_m + \overline{W}_r + \overline{W}_d) = 0 \quad (\text{II.65})$$

where  $\overline{W}_m$ ,  $\overline{W}_r$  and  $\overline{W}_d$  are the averaged value, on a cycle basis, of the respective powers.

Under these conditions, the power adsorbed by the system (negative) is the driving power (positive) changed in sign and divided by the hydraulic motor total efficiency

$$\overline{W}_a = -\frac{\overline{W}_m}{\eta_T} = -\frac{\overline{C}\omega}{\eta_H \eta_M \eta_V} = -\Delta p \cdot V \quad (\text{II.66})$$

The main quote of this power is used for the cutting action ( $\overline{W}_r$ ), while the rest is dissipated ( $\overline{W}_d$ ) [8, 30]:

$$\overline{W}_a = \frac{\overline{W}_r}{\eta_T} + \frac{\overline{W}_d}{\eta_T} \quad (\text{II.67})$$

The dissipative power is mainly due to mechanism frictions, while secondly it is due even to the losses in cutting action and plant deflection and transportation [2, 46]. Neglecting the second kind of contribute in respect to the first one<sup>14</sup>, the dissipative power average value can be easily evaluated measuring the total power adsorbed by the system with nothing to cut (i.e. in *void working conditions*):

$$\overline{W}_a|_{R=0} = \frac{\overline{W}_d}{\eta_T} \quad (\text{II.68})$$

In this way, remembering equation (II.54) and applying a linear regression proceeding, an experimental measurement of the friction coefficient can be obtained.

Substituting then equation (II.66) into equation (II.67) and using equation (II.68), it becomes:

$$\overline{W}_r = -(\Delta p \cdot V + \overline{W}_a|_{R=0}) \cdot \eta_T \quad (\text{II.69})$$

<sup>14</sup> Even in the preceding Paragraph it has been tacitly neglected the second contribute. Indeed this contribute is generally highly lower than the first one, in case of grass and forage cutting [2], and it could be supposed to be even lower in case of larger shrubs.

## Models

where  $(\Delta p \cdot V)$  and  $\overline{W}_a|_{R=0}$  have opposite signs. Hence, the power quote effectively used for the cutting action, the *net cutting power* average value  $\overline{W}_r$ , can be easily evaluated measuring both the powers adsorbed in void and standard working conditions. Having this value, moreover, and remembering equations (II.11) and (II.53), the specific cutting energy  $E$  can be experimentally evaluated.



# III

## SENSITIVITY ANALYSIS

---



### III.1 INTRODUCTION

Using the characteristics of a common cutter bar and using standard working conditions, the equation of motion (II.57) has been numerically integrated<sup>15</sup>, obtaining the motion law and all the  $\vartheta$  dependent function trends in time.

Having these functions, the disequilibrium can be characterized in terms of any force contribution or even in terms of the overall forces and torques magnitudes and fluctuations in and around each direction. However, as it can be well understood from the equations in the preceding Chapter, these functions depend upon a lot of different factors. Hence, the variance of anyone of these factors implies a change in these functions and in their shapes so, finally, a change in the overall disequilibrium. To look at the disequilibrium modifications by means of changing the influencing parameter take the name of *sensitivity analysis*.

In this chapter, the sensitivity analysis has been conducted analyzing the variance of the most important functions with some of the cutter bar main operational parameters. The influencing parameters chosen are total filling coefficient  $p$  (estimated nominal at 16.67%), average rotational speed  $\omega$  (nominal at 31.40 rad s<sup>-1</sup>) and rotational inertia  $J_T$ , simulating different crank disc diameters  $D$  (nominal at 0.13 m). Then the influence of some other parameters has been investigated, such as conrod length  $l$  (nominal at 0.39 m) and clamping force  $F_s$  (estimated nominal at 500 N). The mentioned nominal values are obtained directly from the manufacturer and experimentally by the used cutter bar. The disequilibrium functions has been all analyzed under the variance of these parameters, but only the most influenced ones has been shown in the following, that are the rotational speed and the driving torque.

With the sensitivity analysis on the coefficient  $p$  it is possible to highlight what the differences are in motion shape and cutter bar disequilibrium while the cutter bar is working with more or less or even without shrubs. The latter is a useful case to observe the cutter bar's own disequilibrium, and to characterize the presence and the damping effect of shrubs during the work activity.

Moreover, the analysis based on the variation of the average rotational speed allows not only to individuate the optimal running speed by which the system minimizes the existing overall disequilibrium, but also to clarify the motion irregularity against such a variable resistance torque.

---

<sup>15</sup> For the code lists see Appendix B.

Finally, simulating different crank disc sizes it is possible to highlight the influence of the disc itself on the motion irregularity, obtaining useful information for the system design as well as from the analysis of others influencing factors like the conrod length.

### III.2 SENSITIVITY ANALYSIS RESULTS

In the following the motion law has been analyzed on the basis of a single cycle, i.e. one crank revolution, between the times  $t$  and  $(t + T)$ , where  $t$  is a general point in time and  $T$  is the cycle period in seconds. Each function has been then expressed and analyzed as a function of the normalized and dimensionless time  $\hat{t} = t/T$ , for comparison purposes. The analysis regards the variances in the trend of the rotational speed  $\dot{\vartheta}(\hat{t})$  and in the trend of the driving torque  $C(\hat{t})$ , while other  $\vartheta$  dependant functions are highlighted at the end of the Chapter.

#### III.2.1 Rotational speed trend in time

The motion law analysis points out, firstly, a periodic oscillatory time – shape for the rotational speed  $\dot{\vartheta}(\hat{t})$ , with period  $T$ , average value

$$\omega = \frac{1}{T} \int_t^{t+T} \dot{\vartheta}(t) dt \quad (III.1)$$

and discontinuities just in correspondence to the cutting resistance beginning and ending (Figure III. 1). This preliminary result bears out the initially assumed hypothesis of a non – uniform crank rotational speed.

The periodic trend of the rotational speed can be understood by looking better at the equation of motion. Indeed, assuming  $\delta(\vartheta) = \dot{\vartheta}(\vartheta)$ <sup>16</sup> equation (II.57) can be rewritten as

$$\left[ J_T + A(\vartheta) f^2(\vartheta) \right] \cdot \frac{dz(\vartheta)}{dt} \delta(\vartheta) + \left[ A(\vartheta) f(\vartheta) f'(\vartheta) \right] \cdot \delta^3(\vartheta) - k \cdot \delta^2(\vartheta) + B(\vartheta) \cdot \delta(\vartheta) = F(\vartheta) \quad (III.2)$$

that is an ordinary non – homogeneous nonlinear first order differential equation in  $\delta(\vartheta)$ , with  $\vartheta$  dependent coefficients. This change of variable can be made since the DOF  $\vartheta$  appears only by means of its first and second derivatives, other than in the multiplicative coefficients.

This change corresponds to considering an equivalent system, with  $\vartheta$  as independent variable and  $\delta(\vartheta)$  as unique DOF. Beneath this perspective, equation (III.2) represents the nonlinear

---

<sup>16</sup> The instantaneous rotational speed is represented here in function of the unique DOF  $\vartheta$  because of what has been written in Paragraph II.3.3.

## Sensitivity Analysis

forced vibration of the equivalent system, which vibrates in  $\delta(\vartheta)$  with the following forcing function:

$$F(\vartheta) = -\frac{D(\vartheta)A(\vartheta)}{m_T r^2} = -\frac{D(\vartheta)}{1 - \mu g(\vartheta)} = F(\vartheta, R(\vartheta)) \quad (\text{III.3})$$

with  $D(\vartheta)$  given by (II.60).

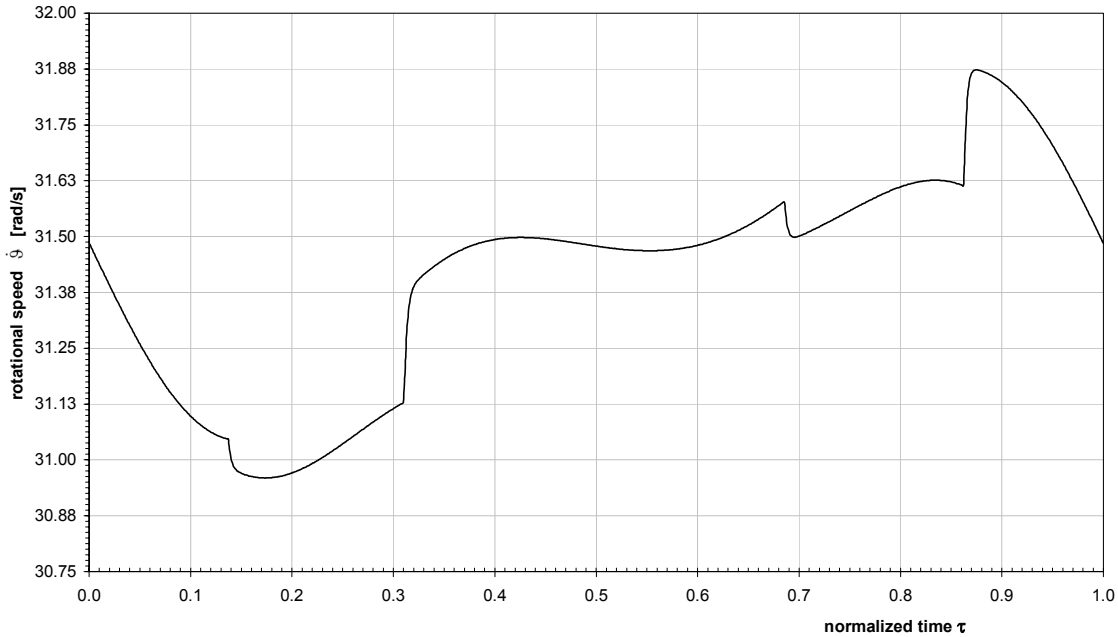


**Figure III. 1 – Rotational speed trend in function of the normalized time. Four points of discontinuity appear in correspondence of the cutting resistance beginning and ending, both for the case of forward and return strokes. For this assertion please compare figures at page 33.**

Hence, after a short transient in which  $\delta(\vartheta)$  (i.e. the rotational speed) follows the trend given by the general solution of the associated homogeneous equation, it enters in a periodic steady state given by the particular solution of equation (III.2).

As it is well known, this particular solution depends only upon the forcing function  $F(\vartheta)$ , that is a periodic function of  $\vartheta$  and, precisely, follows the trend of the cutting resistance  $R(\vartheta)$  somehow modified by the sine of  $\vartheta$ . Indeed, as it could be observed in Figure III. 1, the particular solution for the rotational speed has a periodic steady trend in which the cutting resistance peaks arise, smoothed and lightly modified by an overall sinusoidal baseline trend.

Furthermore, assuming the value of the average rotational speed  $\omega$ , the value of the forcing period  $T$  results from:

$$T = \frac{1}{\omega} \int_{\vartheta}^{\vartheta+2\pi} d\vartheta = \frac{2\pi}{\omega} \quad (\text{III.4})$$

that is the period of the rotational speed oscillatory trend too. From this, equation (III.1) is determined:

$$\omega = \frac{1}{T} \int_{\vartheta}^{\vartheta+2\pi} d\vartheta = \frac{1}{T} \int_t^{t+T} \frac{d\vartheta}{dt} dt = \frac{1}{T} \int_t^{t+T} \dot{\vartheta} dt \quad (\text{III.5})$$

A useful parameter to clarify the trend of  $\dot{\vartheta}(t)$  is the motion irregularity, commonly adopted for non-uniform rotational speed analysis and defined as the rotational speed maximum amplitude in percentage of its average value:

$$\phi_{\dot{\vartheta}} = \frac{(\dot{\vartheta}_{MAX} - \dot{\vartheta}_{MIN})}{\omega} \times 100 \quad (\text{III.6})$$

which is also calculated on the basis of a single cycle.

Figure III. 2 shows the changes in this shape for different total filling percentages. It can be clearly seen that, as it was expected to be, the higher is the percentage (i.e. the greater is the cutting resistance) the wider is the irregularity in motion, with consequently higher discontinuity (depressive) peaks. A secondary consequence is that, to face up to higher discontinuity peaks, and also to maintain the imposed<sup>17</sup> average speed value, the rotational speed values increase out of these depressive peaks.

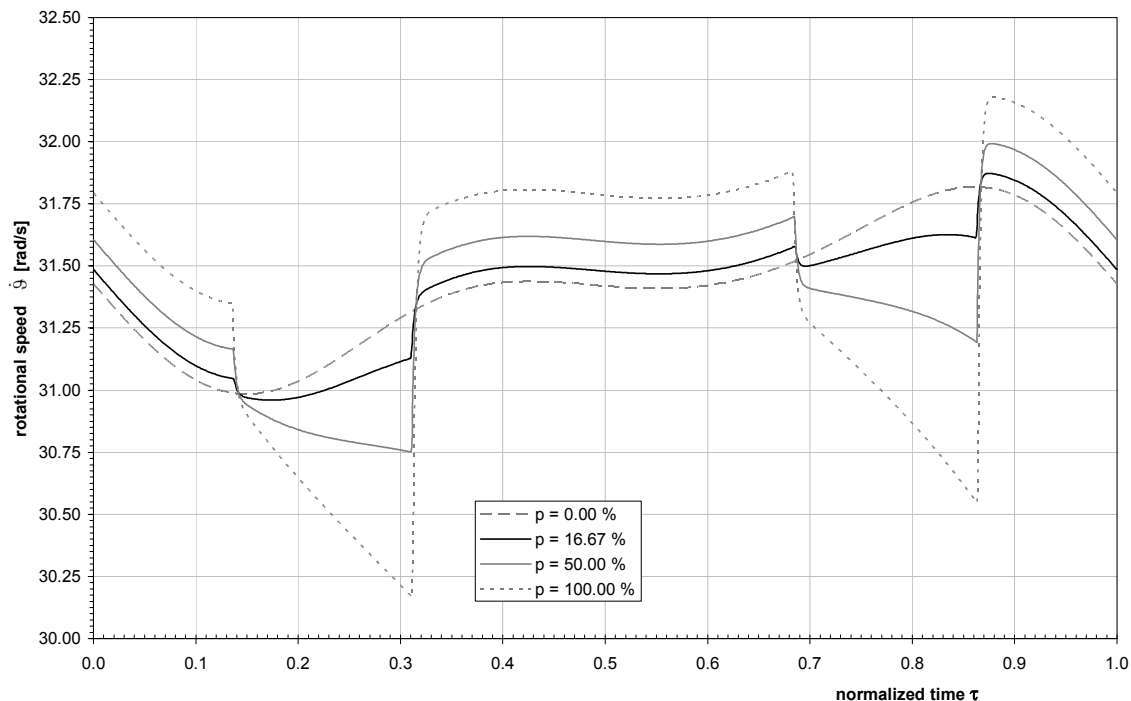


**Figure III. 2 – Rotational speed as a function of normalized time, for different values of filling percentage  $p$ .**

<sup>17</sup> The averaged value of the rotational speed is externally imposed by the tractor gas throttle (see note 11 at page 43).

## Sensitivity Analysis

With null cutting resistance ( $p = 0\%$ ) the motion irregularity  $\phi_{\dot{\vartheta}}$  is about 2.50%, that means the existence of a characteristic irregularity due to the implicit nature of the mechanism, while at the nominal working condition this irregularity is about 3%, increasing to 6.50% with total filling ( $p = 100\%$ ). So it can be seen that, under the nominal working conditions, the irregularity is mainly due to the system itself (in a quote of 2.50%) and only a little to the plant resistance  $R$  (0.50%).

The reason for the rotational speed to be so highly dependant upon the total filling percentage is due always to the forcing function (III.3), which is proportional to the following parameters:

$$F(\vartheta) \propto (p, z, E, \dot{x}_3, r, l, e) \quad (\text{III.7})$$

But while  $p$  and  $E$  can change instantaneously, the number of teeth  $z$ , forward speed  $\dot{x}_3$ , and crank radius  $r$  are unchangeable<sup>18</sup>.

Figure III. 3 shows the variance in rotational speed shape with different crank disc diameters. Here the analysis highlight that the influence of crank disc inertia on  $\dot{\vartheta}(\tau)$  is absolutely negligible with  $D$  less than once or even twice the nominal value, as it can be well seen from the figure zoom. Increasing the diameter further,  $\phi_{\dot{\vartheta}}$  reduces to 1% for  $D$  about four times the nominal one and it approximately disappears for  $D = 1.30$  m, i.e. ten times the commonly used diameter. Hence, the nominal crank disc ( $D = 0.13$  m) is clearly shown to be inefficient for motion regularization, while its presence begin to be useful for diameters in the orders of half a metre.

The reason for this crank disc influence is not explainable by looking at the forcing function  $F(\vartheta)$ . Indeed, an increase in the crank disc acts directly on the total inertia momentum  $J_T$ , increasing the inertia torque and making the rotational speed to be directly more uniform.

Finally, Figure III. 4 shows the variance in rotational speed shape for different values of the imposed average value  $\omega$ . To enable a comparison even with different absolute scales, the diagram represents the rotational speed percentage variation rather than the absolute value.

This speed percentage variation is defined as the instantaneous difference between the rotational speed and its average value, as a percentage of the average value itself

$$\Delta \dot{\vartheta}_{\%} = \frac{(\dot{\vartheta} - \omega)}{\omega} \times 100 \quad (\text{III.8})$$

<sup>18</sup> In the above analysis, the total filling percentage  $p$  can be easily replaced by the specific cutting energy  $E$ , being the forcing function directly proportional to both parameters and having them been assumed as constant but, actually, both variable instantaneously in time (see page 34, Paragraph II.2.2).

Moreover, while the forward speed is externally imposed, choosing a certain cutter bar it means to have a fixed number of teeth  $z$ , and having each tooth standard dimensions, even the crank radius is fixed, as the double of the tooth major base.

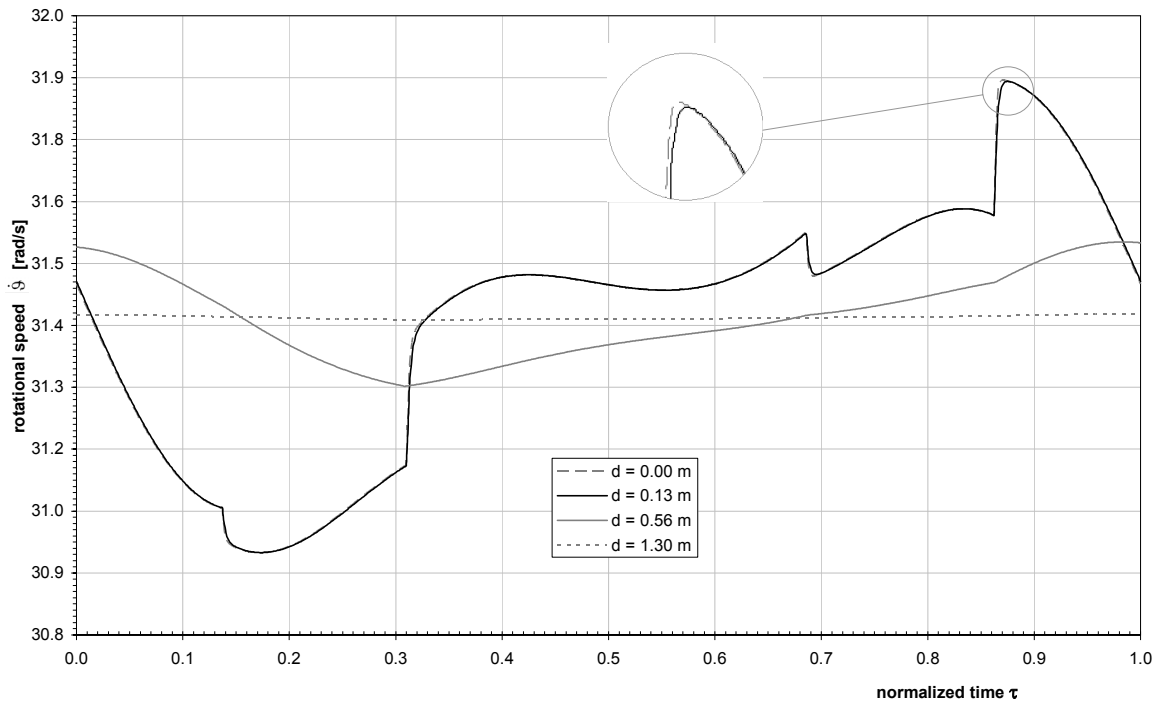


Figure III. 3 – Rotational speed as a function of normalized time, for different crank disc diameter values.

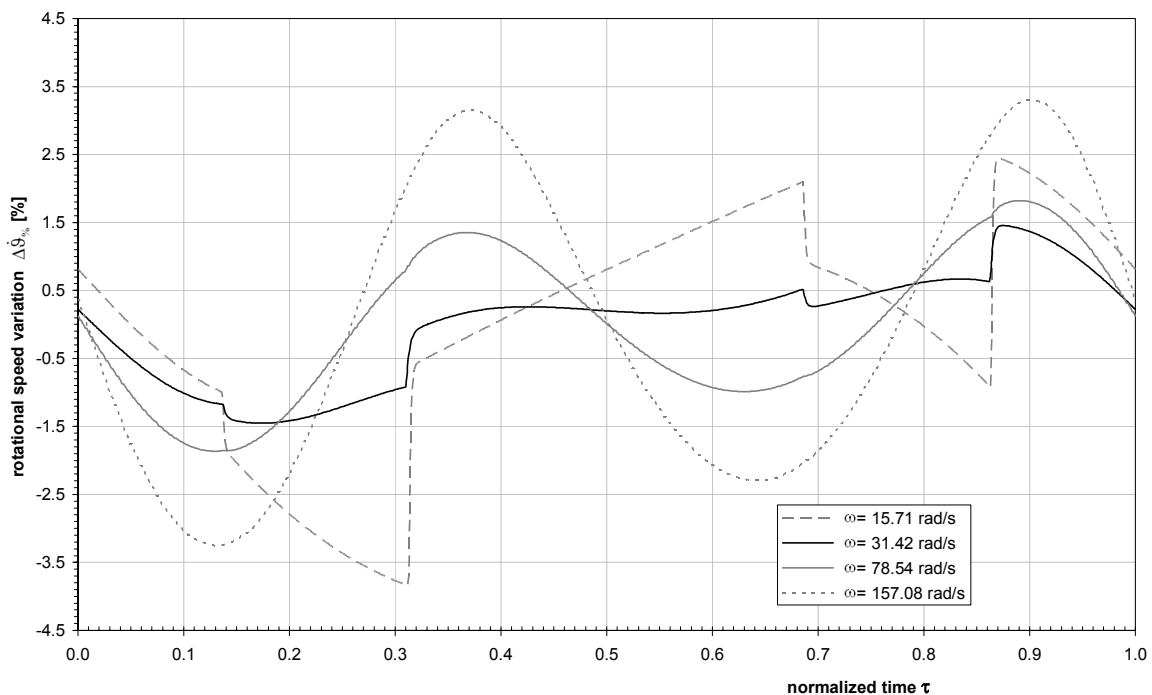


Figure III. 4 – Rotational speed variation as a function of normalized time, for different average running speeds. The speed percentage variation, has been used rather than the absolute speed for comparing scale.

Raising the average rotational speed from the value of  $15.71 \text{ rad s}^{-1}$  (150 rpm),  $\phi_{\dot{\theta}}$  firstly reduces to the minimum value of 2.50%, at an average speed of  $52.40 \text{ rad s}^{-1}$  (500 rpm) while, after this point of minimum,  $\phi_{\dot{\theta}}$  begins to increase proportionally to the average speed. This

## Sensitivity Analysis

means the existence of an optimum rotational speed, that is approximately 500 rpm but can be more accurately investigated, that minimizes the motion irregularity, as shown in Figure III. 4. Moreover, it has to be noticed that with an increase in the average speed value the fluctuation shape is gradually more smoothed, due to the fact that the cutting resistance  $R$  becomes increasingly negligible<sup>19</sup>.

### III.2.2 Driving torque trend in time

As it can be seen, the motion irregularity is not very pronounced. Anyway, as a consequence of this irregularity, the driving torque follows the same fluctuation, with a similar discontinuous and periodic trend over time, but with a really not-negligible fluctuation amplitude (Figure III. 5). This is important because, as it has been mentioned for the equilibrium equations analysis (Paragraph II.4), the driving torque makes the major and unavoidable contribution to the system unbalancing.

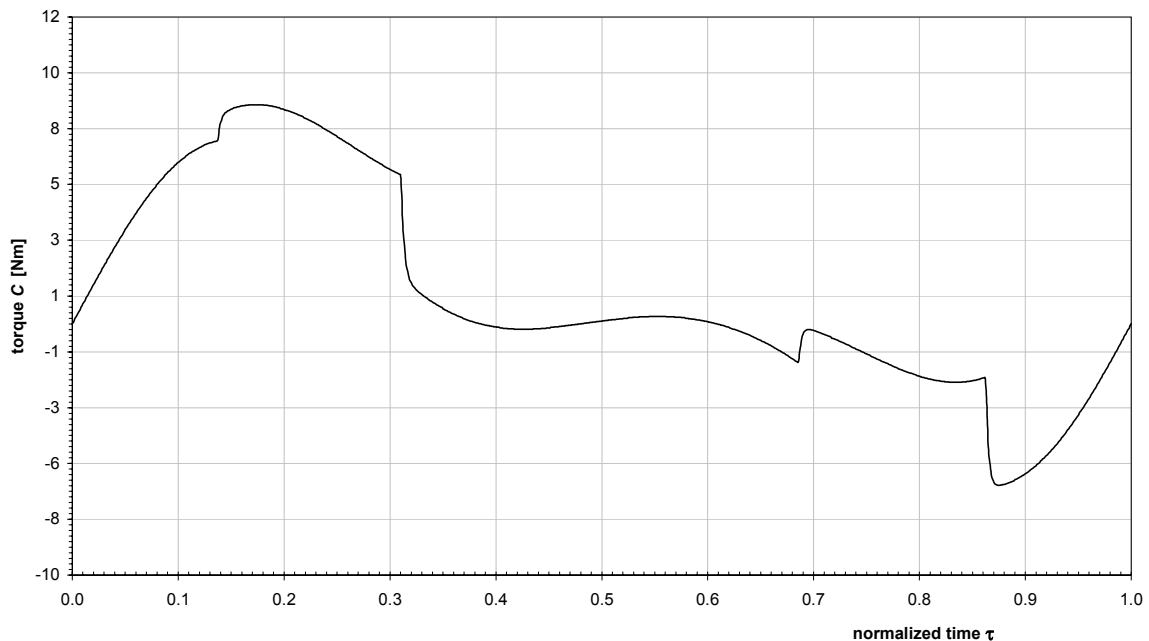


**Figure III. 5 – Driving torque as a function of normalized time. The trend is similar to the rotational speed one, being the torque recognized to be linearly dependent upon it.**

As a matter of fact, the torque trend in time can be qualitatively foreseen looking at the preceding diagrams, because of the driving torque has been recognized to depend linearly upon the instantaneous rotational speed (II.50), with  $k$  being a negative number and assumed to be constant.

<sup>19</sup> For this assertion please compare with Figure II. 5.

Hence, the driving torque also has a periodic oscillatory time – shape, with the same period  $T$  of the rotational speed and average value

$$\bar{C} = \frac{1}{T} \int_t^{t+T} C(t) dt \quad (\text{III.9})$$

Figure III. 6 shows the variance in driving torque with different filling percentages  $p$ . As before, two discontinuities appear in correspondence to the cutting resistance beginning and ending, yielding high torque irregularity with the filling percentage increase. Anyway, differently from before where the peaks intensity influenced the whole motion shape, it could be seen here that it doesn't happen. This happens because the torque average value is not externally imposed, but depends upon the resistance and inertia torques<sup>20</sup>, the main consequence being the torque average value itself increases with the filling percentage.

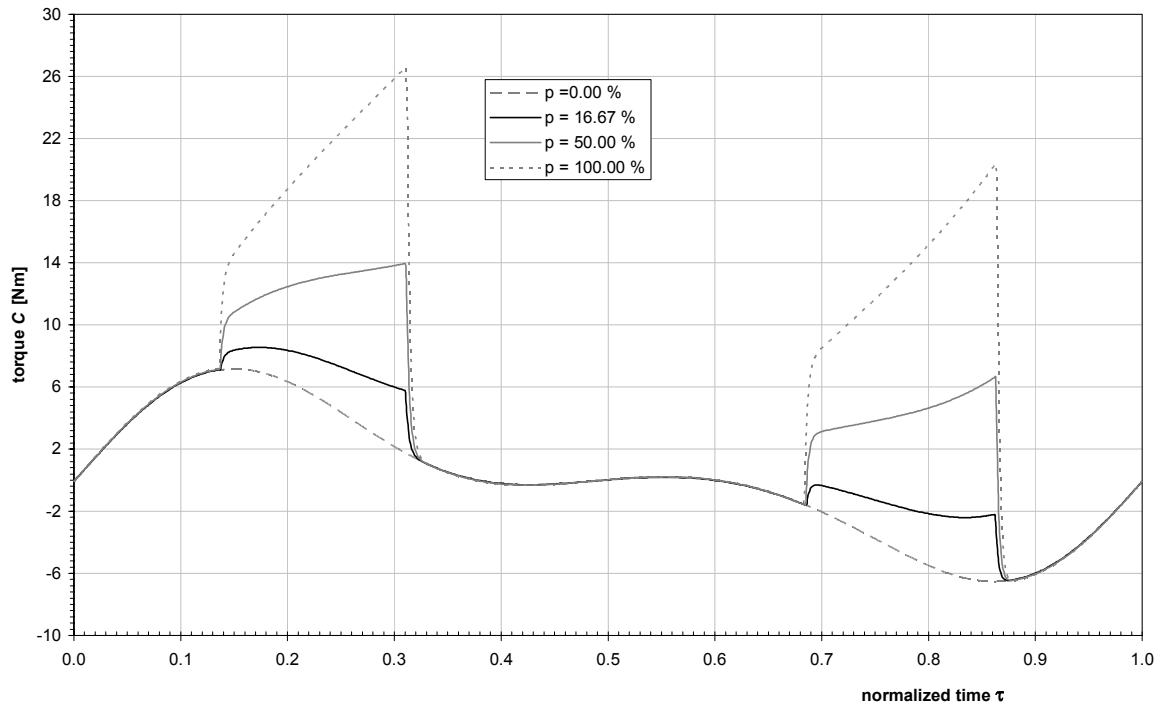


**Figure III. 6 – Torque as a function of normalized time, for different values of the filling percentage  $p$ .**

With a null cutting resistance the torque average value is about 3 Nm for the forward stroke and -2.80 Nm for the return one, almost but not null on the entire cycle only because of the friction and the inertia forces, with an overall fluctuation amplitude of about 13.70 Nm. These values characterize the cutter bar's own disequilibrium. The mentioned values increase respectively to 3.90 Nm, -1.80 Nm and 15 Nm under the nominal working condition and up to 8.50 Nm, 3.70 Nm and 33 Nm in the case of total filling.

<sup>20</sup> For this assertion please see note 11 at page 43.

## Sensitivity Analysis

Diagram of Figure III. 6, if used in conjunction with the hydraulic engine functional diagram  $C = C(\dot{\theta})$ , provides an important tool to avoid system's jams or breakings due to an overfilling. Indeed, knowing the plant characteristics  $\Delta p$  and  $Q$  (note 11 at page 43) the optimal and maximum torque values which can be supplied by the hydraulic motor are defined by the functional diagram. Hence, if the supposed filling percentage in working conditions leads to a driving torque peak values greater than the maximum provided by the plant, it could be foreseen the need of a more powerful plant, or the system risks to jam or break.

With a torque sensitivity analysis based on the variation of the crank disc diameter (Figure III. 7) it is possible to understand the usefulness of the crank disc inertia, as stated by other Authors [54]. The disc does not significantly influence the average value of the torque, either for the forward or return stroke, but has some effect on the torque overall shape and amplitude only when its value is very high. Under the nominal working conditions and with the commonly used diameter, the disc produces a totally negligible inertia torque for the driving torque smoothing, with a cycle peak about eight times higher than the average value. The nominal situation is practically like if there was no disc, as it is clearly highlighted by the figure zoom. The peak values diminish to three times the average torque for a diameter about four times the nominal one, until an approximately one to one proportion in the improbable case of a 1.30 m disc diameter.

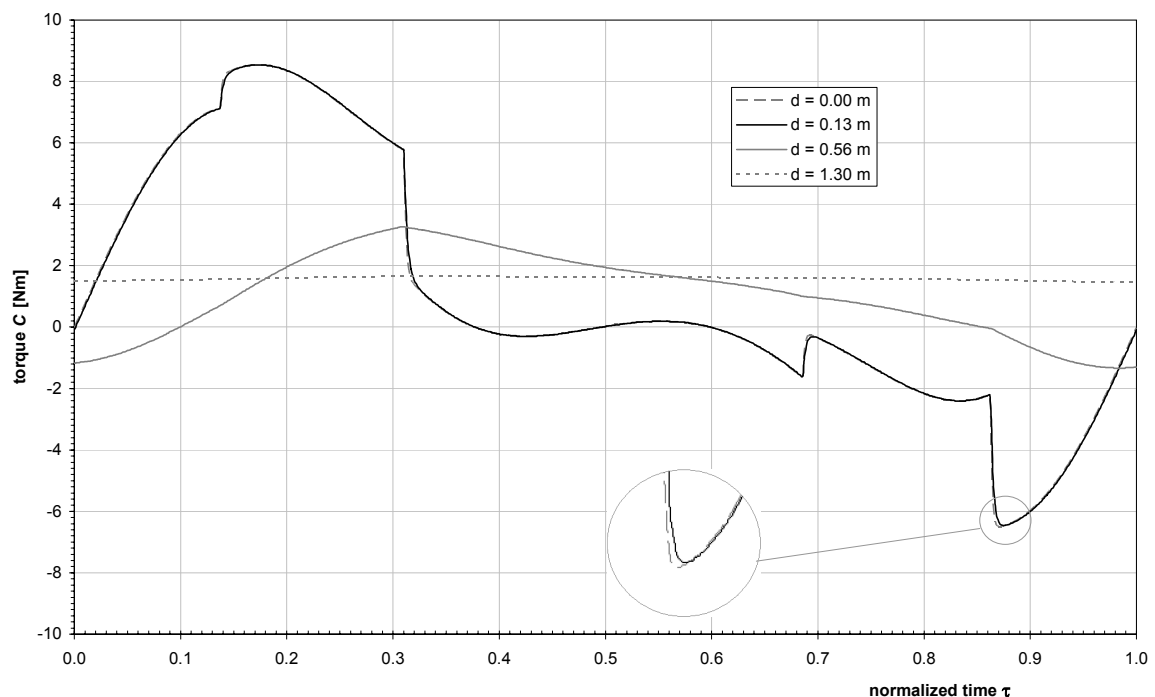
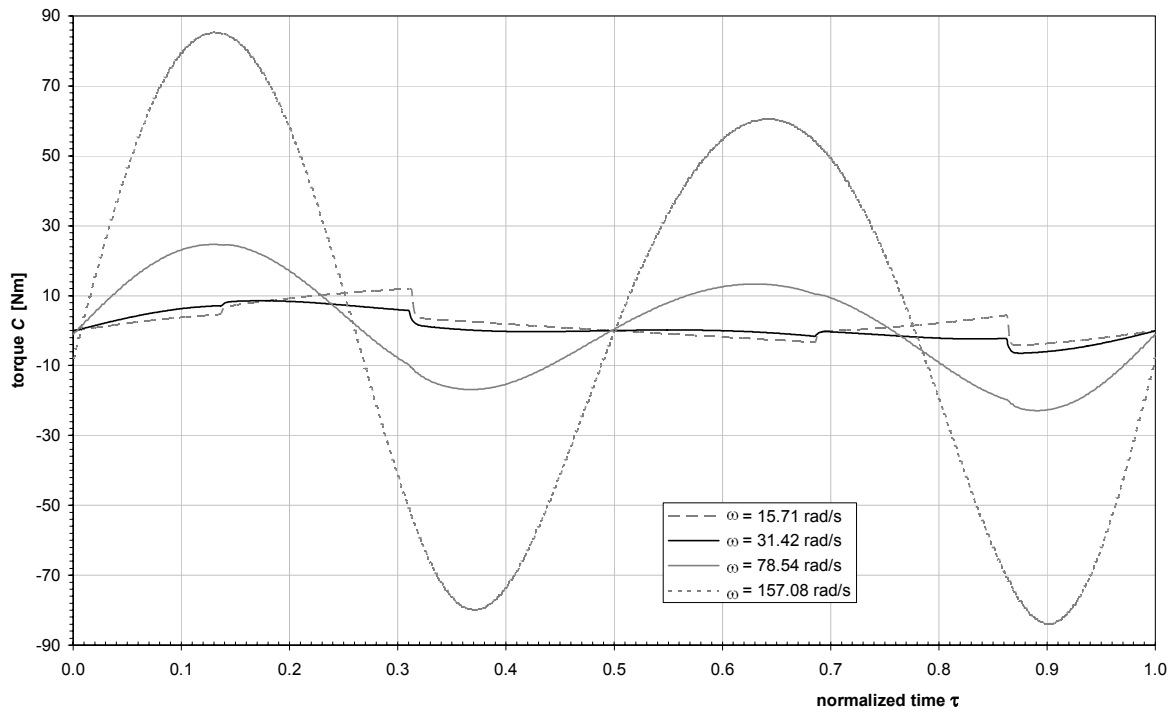


Figure III. 7 – Torque as a function of normalized time, for different crank disc diameters.

The disc ineffectiveness is mainly due to the really low average rotational speed, which is a particular characteristic of this kind of cutting system [30], while as it is well known the additive inertia carried by flywheels plays its role at high rotational speed. So, as it is shown in Figure III. 8 where the driving torque variance is analyzed in function of different running speeds, with an increasing average rotational speed the torque irregularity at first diminishes, because of the disc inertia increases its effect. Besides, raising further the rotational speed this effect overlaps with the pure average running speed effect, which tends to increase the driving torque peaks intensity, accordingly to equation (II.50). Consequently, with the nominal diameter even the torque fluctuation amplitude has a minimum value being near the average rotational speed of  $52.40 \text{ rad s}^{-1}$ . Raising further on the speed, the overall amplitude increases again and the discontinuities due to cutting resistance become increasingly smoothed.



**Figure III. 8 – Torque as a function of normalized time, for different average running speeds.**

The driving torque sensitivity analysis has also been conducted for variations in clamping force and conrod length values. In the former case, as it was expected to be, the torque increases with clamping force, but without changes to the overall shape and average value (Figure III. 9). This because the clamping force  $F_s$  appears in the equation of motion (III.2) only through the multiplicative coefficient  $B(\vartheta)$  and not in the forcing function  $F(\vartheta)$ . In addition, in the case of an increase in conrod length the torque fluctuation amplitude also slightly increases, clashing

## Sensitivity Analysis

with the common use of a longer conrod to better balancing the system (Figure III. 10), while the torque average value doesn't significantly change even doubling the conrod length.

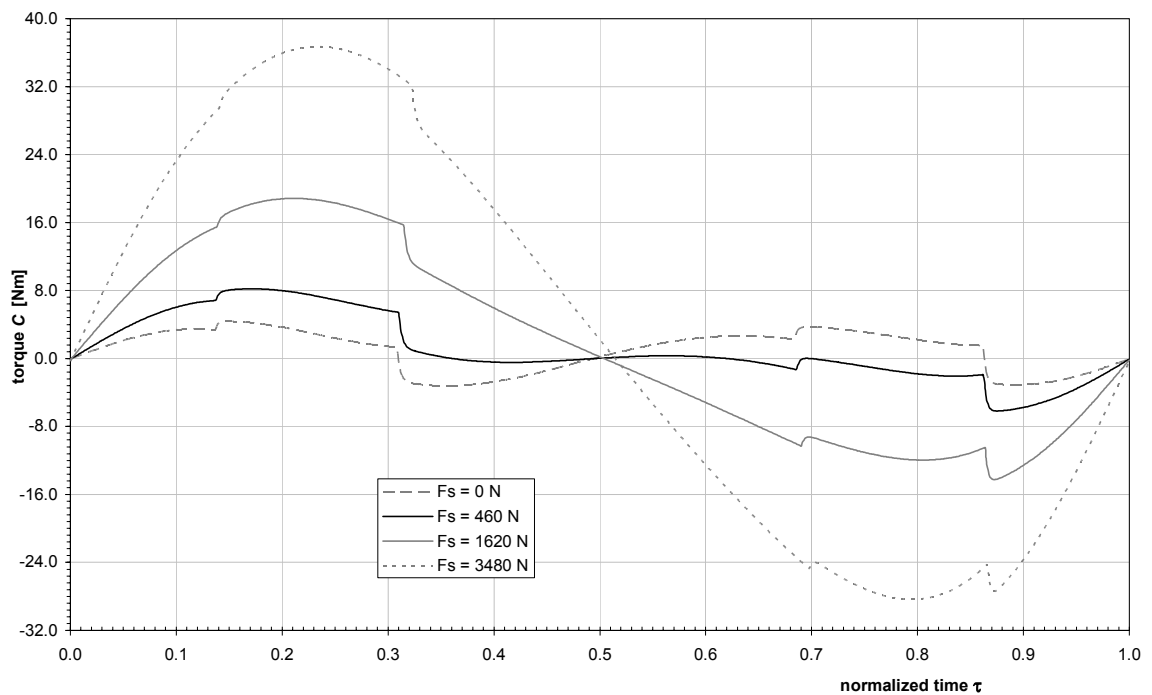


Figure III. 9 – Torque as a function of normalized time, for different values of clamping force  $F_s$ .

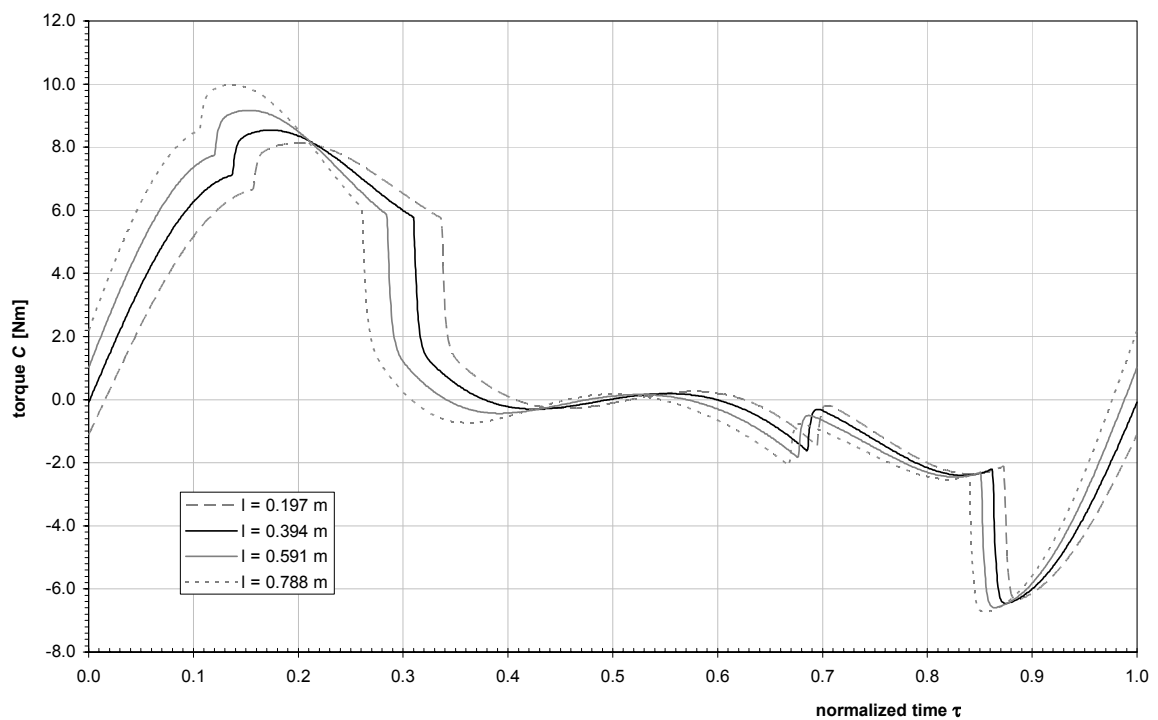


Figure III. 10 – Torque as a function of normalized time, for different values of conrod length  $l$ .

### III.2.3 Other functions trend in time

Another function that could be useful to analyze from a sensitivity point of view is the overall unbalancing torque  $T_3$  that lead to the rotational disequilibrium around the  $X_3$  axis (II.40):

$$T_3 = J_T \ddot{\vartheta} - C - m_T \ddot{x}_1 \cdot (x_{GL2} - x_{GS2}) \quad (\text{III.10})$$

As it could be seen from Figure III. 11, this function is practically not influenced by the variance of the crank disc inertia. While the contribute led by the driving torque  $C$  is influenced as shown in Figure III. 7, diminishing with the disc inertia increasing, and the torque due to the blade inertia  $-m_T \ddot{x}_1 \cdot (x_{GL2} - x_{GS2})$  is independent against changing in the disc inertia, the contribute led by the inertia torque  $J_T \ddot{\vartheta}$  compensates the variance of the first one, increasing proportionally to the disc inertia and leaving the overall torque practically unaltered.

This has a great importance, showing finally the total usefulness of the disc for the system balancing improvement.

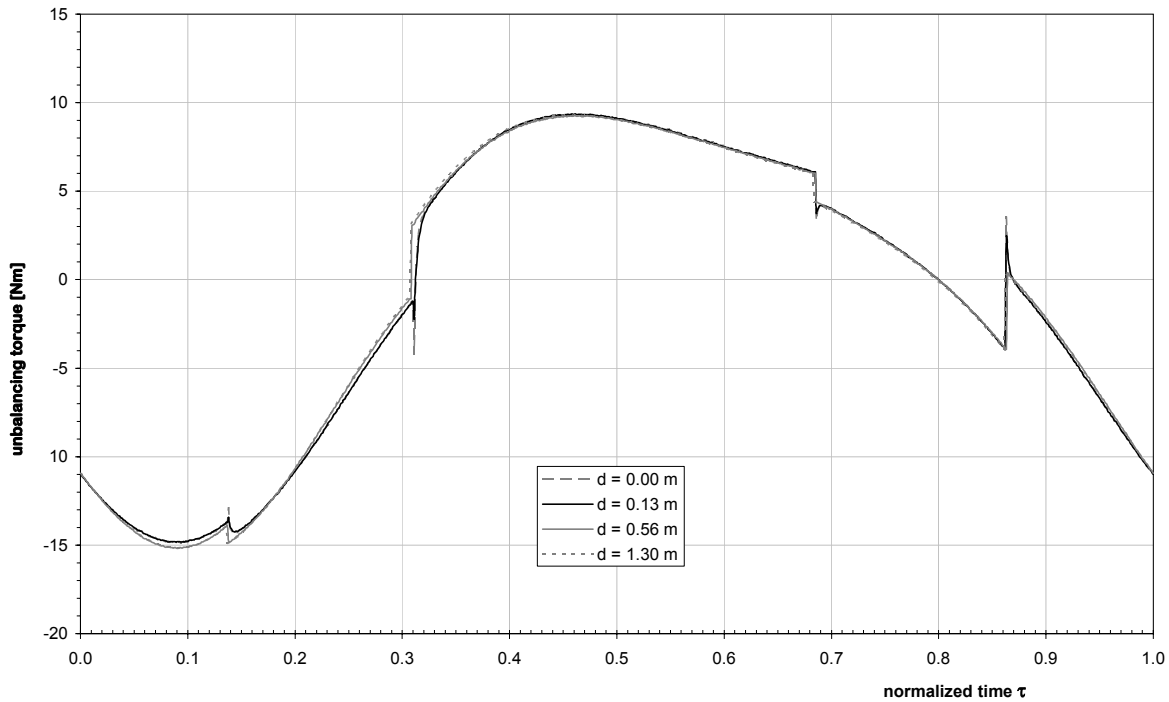


**Figure III. 11 – Resistance Torque  $T_3$  as a function of normalized time, for different crank disc diameters  $d$ .**

Considering the variance of the filling percentage coefficient  $p$ , moreover, the disequilibrium torque is influenced only because of the driving torque contribute and, indeed, it assumes the same shape over time, with the same kind of discontinuities (Figure III. 12).

## Sensitivity Analysis

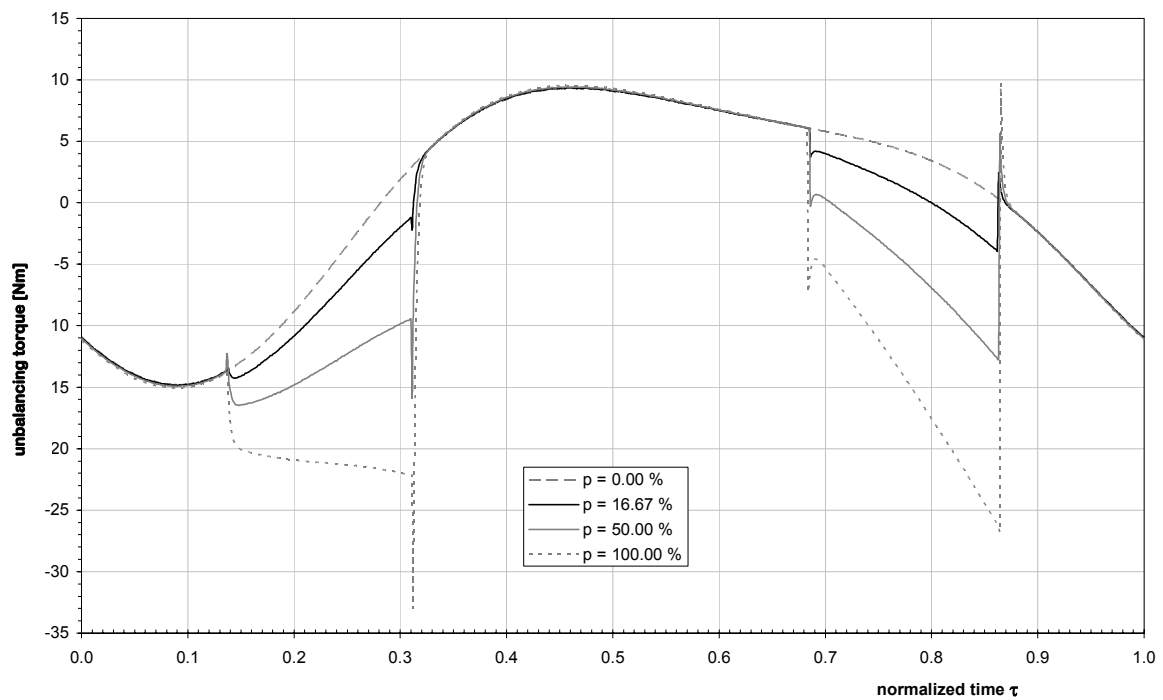


Figure III. 12 – Resistance Torque  $T_3$  as a function of normalized time, for values of the filling percentage  $p$ .

Finally, increasing the average running speed the amplitude of the disequilibrium torque fluctuation increase proportionally, being the torque due to the blade inertia increasingly important (Figure III. 13).

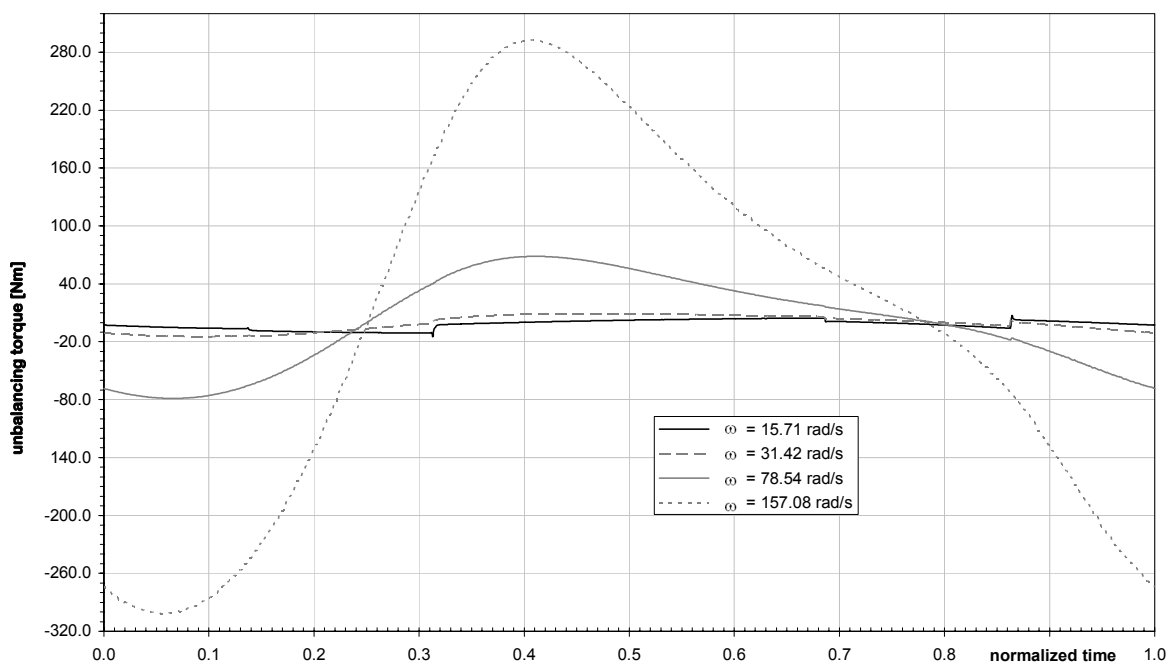


Figure III. 13 – Torque as a function of normalized time, for different average running speeds.



# IV ALTERNATIVE SOLUTION

---



IV.1 INTRODUCTION

As it has been shown in Paragraph II.3.3, the system works in a periodic running condition, with a not-constant rotational speed. Moreover, following what described in Paragraph II.4 let us analyze again the disequilibrium torque around the  $X_3$  direction, that is the right member of equation (II.40):

$$T_3 = J_T \ddot{\vartheta} - C - m_T \ddot{x}_1 \cdot (x_{GL2} - x_{GS2}) \quad (IV.1)$$

Neglecting the last term which could be geometrically avoided, using equation (II.24) the unbalanced torque becomes:

$$T_3 \approx J_T \ddot{\vartheta} - C = -F_c(\vartheta, \dot{\vartheta}, \ddot{\vartheta}) \cdot b(\vartheta) \quad (IV.2)$$

that is finally the resistance torque, strongly dependant on  $\vartheta$  and its derivatives, and with the trend represented in Figure IV. 1

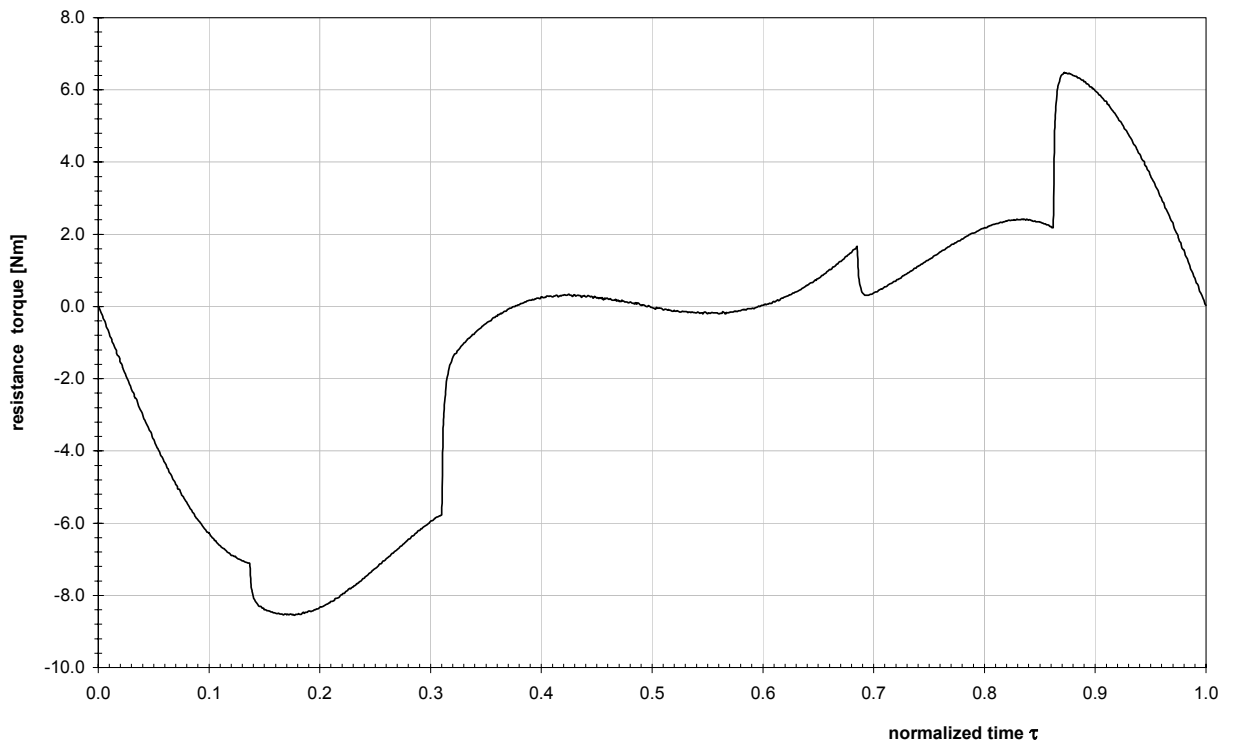


Figure IV. 1 – Resistance torque trend in function of the normalized time, standard conditions.

In other situations, like for internal combustion engines, the disequilibrium torque is represented exclusively by the driving torque, that make the chassis structure vibrate. Hence, commonly, the purpose is to regularize the driving torque, having the rotational speed as more uniform as possible, because of the existence of a direct correlation between driving torque and

rotational speed. A large flywheel is set on the engine output revolution axis, because the engine causes the disequilibrium, while the operating machine has to run uniformly [1, 25].

In the case here analyzed the situation is totally different. The disequilibrium is caused by the resistance torque and not by the driving one, because of the crank – conrod mechanism is here part of the operating machine, and not part of the engine. Hence, in this particular case it is totally useless to have a flywheel on the output axis of the hydraulic motor, because the motor itself is not the source of the disequilibrium.

Following the sensitivity analysis upon the crank disc diameter it could be thought that a larger diameter helps to reduce the disequilibrium, but it is not. Having a bigger flywheel instead of the standard one on the motor axis, make the rotational speed to be more uniform, the driving torque as well, but not the resistance torque that is the sum of driving torque and inertia torque.

With an increase in the flywheel diameter the resistance torque becomes slightly more uniform but greatly less than the driving one, because while both driving torque and rotational speed become more uniform, and hence the rotational acceleration decrease, the inertia term  $J_T$  increase significantly, making the resistance torque remain not uniform. Hence the disequilibrium remains even if the driving torque and the rotational speed are regularized with a large crank disc (Figure IV. 2).

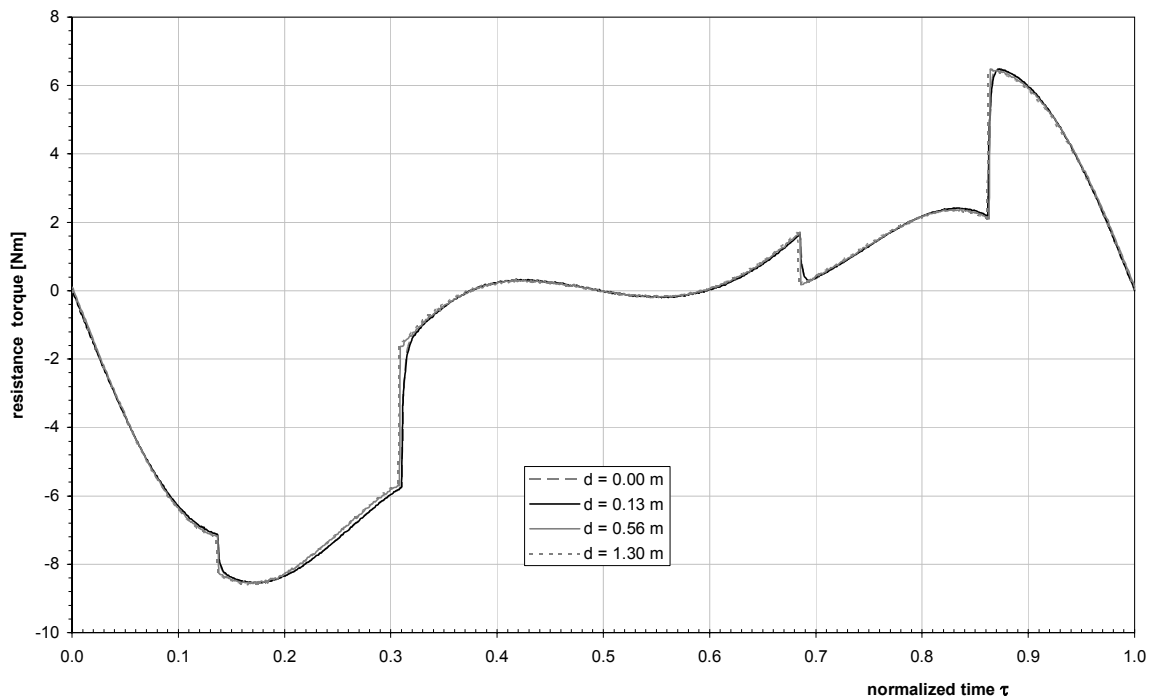


**Figure IV. 2 – Changes in the resistance torque trend in function of the crank disc diameter  $d$ . As it could be clearly seen, and differently from the driving one, the resistance torque is not influenced by the crank disc diameter.**

IV.2 ADDITIVE SHAFT WITH NON CIRCULAR GEARING

The basic principia on which the flywheel act is to introduce an additive (inertia) torque between the driving and the resistance torques [1, 25, 30]. In the following, on the same basic principia, an alternative solution is adopted to introduce an additive torque on the motor rotational axis, which makes use of a flywheel and a pair of non circular gears. But where the purpose was to regularize the driving torque, here it is to regularize the resistance one (Figure IV. 3).

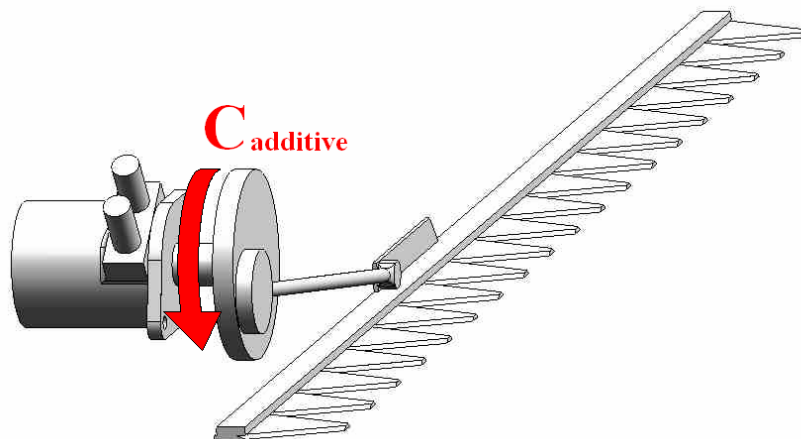


**Figure IV. 3 – An additive torque is introduced between the motor and the crank, with the purpose of regularize the resistance torque.**

Although variable radius gears are not very diffuse, they are essential for automatic equipment and other applications where there is not only a need for speed variation control during the working cycle, but also if a purely mechanical system is desired [17, 18].

Except for elliptical gears [6], until recently variable radius gears have been limited in their diffusion because of the production costs and because of the lack of generalized knowledge about production methodologies. Anyway, different and costless methodologies has been recently implemented for cylindrical gears cutting, like wire cutting, which has changed the prospective upon the non circular gears utilization even for cheap mechanisms [4, 50].

Therefore, the first goal has been here to establish a useful application for the non circular gearing on which basis the above mentioned additive torque could be supplied to regularize the resistance torque, the fundamental idea being to supply a cyclically variable additive torque by means of a cyclically variable gear ratio [18, 20, 21, 33, 41 and 57]. This application, anyway, had to be as less invasive as possible, so that the overall mechanism had not to be deeply modified in its own structure and its cost had presumably not to grow up too much.

After the application scheme has been developed, the gear design has to be realized on the basis of the single necessary condition of resistance torque regularization. From this condition

the gear ratio trend in time could be obtained, while the two gear pitch lines could be determined on the basis of the gear ratio and of geometrical constraints.

*IV.2.1 Arrangement description and gear ratio calculation*

Let us define the motor rotational axis as the primary shaft (1) and remove the crank disc, setting on its original position a non circular pinion gear [18, 20, 21 and 41]. Rewriting the rotational equilibrium around the  $X_3$  axis it is:

$$C + C_{ADD} - F_c \cdot b = J_1 \ddot{\vartheta} \tag{IV.3}$$

where  $J_1$  is the total inertia momentum of the primary shaft in the new configuration, with the pinion but without the disc, while  $C_{ADD}$  is an additive time-variable torque led through the pinion and such as the resistance torque becomes constant:

$$F_c \cdot b = C + C_{ADD} - J_1 \ddot{\vartheta} = \text{constant} \tag{IV.4}$$

The latter is the *functional equation* needed for the proceeding. This additive torque is supplied by a secondary parallel shaft (2), which carries a flywheel and a non circular driven gear which meshes with the primary shaft's pinion (Figure IV. 4).

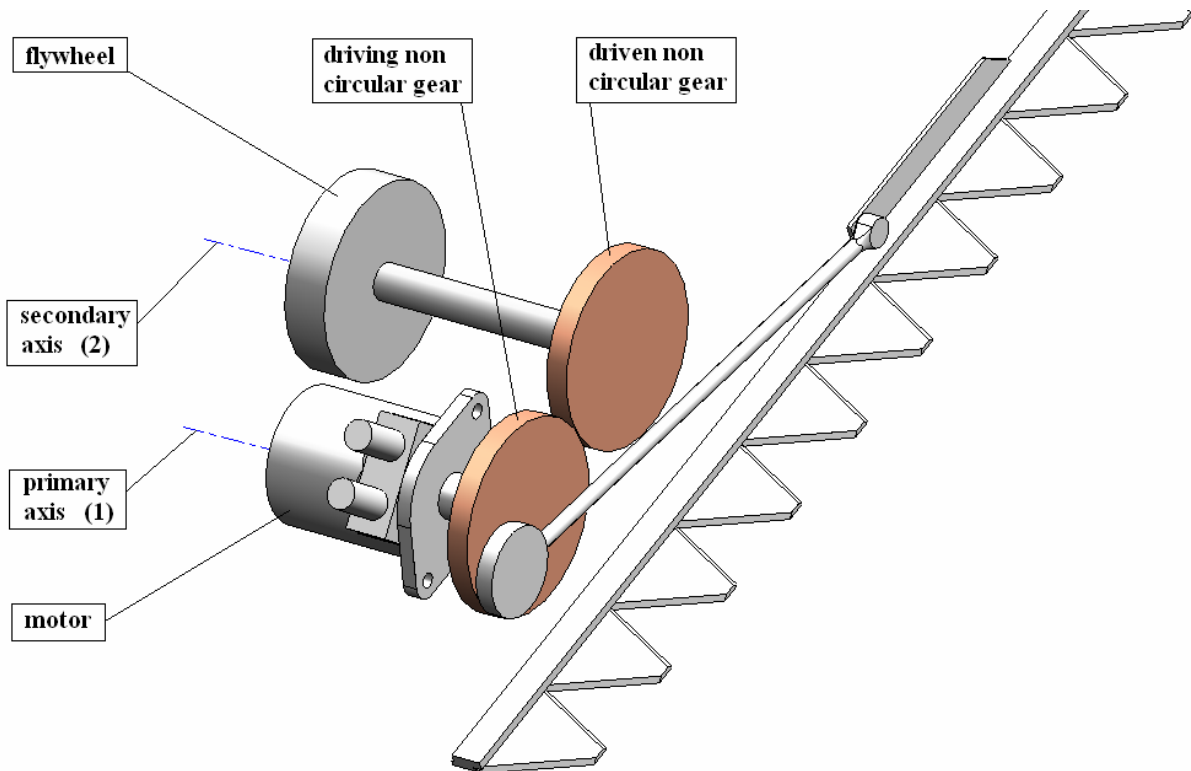


**Figure IV. 4 – Arrangement for the application of non circular gearing. The driving gear acts even as crank for the crank – conrod mechanism, while the secondary shaft carries both the driven non circular gear and the flywheel.**

## Alternative solution

In this way the additive torque is supplied between the driving one, provided by the motor, and the resistance one, provided through the crank – conrod mechanism. Writing the kinematic energy theorem for the secondary shaft:

$$W_{IN} + W_{OUT} = \frac{dE_2}{dt} \quad (IV.5)$$

where  $W_{IN}$  is the input power, adsorbed by the secondary from the primary shaft,  $W_{OUT}$  is the output power, supplied by the secondary to the primary shaft, while  $E_2$  is the kinematic energy of the secondary shaft. With the commonly adopted sign convention, the adsorbed power is positive while the supplied one is negative, so that the energy contents of the secondary shaft decreases (increases) when the power flows from it (from the primary shaft) to the primary shaft (to it). Anyway, the power exchange between the two shafts occurs only through the non circular gearing and hence the power cannot be adsorbed and supplied simultaneously. When the power is adsorbed it cannot be supplied, and vice versa. Hence, it can be written generally:

$$C_2 \cdot \dot{\vartheta}_2 = \frac{d}{dt} \left( \frac{1}{2} J_2 \dot{\vartheta}_2^2 \right) = J_2 \dot{\vartheta}_2 \ddot{\vartheta}_2 \quad (IV.6)$$

where  $C_2$ ,  $\dot{\vartheta}_2$  and  $J_2$  are respectively the torque, instantaneous rotational speed and total inertia momentum of the secondary shaft. It follows that

$$C_2 = J_2 \cdot \ddot{\vartheta}_2 \quad (IV.7)$$

Moreover, because of the power conservation between the meshed gears it is:

$$C_2 \cdot \dot{\vartheta}_2 = C_{ADD} \cdot \dot{\vartheta}$$

and hence, the additive torque supplied from the secondary to the primary shaft is

$$C_{ADD} = C_2 \cdot \frac{\dot{\vartheta}_2}{\dot{\vartheta}} = J_2 \ddot{\vartheta}_2 \tau(t) \quad (IV.8)$$

where  $\tau(t)$  is the time-variable gear ratio.

Equation (IV.4) is satisfied writing:

$$\frac{d}{dt} (F_c \cdot b) = 0 \quad (IV.9)$$

and so:

$$\frac{d}{dt} (C - J_1 \ddot{\vartheta} + J_2 \ddot{\vartheta}_2 \tau(\vartheta)) = 0 \quad (IV.10)$$

Let us analyze each term separately and write them in function of the DOF, its derivatives and in function of the gear ratio. From equation (II.50) it is:

$$\frac{d}{dt} C = k \cdot \ddot{\vartheta} \quad (IV.11)$$

while

$$\frac{d}{dt}(-J_1\ddot{\vartheta}) = -J_1\ddot{\ddot{\vartheta}} \quad (\text{IV.12})$$

where  $\ddot{\ddot{\vartheta}}$  is the rotational jerk of the primary shaft. Moreover it is:

$$\dot{\vartheta}_2 = \tau(t) \cdot \dot{\vartheta} \quad (\text{IV.13})$$

and hence the rotational acceleration and jerk of the secondary shaft are respectively:

$$\ddot{\vartheta}_2 = \frac{d}{dt}(\tau(t) \cdot \dot{\vartheta}) = \frac{d\tau}{dt} \cdot \dot{\vartheta} + \tau \cdot \ddot{\vartheta} \quad (\text{IV.14})$$

and

$$\frac{d\ddot{\vartheta}_2}{dt} = \ddot{\ddot{\vartheta}}_2 = \frac{d}{dt} \left( \frac{d\tau}{dt} \cdot \dot{\vartheta} + \tau \cdot \ddot{\vartheta} \right) = \frac{d^2\tau}{dt^2} \cdot \dot{\vartheta} + 2 \cdot \frac{d\tau}{dt} \cdot \ddot{\vartheta} + \tau \cdot \ddot{\ddot{\vartheta}} \quad (\text{IV.15})$$

So considering the last term of equation (IV.10):

$$\frac{d}{dt}(J_2\ddot{\vartheta}_2\tau) = J_2 \left( \ddot{\ddot{\vartheta}}_2 \cdot \tau + \ddot{\vartheta}_2 \cdot \frac{d\tau}{dt} \right) \quad (\text{IV.16})$$

and substituting it becomes:

$$\frac{d}{dt}(J_2\ddot{\vartheta}_2\tau) = J_2 \left( \dot{\vartheta} \cdot \frac{d^2\tau}{dt^2} \tau + 3\ddot{\vartheta} \cdot \frac{d\tau}{dt} \tau + \ddot{\vartheta} \cdot \tau^2 + \dot{\vartheta} \cdot \left( \frac{d\tau}{dt} \right)^2 \right) \quad (\text{IV.17})$$

Finally, introducing equations (IV.11, IV.12 and IV.17) into (IV.10) and collecting in respect of the DOF derivatives, it becomes

$$\left[ \frac{d^2\tau}{dt^2} \tau + \left( \frac{d\tau}{dt} \right)^2 \right] \cdot \frac{d\vartheta}{dt} + \left[ 3 \frac{d\tau}{dt} \tau + \frac{k}{J_2} \right] \cdot \frac{d^2\vartheta}{dt^2} + \left[ \tau^2 - \frac{J_1}{J_2} \right] \cdot \frac{d^3\vartheta}{dt^3} = 0 \quad (\text{IV.18})$$

that could be further simplified with a variable change. Naming

$$\frac{d\gamma}{dt} = \frac{d\tau}{dt} \tau \quad (\text{IV.19})$$

it is consequently:

$$\frac{d^2\gamma}{dt^2} = \frac{d^2\tau}{dt^2} \tau + \left( \frac{d\tau}{dt} \right)^2 \quad (\text{IV.20})$$

and the dimensionless substituting variable

$$\gamma = \int \frac{d\gamma}{dt} dt = \int \frac{d\tau}{dt} \tau dt = \frac{1}{2} \tau^2 \quad (\text{IV.21})$$

Substituting these quantities into equation (IV.18) it finally becomes:

## Alternative solution

$$\left[ \frac{d\vartheta}{dt} \right] \cdot \frac{d^2\gamma}{dt^2} + \left[ 3 \frac{d^2\vartheta}{dt^2} \right] \cdot \frac{d\gamma}{dt} + \left[ 2 \frac{d^3\vartheta}{dt^3} \right] \cdot \gamma = \frac{J_1}{J_2} \cdot \frac{d^3\vartheta}{dt^3} - \frac{k}{J_2} \cdot \frac{d^2\vartheta}{dt^2} \quad (\text{IV.22})$$

Moreover, the application of a secondary shaft parallel and geared to the primary one doesn't introduce any change in the equation of motion. Indeed, the kinematic energy theorem (II.51) for the whole system becomes:

$$W_m + W_r + W_d + W_{ADD} = \frac{dE}{dt} + \frac{dE_2}{dt} \quad (\text{IV.23})$$

where  $W_{ADD}$  is the additive power given to the system by the secondary shaft

$$W_{ADD} = C_2 \cdot \dot{\vartheta}_2 \quad (\text{IV.24})$$

But remembering equation (IV.6) and simplifying, it is finally again:

$$W_m + W_r + W_d = \frac{dE}{dt} \quad (\text{IV.25})$$

That leads to the same equation of motion that has been developed in Paragraph II.3.3 with the only change in the new value of the total inertia momentum of the primary shaft:

$$\begin{aligned} & \left[ J_1 + A(\vartheta) f^2(\vartheta) \right] \cdot \left( \frac{d^2\vartheta}{dt^2} \right) \left( \frac{d\vartheta}{dt} \right) + \left[ A(\vartheta) f(\vartheta) f'(\vartheta) \right] \cdot \left( \frac{d\vartheta}{dt} \right)^3 - k \cdot \left( \frac{d\vartheta}{dt} \right)^2 + B(\vartheta) \cdot \left( \frac{d\vartheta}{dt} \right) + \\ & + (D(\vartheta)A(\vartheta))/m_T r^2 = 0 \end{aligned} \quad (\text{IV.26})$$

Functional equation (IV.22) together with the new equation of motion (IV.26), that is the constitutive equation, forms an ordinary non-linear and non-homogeneous differential equation system, with  $\vartheta$  – dependent coefficients, that is of second order in respect of  $\gamma(t)$  and of third order in respect of  $\vartheta(t)$ . The solution of this equation is the gear ratio trend in time (IV.21)

$$\tau = \sqrt{2\gamma} \quad (\text{IV.27})$$

and the new (practically unchanged) motion law of the primary shaft.

Because of what mentioned in Paragraph II.3.3, every quantity that appears in these expressions depends only upon the DOF  $\vartheta$ . As a consequence, always under deterministic conditions, even the function  $\gamma$  and so the gear ratio have to have the same dependence

$$\tau = \tau(\vartheta) = \sqrt{2\gamma(\vartheta)} \quad (\text{IV.28})$$

and a periodic trend with period  $T = 2\pi/\omega$ <sup>21</sup>. Hence the secondary shaft has a periodic motion too.

<sup>21</sup> Please refer to equation III.1.

Since the gear ratio  $\tau$  is absent from the new equation of motion (IV.26) and the DOF  $\vartheta$  is absent from the functional equation (IV.22)<sup>22</sup>, it is now clear that the trend of  $\vartheta(t)$  is not influenced by the presence of the secondary shaft and by the non circular gearing. It can be said that the two variables are directly de-coupled.

Hence, because of the particular application and because of the procedure by which it has been obtained, it is the gear ratio trend that follows the motion law by means of the rotational speed, acceleration and jerk trends in time, in a way such as to satisfy the functional equation and hence to annihilate the resistance torque variance, with the aid of the secondary shaft inertia.

The only change in the motion law, in respect to the shape analyzed in Chapter III, is due to the absence of the disc and its substitution with the gear pinion.

#### IV.2.2 Generation of variable radius pitch lines

Both the two non circular gear pitch lines can be obtained from the functional equation together with respecting a series of geometrical and kinematic constraints [18, 57]. The first condition regards the wheelbase satisfaction, i.e. the distance between the two gear axes must be constant and equal to a certain given value at any instant:

$$R_1(\vartheta) + R_2(\vartheta_2(\vartheta)) = \Delta \quad (\text{IV.29})$$

where  $\Delta$  is the (constant) wheelbase value while  $R_1(\vartheta)$  and  $R_2(\vartheta_2(\vartheta))$  are corresponding values of respectively the primary and secondary gear radii. The second condition regards the gearing mesh continuity, that means at any rotation of the primary shaft pitch line it has to correspond a rotation of the secondary one. This condition has to be satisfied independently from the two pitch lines overall lengths, so reasoning for infinitesimal quantities it is:

$$ds_1 = ds_2 \quad (\text{IV.30})$$

where  $ds_i$  represent the arc length, on the  $i$  – shaft, of the pitch line movement, that is:

$$R_1(\vartheta)d\vartheta = R_2(\vartheta_2(\vartheta))d\vartheta_2 \quad (\text{IV.31})$$

This means, as well, the absence of sliding between the two gears.

However, it is clear that in order to obtain a not only continuous but also periodic variation of the gear ratio  $\tau(\vartheta)$ , the ratio between the lengths of the two pitch lines must be a rational number. Hence, the gear ratio average value  $\bar{\tau}$ , evaluated on the basis of a single cycle of period  $T$ , has to be an integer number too. As a consequence, each tooth will mesh always with another tooth, or with a fixed number of teeth if  $\bar{\tau}$  is greater than 1. That is, at any angle  $\vartheta$  will

---

<sup>22</sup> It is present but only by means of its first and second derivatives.

Alternative solution

correspond to a specific radius or a fixed number of radii of the secondary gear, this number depending upon the gear ratio average value itself.

Hence, imposing the gear ratio average value to be an integer number

$$\int_{\vartheta}^{\vartheta+2\pi} \tau(\vartheta) d\vartheta = 2\pi q \quad (IV.32)$$

where  $q$  is integer. Hence, it means

$$\bar{\tau} = \frac{1}{2\pi} \int_{\vartheta}^{\vartheta+2\pi} \tau(\vartheta) d\vartheta = q \quad (IV.33)$$

And the two above conditions become:

$$R_1(\vartheta) + R_2(\vartheta) = \Delta \quad (IV.34)$$

$$R_1(\vartheta) d\vartheta = R_2(\vartheta) d\vartheta_2 \quad (IV.35)$$

But since

$$\tau(\vartheta) = \frac{\dot{\vartheta}_2}{\dot{\vartheta}} = \frac{d\vartheta_2}{dt} \frac{dt}{d\vartheta} = \frac{d\vartheta_2}{d\vartheta} \quad (IV.36)$$

from condition (IV.35) it is

$$\frac{R_1(\vartheta)}{R_2(\vartheta)} = \frac{d\vartheta_2}{d\vartheta} = \tau(\vartheta) \quad (IV.37)$$

and substituting into condition (IV.34) it is

$$R_2(\vartheta) = \frac{\Delta}{1 + \tau(\vartheta)} \quad (IV.38)$$

and consequently again from condition (IV.35) it is:

$$R_1(\vartheta) = \frac{\Delta \tau(\vartheta)}{1 + \tau(\vartheta)} \quad (IV.39)$$

The two radii obtained above describe the pitch lines of a non circular gear pair that is able to generate the prescribed motion law and additive torque, which annihilate the resistance torque variance as needed.

### IV.2.3 Other constraints

Some observation has still to be marked about the constraints that have to be satisfied other than what already assumed and imposed.

The first assumption was the periodic trend of  $\tau$ , which descend directly from the fact that  $\tau$  must be a function of the solely DOF. The satisfaction of this fundamental condition is implicitly guaranteed by equation system (IV.22, IV.26), because all the coefficients involved in this system are  $\vartheta$  – dependent. Moreover, the only three constraints imposed were the

integer value for the average gear ratio  $\bar{\tau}$  (IV.33), the constancy of the wheelbase  $\Delta$  (IV.34) and the meshing continuity (IV.35)

Anyway, some other constraints are important for the good design of the gear pair. First of all, it is necessary the two pitch lines to be both closed geometries, always to guarantee the continuity of motion. But while the closeness constraint upon the driving gear is obviously guaranteed by the periodicity of the DOF itself, the pitch closeness for the driven gear can be expressed by the following boundary condition:

$$\begin{cases} \vartheta_2(\vartheta(t_0)) = \vartheta_{20} \\ \vartheta_2(\vartheta(t_0) + 2q\pi) = \vartheta_2(2z\pi) = \vartheta_{20} + 2q\pi \end{cases} \quad (\text{IV.40})$$

where  $t_0$  is an arbitrary point in time. But as it has been said, the driven gear angle of rotation  $\vartheta_2$  depends only upon the DOF  $\vartheta$  and hence, always because of its periodicity,  $\vartheta_2$  is periodic as well. Hence, by the assumption of periodicity for  $\tau$  the constrain equation (IV.40) is also satisfied.

In the same way, this assumption of periodicity guarantees also the continuity (and differentiability up to the second order) for the driven gear angle of rotation  $\vartheta_2$ , essential conditions for the smoothness of running. In fact, while this condition upon the driving gear angle of rotation is guaranteed by the integrability of the motion law, the same condition upon the driven gear could be written as

$$\begin{cases} \left. \frac{d\vartheta_2}{d\vartheta} \right|_{\vartheta(t_0)} = \left. \frac{d\vartheta_2}{d\vartheta} \right|_{\vartheta(t_0) + 2q\pi} \\ \left. \frac{d^2\vartheta_2}{d\vartheta^2} \right|_{\vartheta(t_0)} = \left. \frac{d^2\vartheta_2}{d\vartheta^2} \right|_{\vartheta(t_0) + 2q\pi} \end{cases} \quad (\text{IV.41})$$

and remembering (IV.37):

$$\begin{cases} \tau(\vartheta(t_0)) = \tau(\vartheta(t_0) + 2q\pi) \\ \left. \frac{d\tau(\vartheta)}{d\vartheta} \right|_{\vartheta(t_0)} = \left. \frac{d\tau(\vartheta)}{d\vartheta} \right|_{\vartheta(t_0) + 2q\pi} \end{cases} \quad (\text{IV.42})$$

These two equations represent respectively the periodicity and first derivability of the gear ratio, in respect to  $\vartheta$ . While the first one is clearly satisfied by the assumption of periodicity for  $\tau$ , the second one needs some explanations. This equation could be rewritten as:

$$\left. \left( \frac{d\tau(\vartheta)}{dt} \cdot \frac{dt}{d\vartheta} \right) \right|_{\vartheta(t_0)} = \left. \left( \frac{d\tau(\vartheta)}{dt} \cdot \frac{dt}{d\vartheta} \right) \right|_{\vartheta(t_0) + 2q\pi} \quad (\text{IV.43})$$

that is:

Alternative solution

$$\left. \frac{\dot{\tau}}{\dot{\vartheta}} \right|_{\vartheta(t_0)} = \left. \frac{\dot{\tau}}{\dot{\vartheta}} \right|_{\vartheta(t_0)+2q\pi} \quad (\text{IV.44})$$

This equation is satisfied always by the periodicity of  $\tau$ , which implies the periodicity of its first derivative  $\dot{\tau}$ , and by the periodicity of  $\vartheta$  too, which as seen implies the periodicity of its first derivative  $\dot{\vartheta}$ .

Hence any other important condition is implicitly satisfied by the three imposed constraint together with the assumption of periodicity for  $\tau$ .

Last but not least, the pitch lines mustn't contain reverse portions, to avoid retrograde motion for the driven gear. This condition is satisfied by imposing the gear ratio function to be positive everywhere upon its domain:

$$\tau(\vartheta) > 0 \quad \forall \vartheta \quad (\text{IV.45})$$

Moreover to have a sort of uniformity in the gear dimensions, and for limiting the system overall dimensions, it is helpful if  $\bar{\tau}$  is not too far from the unity.

### IV.3 SOLUTION APPLICATION IN VOID WORKING CONDITIONS

The alternative solution above analyzed was numerically applied using the characteristics of a specific cutter bar case study<sup>23</sup>. For this purpose, equations (IV.22) and (IV.26) were numerically integrated (see Appendix C) in the special case of void working conditions [34]. The boundary conditions was the values of the gear ratio at the minimum and maximum values of the integration time, chosen in a way such as the averaged one results to be integer, together with the two values of the rotational speed, assumed to be equal to the rotational speed average value as well as in Paragraph II.3.3.

The choice to design the solution in the special case of void working conditions is due to the fact that the cutting resistance assumed here for the analysis is a model. And, as it has been said, this is a qualitative model, useful for understanding the unbalance and the system behavior. But, this model influences the motion law greatly, as it could be seen form the figures in Paragraph III.2.1. Consequently, because of the gear profiles derive directly from the motion law together with the imposed functional condition, it would not be useful to have a gear profiles that reflect exactly a qualitative cutting resistance model, which has been supposed not to be directly comparable with the real trend of the cutting resistance.

---

<sup>23</sup> The same specific cutter bar case study adopted for the analysis of the equation of motion has been used.

Hence, the gears was designed to annihilate the unbalancing torque without any shrub under cut while, subsequently, the benefit introduced even in standard working conditions was evaluated.

#### IV.3.1 Gear profiles and discussion

The gear pitch line profiles obtained numerically are shown in Figure IV. 5, where the scale is in metres. The solution presented is set for a unitary average gear ratio, and for a secondary shaft inertia momentum equivalent to the standard primary one (i.e. the standard crank disc is used as flywheel but on the secondary shaft).

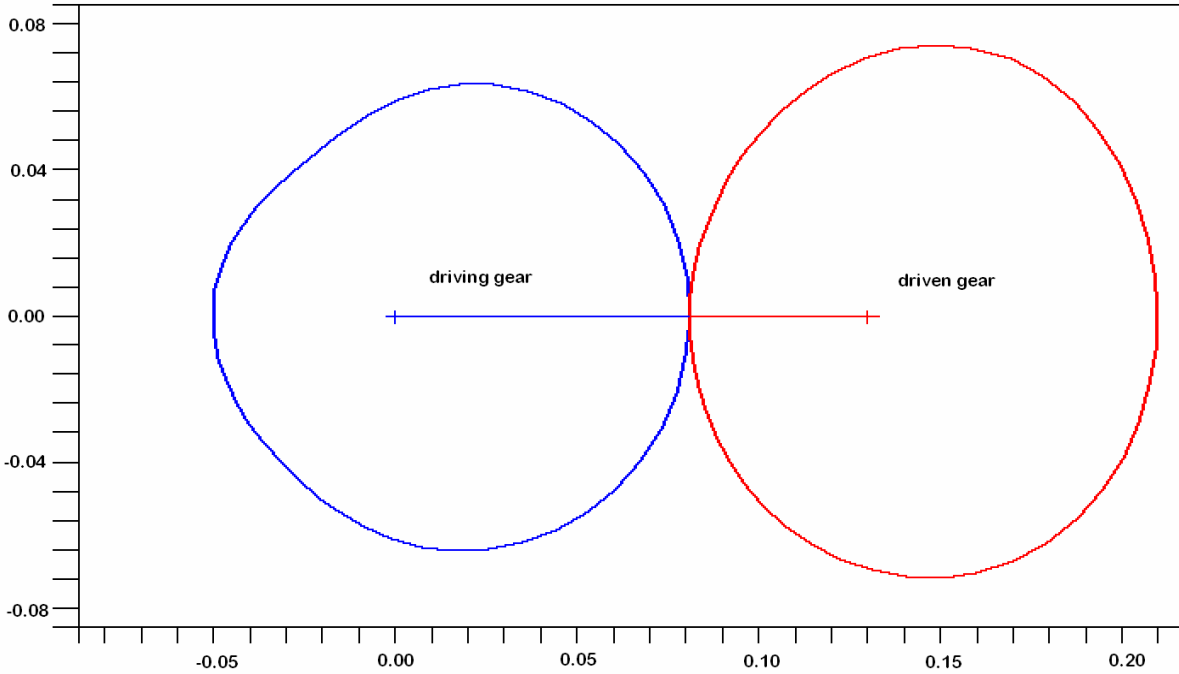


**Figure IV. 5 – Non circular gear pitch lines profile.**

It has to be noticed that the gear ratio, and hence even both the pitch line profiles, depend on the motion law  $\vartheta(t)$ , independently defined, on the primary and secondary inertia momentums  $J_1$  and  $J_2$  and on the motor stiffness  $k$ , (IV.22):

$$\left[ \frac{d\vartheta}{dt} \right] \cdot \frac{d^2\gamma}{dt^2} + \left[ 3 \frac{d^2\vartheta}{dt^2} \right] \cdot \frac{d\gamma}{dt} + \left[ 2 \frac{d^3\vartheta}{dt^3} \right] \cdot \gamma = \frac{J_1}{J_2} \cdot \frac{d^3\vartheta}{dt^3} - \frac{k}{J_2} \cdot \frac{d^2\vartheta}{dt^2} \quad (\text{IV.46})$$

This differential equation can be rewritten as:

$$\left[ \dot{\vartheta} \right] \cdot \frac{d^2\gamma}{dt^2} + \left[ 3 \frac{d\dot{\vartheta}}{dt} \right] \cdot \frac{d\gamma}{dt} + \left[ 2 \frac{d^2\dot{\vartheta}}{dt^2} \right] \cdot \gamma = \frac{J_1}{J_2} \cdot \frac{d^2\dot{\vartheta}}{dt^2} - \frac{k}{J_2} \cdot \frac{d\dot{\vartheta}}{dt} \quad (\text{IV.47})$$

## Alternative solution

where the DOF  $\vartheta$  doesn't appear anymore. This is, precisely, an ordinary linear non – homogeneous second order differential equation in  $\gamma(\dot{\vartheta})$ , with coefficients dependent upon the instantaneous rotational speed  $\dot{\vartheta} = d\vartheta/dt$  and its first and second derivatives.

This corresponds to considering a system with  $\dot{\vartheta}$  as independent variable and  $\gamma(\dot{\vartheta})$  as unique DOF. Hence, equation (IV.47) represents the linear forced vibration of this system, which vibrates in  $\gamma(\dot{\vartheta})$  with forcing function:

$$G(\dot{\vartheta}) = \frac{J_1}{J_2} \cdot \frac{d^2 \dot{\vartheta}}{dt^2} - \frac{k}{J_2} \cdot \frac{d \dot{\vartheta}}{dt} = G\left(\frac{d \dot{\vartheta}}{dt}, \frac{d^2 \dot{\vartheta}}{dt^2}, J_1, J_2, k\right) \quad (\text{IV.48})$$

After a short transient, the gear ratio  $\gamma(\dot{\vartheta})$  (IV.21) enters in a periodic steady trend given by the particular solution of equation (IV.47) that depends only upon the forcing function  $G(\dot{\vartheta})$ . The latter is periodic with  $\dot{\vartheta}$  first and second derivatives (Figure IV. 6) and is influenced by the values of  $J_1$ ,  $J_2$  and  $k$ .

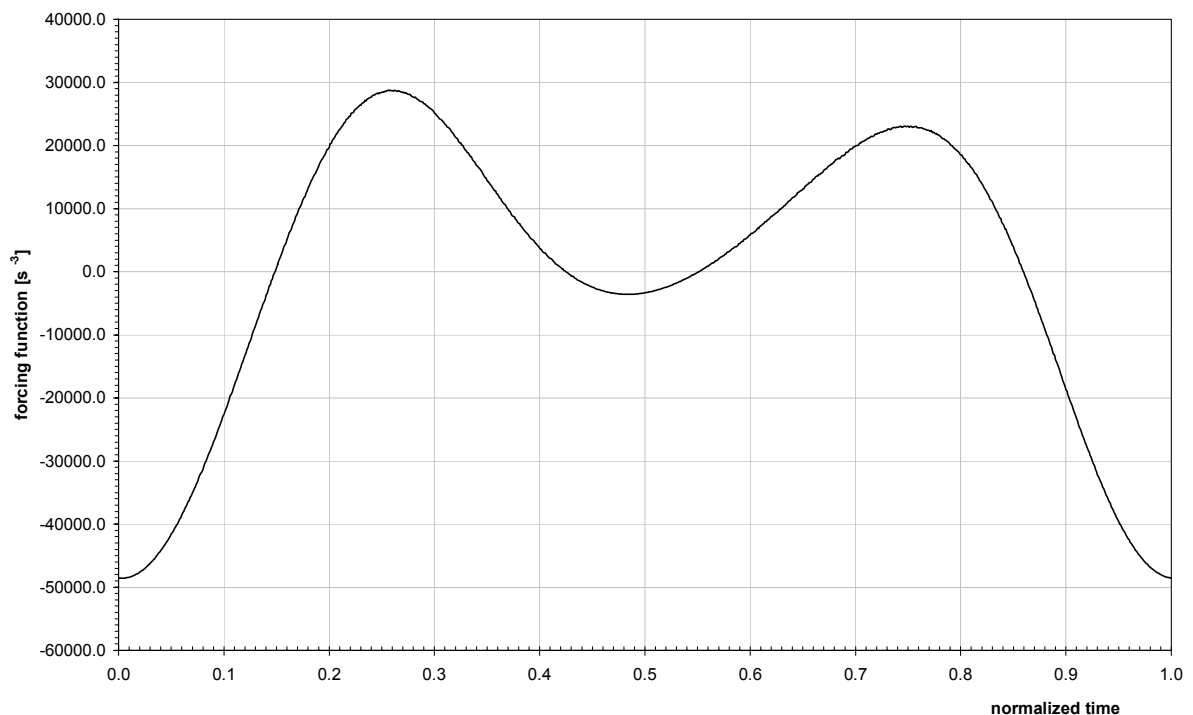


**Figure IV. 6 – Trend of the forcing function of the gear ratio differential equation, in function of normalized time.**

Looking at these parameters and how they appear in the forcing function, it is generally:

$$\frac{J_1}{J_2} \ll \frac{k}{J_2} \quad (\text{IV.49})$$

that is, the *jerk component* of the forcing function  $J_1/J_2 \cdot d^3\vartheta/dt^3$  is absolutely negligible in respect to the *acceleration component*  $-k/J_2 \cdot d^2\vartheta/dt^2$ , as it could be seen from Figure IV. 7.

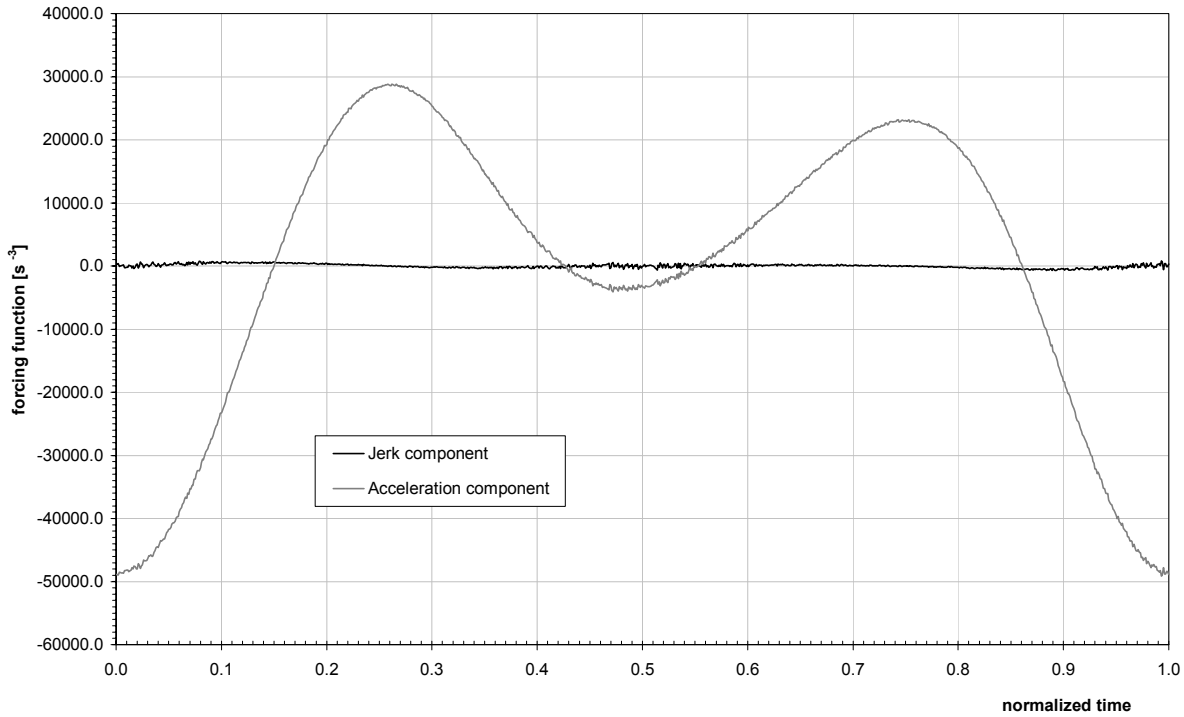


Figure IV. 7 – Comparison between the trend of the two components of the forcing function of the gear ratio differential equation.

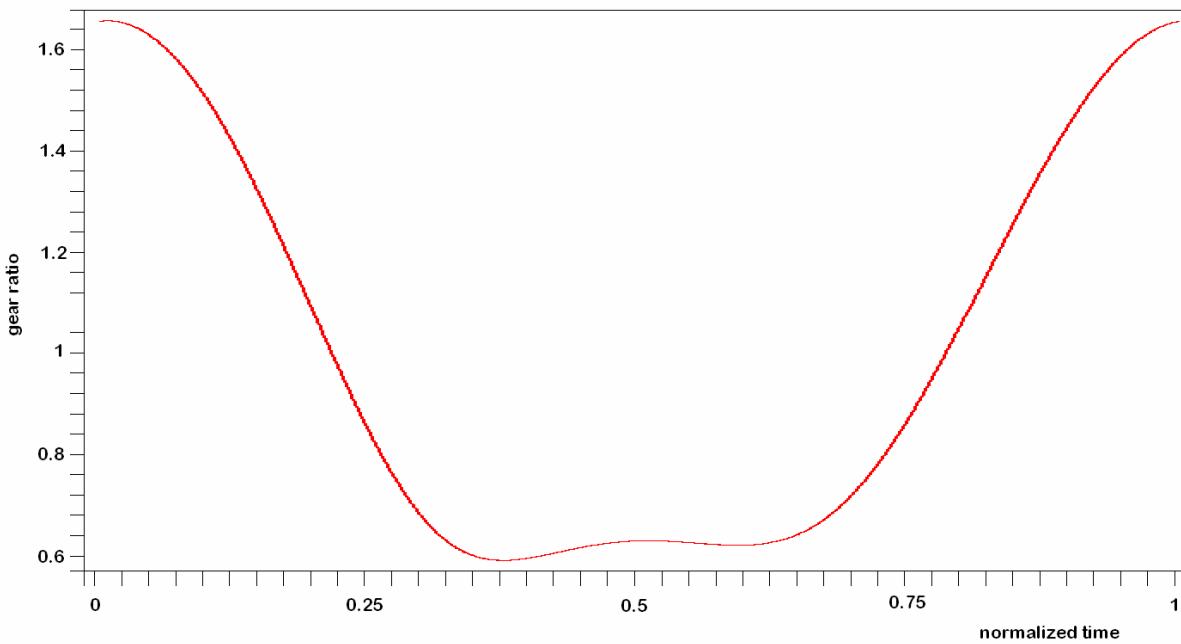
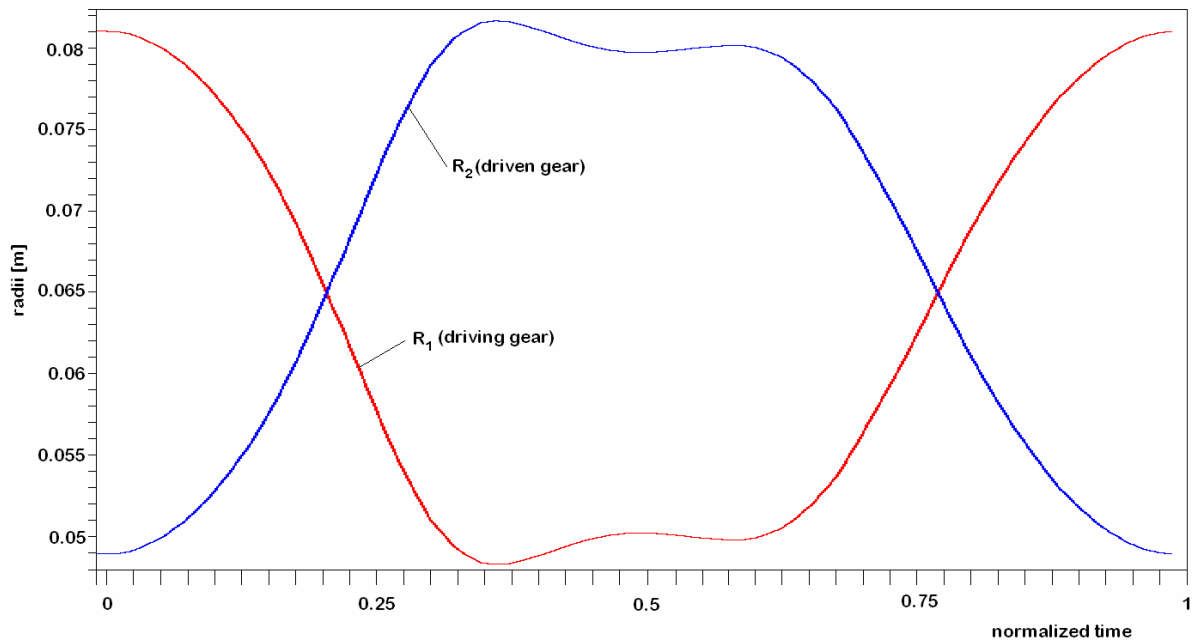


Figure IV. 8 – Gear ratio trend in function of normalized time



**Figure IV. 9 – Gear radii in function of normalized time.**

Hence, the strongest influence on the gear ratio is given by the rotational acceleration trend and by the ratio between the motor stiffness  $k$  and the secondary inertia momentum  $J_2$ , while the inertia momentum of the primary shaft doesn't have any considerable effect.

So, it is clear that having certain hydraulic motor and supplying plant (i.e. reasoning for a fixed value of  $k$ ), the gear ratio trend remains solely and univocally defined by the value of the secondary shaft inertia momentum  $J_2$ , together with the primary shaft rotational acceleration trend, the latter being determined by the independently defined motion law of the mechanism.

Finally the gear ratio and the two radii trends are shown respectively in Figure IV. 8 and Figure IV. 9 in function of normalized time.

#### *IV.3.2 Benefits in void and standard working conditions*

Figure IV. 10 shows the unbalancing torque trend in time in the case of void working conditions. The torque considered is defined by equation (IV.2), i.e. presuming that the torque contribute due to the blade inertia force had been made pointless by a geometric change in the system layout. The two curves represent respectively the standard mechanism case (the dotted curve) and the case of non circular gear application (the continuous curve). The benefits obtained by the application of this solution are clear, the unbalancing torque becoming constant as needed.

Hence, in the case of void working conditions the proposed solution is able to reach the scope of annihilating the unbalancing torque, completely.

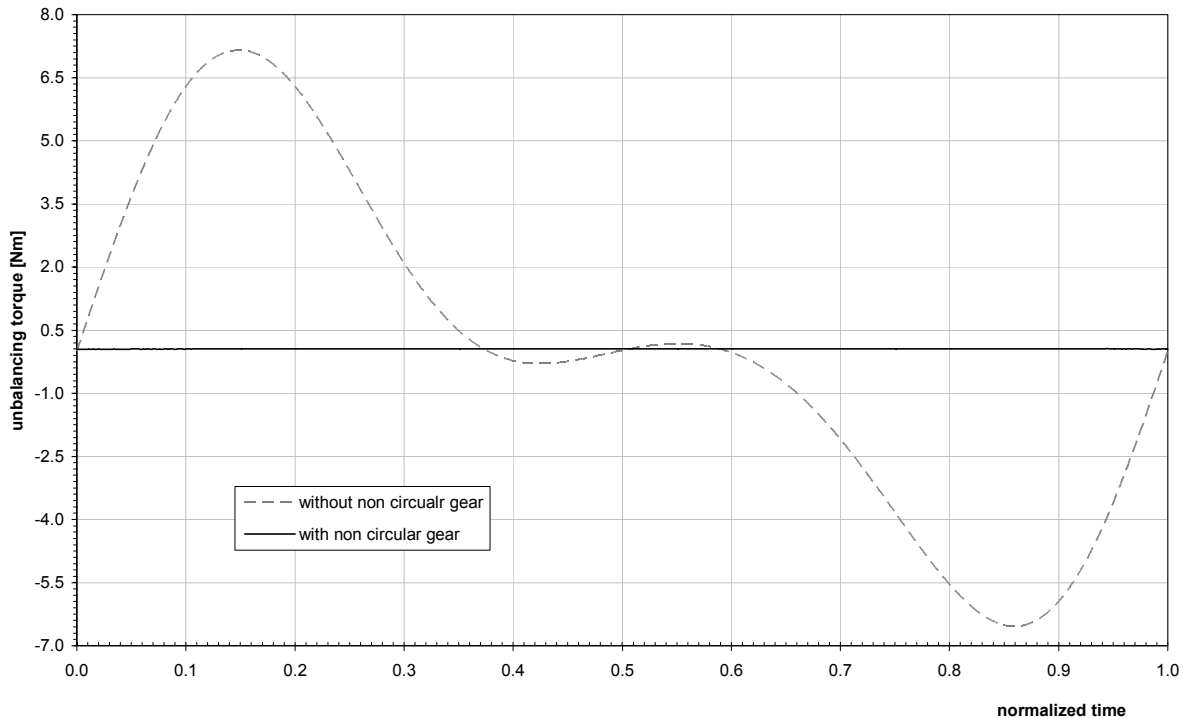


**Figure IV. 10 – Unbalancing torque in function of normalized time, in the specific case of void working condition ( $p = 0\%$ ).**

Anyway, the void working conditions is only a reference situation, while the situation to look at for understanding the real benefits is with standard working conditions. For this purpose Figure IV. 11 shows the sensitivity analysis of the adopted solution for different value of the filling percentage  $p$ , that is from the design situation of void working conditions to the total filled condition. From this perspective, it is evident that the higher is the percentage of filling, the worse the alternative solution works, but a certain benefit is still present.

Indeed referring to Figure III. 12 at page 67, which shows the unbalancing torque trend in time in function of the filling percentage but without the application of the non circular gearing, the amount of this benefit can be calculated. It could be seen that the amplitude of the torque oscillation was nearly 25 Nm in both void and standard working conditions ( $p = 16.67\%$ ), while it increased to 27 Nm for  $p = 50\%$  up till 37 Nm for the total filled condition. Looking at Figure IV. 11, the adopted solution reduces this amplitude respectively to 0 Nm, 4.30 Nm, 13 Nm and 26.4 Nm, with a positive gain on the unbalancing torque respectively of 100% in void working conditions, 83.70% for standard working conditions, 52% for half filled conditions and 28.70% for the condition of total filling.

## Alternative solution

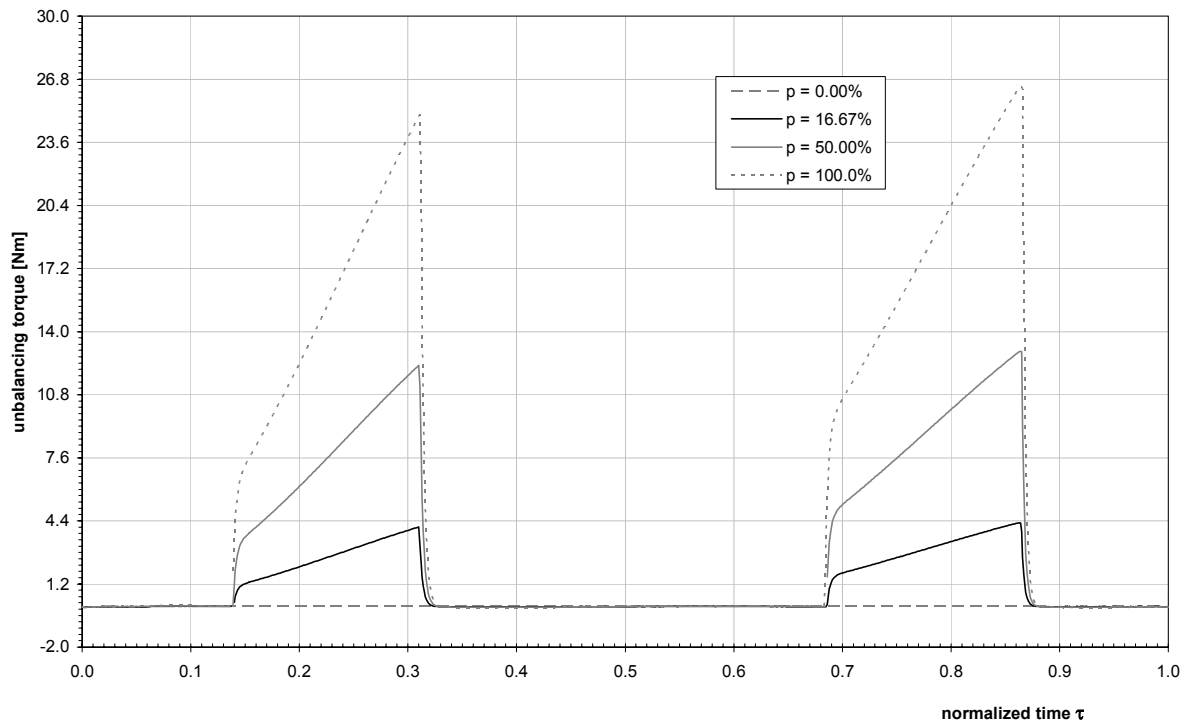


**Figure IV. 11 – Unbalancing torque in function of normalized time, for different values of the total filling percentage.**



V

CONCLUSIONS

---



## Conclusions

Beginning with the development of the necessary models, and continuing through the analysis of the system till the evaluation of an alternative innovative solution, this thesis has been able to give a contribution in the comprehension and optimization of cutter bar mechanisms, under the most general standpoint. The aim, which was to develop a study such as to finally achieve an improvement in the operational quality of the system, has been attained.

Firstly, a new and simplified model for the plant cutting resistance has been developed, on a theoretical basis which comes from a complete and deep literature analysis. This model, which has a kinematic character and can cover different kind of plants by means of the specific cutting energy parameter, has been successively useful for highlighting the cutting parameters influence on the whole system behavior.

Secondly, a complete dynamic model of the single blade cutter bar has been constructed. Although obtained by using characteristics and layout of a specific case study, it has been able to point out the system disequilibrium, independently from the cutter bar characteristics themselves, by means of the counterbar equilibrium equations. These equations are general and can be used for a broad range of application regarding single blade cutter bar systems.

Moreover, by developing the equation of motion of the driving mechanism, this model has been able to describe this disequilibrium in the time domain, in function of the mechanism geometric, kinematic and dynamic characteristics. For this purpose, the developed model has been numerically integrated, allowing the analysis of the variance in the system behavior in function of the variance of several cutter bar parameters. This analysis has succeeded not only in pointing out the system disequilibrium sources, that is the driving torque instability against an extremely variable resistance torque, but also for a general system improvement.

Indeed, through the counterbar equilibrium equations analysis it has been made clear that the main source of vibration is the periodic torque instability, whereas the inertia torque carried by the crank disc is almost negligible because of the low engine rotational speed. Also, the torques caused by the blade inertia force have been found to be another component of the disequilibrium source, but they are all geometrically avoidable by making the counterbar and blade centres of gravity coincide in the respective directions.

The motion law numerical analysis has also highlighted an optimal engine running speed, which is able to minimize the driving torque instability, whereas the crank disc has been clarified to be totally inefficient for this purpose, as it is an increase in conrod length or a reduction in the blade clamping force.

Until this point the analysis has been carried out on the basis of an existing system. Besides the above mentioned results, the analysis has mainly evidenced that the mechanism cannot be

totally equilibrated by means of the solely change in the cutter bar geometric parameters, i.e. the disequilibrium torque has never been totally annihilated within the sensitivity analysis. The only way that has been found able to attain this purpose is to operate on, or to gain some control over the mechanism motion law.

Hence, a double action has been designed for the cutter bar improvement and disequilibrium total abatement.

The first action is, as it has been nodded, to modify the overall layout and hence make the system less eccentric. Precisely, it is necessary to make the counterbar and blade centres of gravity coincide in the direction that belongs both to the plane perpendicular to the tractor forward motion and to the plane perpendicular to the blade motion. This action reduces the oscillation source up to almost an averagely 70% in the above defined direction. It has to be noticed that, however, this first part of the solution has been theoretically highlighted, but its design has been left to the cutter bar manufacturer.

The remaining quote of the unbalance has been found to be not geometrically avoidable. Hence, the second action follows another approach, and precisely it makes use of a secondary shaft, parallel to the motor one, which carries the same standard flywheel that has been removed from the primary shaft. The two shafts are then linked together by means of a keyed and well defined non circular gearing, whose meshing profiles are developed on the basis of a single functional equation and some constitutive conditions.

This second part of the solution has been designed for void working conditions, situation in which it carries a total annihilation of the disequilibrium remain quote, while in standard working conditions it has been found to reduce this quote of approximately the 80%.

However, it has to be remarked that the attained results and the developed solution have a general purpose and can be used widely, even if they have been obtained by the analysis on a specific cutter bar. Moreover, the codes developed for these analysis and design are easily understandable and the values introduced could be changed for the analysis of different cutter bars. Also, the equations written within the codes can be rewritten to conduct the analysis for different kind of mechanism. By this way the analysis and the proposed alternative solution could be then reviewed and extended, with the right modifications, even for double blade cutter bars.

# APPENDIX A

---



## Appendix A

### A.1 MAPLE CODE FOR SOLVING THE EQUATION OF MOTION

Equation of motion (II.57) was numerically integrated to obtain the mechanism's motion law  $\vartheta(t)$ . The code for this purpose was realized with MAPLE 9 and is listed below together with some comments [9, 12, 19, 35, 39, 47 and 55].

The exact values was obtained by the manufacturer and measuring the geometry of a case study, while the others are explained in lateral comments.

#### # INITIAL SETTINGS:

```
restart:
Digits := 8:
with(plots):
with(plottools):
with(LinearAlgebra):
with(process):
_EnvExplicit = true:
with(CurveFitting):
with(RealDomain):
```

#### # EXACT VALUES:

```
n := 300: #average running speed
omega := evalf(2*Pi*n/60):
l:= 0.394: #conrod length
e := 0.0844: #eccentricity
r := 0.038: #crank radius
lambda := r/l: #stroke - conrod ratio
lambda1 := e/l: #eccentricity ratio
h1 := 0.027: #distance
h2 := 0.00373: #distance
Lama := 1.444: #blade length
HD := -0.490: #distance
s1 := 0.015: #thickness
s2 := 0.030: #thickness
d := 0.13: #crank disc diameter
delta := 7845: #steel density
mbmezza := 0.2465: #mass
m := 3.645 + mbmezza: #mass
mnott := 0.3: #mass
betaPME := arcsin(e/(l+r)): #conrod angle at ODC
betaPMI := arcsin(e/(l-r)): #conrod angle at IDC
J:= proc(d)
    (mbmezza+1/2*mnott)*r^2+1/2^5*delta*evalf(Pi)*(d^4*s1+0.05^4*s2-
    .025^4*s1-4*.025^2*s1*r^2):
end proc: #total inertia momentum
mB:=32.7: #mass
xGS1 := 167.56/1000: #baricentric distance,
measured
xGS2 := 16.728/1000: #baricentric distance,
measured
xGS3 := 29.844/1000: #baricentric distance,
measured
xGL2 := (15.77+16.77)/1000 + xGS2: #baricentric distance,
measured
xGL3 := 67.13/1000 + xGS3: #baricentric distance,
measured
```

```

deltaz := xGS3 - xGL3:           #distance
deltay := xGS2 - xGL2:           #distance
theta_PMI := evalf(Pi) + betaPME - betaPMI:   #crank angle at IDC
corsa := (r+1)*cos(betaPME) - (1-r)*cos(betaPMI):   #stroke
nc := 19:                         #teeth number
CHI := 0.2:                         #time parameter
chi := 0.01:                        #time parameter

# ESTIMATED VALUES
va := 8/3.6:                         #forward speed average value
Fs := 500:                             #clamping force average value, measured with a
                                         dynamometer
eta := 0.846:                          #total efficiency, from the hydraulic motor
                                         diagram
E := 3*10^(2):                          #mean value (see note 8 at page 32)
km := -16.4243:                         #motor stiffness, obtained from the hydraulic
                                         motor diagram
mu := 0.225:                             #friction coefficient

# HYPOTHESIS:
BF := 0.015:                             #tooth dimension, measured
LF := 0.0266:                             #tooth dimension, measured
BE := 2*r:                                 #tooth dimension, measured
LE := 0.0466:                             #tooth dimension, measured
xE := 2*r-BE/2-LE/2:                       #cutting window initial value
xF := 2*r-BF/2-LF/2:                       #cutting window final value
p := .1667:                                #total filling percentage

```

The integration of the equation of motion occurs recursively, because the average torque value is not known while it is strictly necessary for the integration of the equation itself. Hence the recurrence occurs with an initial assumed value of the driving torque average value, the same being recalculated at the end of the cycle, after the equation integration, and the whole cycle recalculated. The loop continues till the first and second values coincide.

Moreover, it could be noticed below that the integration of the differential equation is listed as an initial value problem (IVP), with defined initial conditions. On the contrary, this is a boundary value problem (BVP), for the periodicity of the solution which depends essentially on the boundary conditions themselves.

This procedure was adopted because of the difficulty of integration with a BVP solver, within the MAPLE environment. Hence the solution was initially obtained as a boundary value problem, with a BVP solver but with long time integration and great memory usage, and the correspondent initial condition values were calculated. Hence the IVP solver together with the calculated initial conditions is called for any subsequent calculations, using a fewer amount of memory and time saving.

**# CYCLE SETTINGS AND BOUNDARY CONDITIONS:**

## Appendix A

```

Cm_media := 0.1: #initially assumed driving torque average value
Cm_0 := 0: #initial driving torque comparison value

tempo := time():
ciclo := proc()
  global
  j,k,Cm_0,omega,periodo,MIN,MAX,n_giri,theta,x_pt,x_2pt,res1,res2,
  res,Fi,Fa,Cm,eq_moto,sol_moto,th,th_pt,th_2pt,TH2PT,th_3pt,TH3PT,Fbx,
  regime_medio,Cm_media,Cm_medial,Cm_media2,incl_x,R,ti,ci_moto,epsilon,
  beta,x,ni,tempo:
NumericEvent(invalid_operation, 1): #avoid singularities
ti := 1.0: ni := n: #time for initial conditions
ci_moto := theta(ti)=0, D(theta)(ti)=Pi*ni/30: #initial conditions
epsilon := 1/1000: #cycle accuracy on the driving torque

beta := t -> arcsin(lambdal+lambda*sin(theta(t))-betaPME): #conrod angle
x := t -> (r+l)*cos(betaPME)-l*cos(beta(t))-r*cos(theta(t)-betaPME): #blade displacement
omega := evalf(2*Pi*n/60): #running speed
periodo := evalf(60/n): #period
MIN := ti + CHI: #integration minimum value
MAX := MIN + periodo: #integration maximum value
n_giri := (MAX-MIN+2*CHI)*n/60: #total number of rotations

# EQUATION OF MOTION INTEGRATION CYCLE (DRIVING TORQUE AND
# RUNNING SPEED CALCULATION):
for j from 1 while abs(Cm_media-Cm_0)>epsilon do
  Cm_0 := Cm_media:
  x_pt := t -> diff(x(t),t): #blade velocity
  x_2pt := t -> diff(x_pt(t),t): #blade acceleration
  res1 := t -> p*E*nc*va*x(t)/x_pt(t):
  res2 := t -> -p*E*nc*va*(x(t)-corsa)/x_pt(t):
  res := t -> piecewise((x(t)>xE and x(t)<xF and sin(theta(t))>0),
    res1(t), (x(t)>xE and x(t)<xF and sin(theta(t))<0), res2(t));
  #cutting resistance

  Fi := t -> m*x_2pt(t): #blade inertia force
  Fa := t -> mu*(Fs+(res(t)+Fi(t))*tan(beta(t)))/(1-mu*tan(beta(t))): #friction force
  Cm := t -> Cm_0 + km*(diff(theta(t),t)-omega): #driving torque
  eq_moto := Cm(t)*diff(theta(t),t) - res(t)*x_pt(t) - Fa(t)*x_pt(t) -
    J(d)*diff(theta(t),t,t)*diff(theta(t),t) - m*x_pt(t)*x_2pt(t) =
    0: #equation of motion
  sol_moto := dsolve({eq_moto, ci_moto}, numeric, output=listprocedure,
    maxfun=50000, range=MIN-CHI..MAX+CHI): #integration
  th := subs(sol_moto,theta(t)): #solution for the crank angle
  th_pt := subs(sol_moto,diff(theta(t),t)): #solution for the
    instantaneous rotational
    speed
  th_2pt := t -> solve(eq_moto,diff(theta(t),t,t)): #solution for the
    instantaneous rotational
    acceleration

```

## Analysis of Reciprocating Single Blade Cutter Bars

```
Fbx := t -> cos(beta(t))*(Cm(t)-J(d)*th_2pt(t))/(r*sin(theta(t) -
    betaPME + beta(t))):          #horizontal force on the conrod
regime_medio := evalf(60/(2*Pi)*(1/(periodo)))* evalf(Int(th_pt(t),
    t=MIN..MAX, method = _Gquad)):
                                #average rotational speed
Cm_media := 1/periodo*evalf(Int(Cm_0 + km*(th_pt(t)-omega),
    t=MIN..MAX, method = _Gquad)):
                                #average driving torque
end do:
Cm_medial := evalf(2/periodo*Int(Cm_0 + km*(th_pt(t)-omega),t=MIN..MIN+
    periodo/2, method = _Gquad)): #average driving torque on
    the forward stroke
Cm_media2 := evalf(2/periodo*Int(Cm_0 + km*(th_pt(t)-omega), t=MAX-
    periodo/2..MAX, method = _Gquad)):
                                #average driving torque on
    the return stroke
tempo := time() - tempo:
printf("Convergenza in %d iterazioni (%g secondi):\nCoppia motrice media =
    %g Nm, regime medio di rotazione = %g
    giri/min\n",j,tempo,Cm_0,regime_medio);
printf("Coppia motrice media (corsa di andata) = %g Nm\nCoppia motrice media
    (corsa di ritorno) = %g Nm\n",Cm_medial,Cm_media2);
end proc:
evalf(ciclo()):                  #cycle evaluation
gc();
appendto (terminal);
```

# APPENDIX B

---



## Appendix B

The sensitivity analysis was carried out on the basis of the motion law and how it is modified with a discrete variance of a single chosen parameter, for different influencing parameters. Hence the code for the sensitivity analysis, always realized in MAPLE 9 environment, is different for each parameter.

How the motion law and other depending functions are modified in relatively to the chosen parameter variance is shown in Chapter III, where each diagram is obtained as a sequence of points calculated with the following codes and printed out in an EXCEL file.

In the follow codes, only the first is commented, the others being the equivalent code for a different parameter.

### B.1 MAPLE CODE FOR THE SENSITIVITY ANALYSIS ON THE PARAMETER "d"

#### # SETTINGS:

```
d := 0:
MM := 4:
INIZ := 1:
var := d:
VAR := convert(var, string):
```

In Maple, to make a better and easier use of a defined function, i.e. the functions upon which the sensitivity analysis is needed beneath the variance of a certain parameter, it is necessary to redefine it in terms of the equation of motion solutions (angular displacement, speed and acceleration).

#### # DEFINITION OF THE SENSITIVITY FUNCTIONS:

```
X := subs(theta(t)=th(t), x(t)):
X_pt := subs(diff(theta(t),t)=th_pt(t),theta(t)=th(t), x_pt(t)):
Res := subs(diff(theta(t),t)=th_pt(t),theta(t)=th(t), res(t)):
X_2pt := subs(diff(theta(t),t,t)=th_2pt(t), diff(theta(t),t)=th_pt(t),
theta(t)=th(t), x_2pt(t)):
FI := m*X_2pt:
Th_2pt := subs(diff(theta(t),t)=th_pt(t), theta(t)=th(t), th_2pt(t)):
CM := subs(diff(theta(t),t)=th_pt(t), Cm(t)):
FBX := subs(diff(theta(t),t)=th_pt(t), theta(t)=th(t), Fbx(t)):
```

#### # SENSITIVITY ANALYSIS CYCLE AND XLS DIAGRAM CONSTRUCTION:

```
appendto(nomefile);
tempo_inizio_statement := time():
for i from INIZ while i<=MM do
    d := 0.1516*i^2-0.3246*i+0.173; #discrete variance (4 values)
                                     #of the chosen influencing
                                     #parameter
    variabile := convert(evalf(var*1000,3), string);
    legg := cat(VAR," = ",variabile,unità);
    printf("\nVERIFICA DEI PLOT PER LE CURVE N.%d (con %s =
           %g%s)",i,VAR,var,unità);
    tempo := time():
```

```

Cm_media := 0.1:
Cm_0 := 0:
printf("\nCOSTRUZIONE DEI PLOT PER LE CURVE N.%d (con %s = %g%s) -
      Calcolo in corso\n",i,VAR,var,unità);
evalf(ciclo()):
tempo := time() - tempo:
printf("Calcolo riuscito in %d iterazioni (%g secondi):\nCoppia
      motrice media = %g Nm, regime medio di rotazione = %g
      rpm\n",j,tempo,Cm_0,regime_medio);
printf("Coppia motrice media (corsa di andata) = %g Nm\nCoppia motrice
      media (corsa di ritorno) = %g Nm\n",Cm_medial,Cm_media2);
appendto(terminal);
printf("\ninizio calcolo per %s = %g%s",VAR,var,unità);
appendto(nomedata);
printf("\n\n");
risp := rhs(sol_moto[1]),rhs(sol_moto[2]),rhs(sol_moto[3]):
printf("%s",legg);
printf("\ntempo\tangolo di manovella\tvelocità angolare\tvariazione
      percentuale della velocità angolare\tcoppia motrice\tresistenza
      al taglio\tcoppia d'inerzia\tcoppia di Fi nel piano XY\tcoppia
      di Fi nel piano XZ\tforza motrice di taglio");
printf("\n[s]\t[rad]\t[rad/s]\t[Nm]\t[N]\t[Nm]\t[Nm]\t[Nm]\t[N]\n\n");
risoluzione := 1000;
i_incr := 1/(5*risoluzione*n)*300:
MASSIMO := (periodo)/i_incr;
for ii from 0 to MASSIMO do
  printf("%+.5f\t%+.5f\t%+.5f\t%+.5f\t%+.5f\t%+.5f\t%+.5f\t
      %+.5f\n",risp(MIN+ii*i_incr)[1],risp(MIN+ii*i_incr)[2],ris
      p(MIN+ii*i_incr)[3],Cm_0 + km*(th_pt(MIN+ii*i_incr)-
      omega), eval(Res, t=MIN+ii*i_incr),J(d)*eval(Th_2pt,
      t=MIN+ii*i_incr),eval(FI
      *deltaz,t=MIN+ii*i_incr),eval(FI*deltay,t=MIN+ii*i_incr),e
      val(FBX,t=MIN+ii*i_incr));
end do:
tempo := time() - tempo:
appendto(terminal);
printf("\ncalcolo concluso in %g secondi",tempo);
appendto(nomefile);
end do:
tempo_statement := (time() - tempo_inizio_statement)/60:
printf("\n\nCalcolo concluso in %g minuti",tempo_statement);
gc();
appendto(terminal);

```

## B.2 MAPLE CODE FOR THE SENSITIVITY ANALYSIS ON THE PARAMETER “p”

```

# SETTINGS:
p := 0:
MM := 4:
INIZ := 1:
var := p:
VAR := convert(var, string):

```

```

# DEFINITION OF THE SENSITIVITY FUNCTIONS:

```

## Appendix B

```
X := subs(theta(t)=th(t), x(t)):
X_pt := subs(diff(theta(t),t)=th_pt(t),theta(t)=th(t), x_pt(t)):
Res := subs(diff(theta(t),t)=th_pt(t),theta(t)=th(t), res(t)):
X_2pt := subs(diff(theta(t),t,t)=th_2pt(t), diff(theta(t),t)=th_pt(t),
theta(t)=th(t), x_2pt(t)):
FI := m*X_2pt:
Th_2pt := subs(diff(theta(t),t)=th_pt(t), theta(t)=th(t), th_2pt(t)):
CM := subs(diff(theta(t),t)=th_pt(t), Cm(t)):
FBX := subs(diff(theta(t),t)=th_pt(t), theta(t)=th(t), Fbx(t)):

# SENSITIVITY ANALYSIS CYCLE AND XLS DIAGRAM CONSTRUCTION:
appendto(nomefile);
tempo_inizio_statement := time():
for i from INIZ while i<=MM do
  p := 0.0833*i^2-0.0833*i;
  variabile := convert(evalf(var*100,3), string);
  legg := cat(VAR," = ",variabile,unità);
  printf("\nVERIFICA DEI PLOT PER LE CURVE N.%d (con %s = %g%s)",i,VAR,
var,unità);
  tempo := time():
  Cm_media := 0.1:
  Cm_0 := 0:
  printf("\nCOSTRUZIONE DEI PLOT PER LE CURVE N.%d (con %s = %g%s) -
Calcolo in corso\n",i,VAR,var,unità);
  evalf(ciclo()):
  tempo := time() - tempo:
  printf("Calcolo riuscito in %d iterazioni (%g secondi):\nCoppia
motrice media = %g Nm, regime medio di rotazione = %g
rpm\n",j,tempo,Cm_0, regime_medio);
  printf("Coppia motrice media (corsa di andata) = %g Nm\nCoppia motrice
media (corsa di ritorno) = %g Nm\n",Cm_medial,Cm_media2);
  appendto(terminal);
  printf("\ninizio calcolo per %s = %g%s",VAR,var,unità);
  appendto(nomedata);
  printf("\n\n");
  risp := rhs(sol_moto[1]),rhs(sol_moto[2]),rhs(sol_moto[3]):
  printf("%s",legg);
  printf("\ntempo\tangolo di manovella\tvelocità angolare\tvariazione
percentuale della velocità angolare\tcoppia motrice\tresistenza
al taglio\tcoppia d'inerzia\tcoppia di Fi nel piano XY\tcoppia
di Fi nel piano XZ\tforza motrice di taglio");
  printf("\n[s]\t[rad]\t[rad/s]\t[Nm]\t[N]\t[Nm]\t[Nm]\t[Nm]\t[N]\n\n");
  risoluzione := 1000;
  i_incr := 1/(5*risoluzione*n)*300:
  MASSIMO := (periodo)/i_incr;
  for ii from 0 to MASSIMO do
    printf("%+.5f\t%+.5f\t%+.5f\t%+.5f\t%+.5f\t%+.5f\t%+.5f\t
%+.5f\n",risp(MIN+ii*i_incr)[1],risp(MIN+ii*i_incr)[2],
risp(MIN+ii*i_incr)[3],Cm_0 + km*(th_pt(MIN+ii*i_incr)-
omega),eval(Res,t=MIN+ii*i_incr),J()*eval(Th_2pt,
t=MIN+ii*i_incr),
eval(FI*deltaz,t=MIN+ii*i_incr),eval(FI*deltay,
t=MIN+ii*i_incr),eval(FBX, t=MIN+ii*i_incr));
  end do:
  tempo := time() - tempo:
  appendto(terminal);
  printf("\ncalcolo concluso in %g secondi",tempo);
  appendto(nomefile);
end do:
tempo_statement := (time() - tempo_inizio_statement)/60:
```

```
printf("\n\n\nCalcolo concluso in %g minuti",tempo_statement);
gc();
appendto(terminal);
```

### B.3 MAPLE CODE FOR THE SENSITIVITY ANALYSIS ON THE PARAMETER "Fs"

#### # SETTINGS:

```
Fs := 0:
MM := 4:
INIZ := 1:
var := Fs:
VAR := convert(var, string):
```

#### # DEFINITION OF THE SENSITIVITY FUNCTIONS:

```
X := subs(theta(t)=th(t), x(t)):
X_pt := subs(diff(theta(t),t)=th_pt(t),theta(t)=th(t), x_pt(t)):
Res := subs(diff(theta(t),t)=th_pt(t),theta(t)=th(t), res(t)):
X_2pt := subs(diff(theta(t),t)=th_2pt(t), diff(theta(t),t)=th_pt(t),
theta(t)=th(t), x_2pt(t)):
FI := m*X_2pt:
Th_2pt := subs(diff(theta(t),t)=th_pt(t), theta(t)=th(t), th_2pt(t)):
CM := subs(diff(theta(t),t)=th_pt(t), Cm(t)):
FBX := subs(diff(theta(t),t)=th_pt(t), theta(t)=th(t), Fbx(t)):
```

#### # SENSITIVITY ANALYSIS CYCLE AND XLS DIAGRAM CONSTRUCTION:

```
appendto(nomefile);
tempo_inizio_statement := time():
for i from INIZ while i<=MM do
  Fs := 350*i^2-590*i+240;
  variabile := convert(evalf(var*1000,3)/1000, string);
  legg := cat(VAR," = ",variabile,unità);
  printf("\nVERIFICA DEI PLOT PER LE CURVE N.%d (con %s =
    %g%s)",i,VAR,var, unità);
  tempo := time():
  Cm_media := 0.1:
  Cm_0 := 0:
  printf("\nCOSTRUZIONE DEI PLOT PER LE CURVE N.%d (con %s = %g%s) -
    Calcolo in corso\n",i,VAR,var,unità);
  evalf(ciclo()):
  tempo := time() - tempo:
  printf("Calcolo riuscito in %d iterazioni (%g secondi):\nCoppia
    motrice media = %g Nm, regime medio di rotazione = %g
    rpm\n",j,tempo,Cm_0, regime_medio);
  printf("Coppia motrice media (corsa di andata) = %g Nm\nCoppia motrice
    media (corsa di ritorno) = %g Nm\n",Cm_medial,Cm_media2);
  appendto(terminal);
  printf("\ninizio calcolo per %s = %g%s",VAR,var,unità);
  appendto(nomedata);
  printf("\n\n");
  risp := rhs(sol_moto[1]),rhs(sol_moto[2]),rhs(sol_moto[3]):
  printf("%s",legg);
  printf("\ntempo\tangolo di manovella\tvelocità angolare\tvariazione
    percentuale della velocità angolare\tcoppia motrice\tresistenza
    al taglio\tcoppia d'inerzia\tcoppia di Fi nel piano XY\tcoppia
    di Fi nel piano XZ\tforza motrice di taglio");
  printf("\n[s]\t[rad]\t[rad/s]\t[Nm]\t[N]\t[Nm]\t[Nm]\t[Nm]\t[N]\n\n");
```

## Appendix B

```
risoluzione := 1000;
i_incr := 1/(5*risoluzione*n)*300;
MASSIMO := (periodo)/i_incr;
for ii from 0 to MASSIMO do
    printf("%+.5f\t%.5f\t%.5f\t%.5f\t%.5f\t%.5f\t%.5f\t%.5f\t%.5f\t%.5f\t%.5f\n",
        risp(MIN+ii*i_incr)[1], risp(MIN+ii*i_incr)[2], risp(MIN+ii*i_incr)[3],
        Cm_0 + km*(th_pt(MIN+ii*i_incr) - omega), eval(Res, t= MIN+ii*i_incr), J()*eval(Th_2pt, t=MIN+ii*i_incr),
        eval(FI*deltaz, t=MIN+ii*i_incr), eval(FI*deltay, t=MIN+ii*i_incr), eval(FBX, t=MIN+ii*i_incr));
end do;
tempo := time() - tempo;
appendto(terminal);
printf("\ncalcolo concluso in %g secondi", tempo);
appendto(nomefile);
end do;
tempo_statement := (time() - tempo_inizio_statement)/60;
printf("\n\nCalcolo concluso in %g minuti", tempo_statement);
gc();
appendto(terminal);
```

### B.4 MAPLE CODE FOR THE SENSITIVITY ANALYSIS ON THE PARAMETER “n”

#### # SETTINGS:

```
n := 150;
MM := 4;
INIZ := 1;
var := n;
VAR := convert(var, string);
```

#### # DEFINITION OF THE SENSITIVITY FUNCTIONS:

```
X := subs(theta(t)=th(t), x(t));
X_pt := subs(diff(theta(t),t)=th_pt(t), theta(t)=th(t), x_pt(t));
Res := subs(diff(theta(t),t)=th_pt(t), theta(t)=th(t), res(t));
X_2pt := subs(diff(theta(t),t,t)=th_2pt(t), diff(theta(t),t)=th_pt(t), theta(t)=th(t), x_2pt(t));
FI := m*X_2pt;
Th_2pt := subs(diff(theta(t),t)=th_pt(t), theta(t)=th(t), th_2pt(t));
CM := subs(diff(theta(t),t)=th_pt(t), Cm(t));
FBX := subs(diff(theta(t),t)=th_pt(t), theta(t)=th(t), Fbx(t));
```

#### # SENSITIVITY ANALYSIS CYCLE AND XLS DIAGRAM CONSTRUCTION:

```
appendto(nomefile);
tempo_inizio_statement := time();
for i from INIZ while i<=MM do
    n := 150*i^2-300*i+300;
    regime := convert(evalf(n*1000,3)/1000, string);
    legg := cat(" n = ", regime, " rpm");
    printf("\nVERIFICA DEI PLOT PER LE CURVE N.%d (con %s = %g rpm)", i, VAR, var);
    tempo := time();
    Cm_media := 0.1;
    Cm_0 := 0;
    printf("\nCOSTRUZIONE DEI PLOT PER LE CURVE N.%d (con %s = %g rpm) - Calcolo in corso\n", i, VAR, var);
```

```

evalf(ciclo()):
tempo := time() - tempo:
printf("Calcolo riuscito in %d iterazioni (%g secondi):\nCoppia
motrice media = %g Nm, regime medio di rotazione = %g
rpm\n",j,tempo,Cm_0, regime_medio);
printf("Coppia motrice media (corsa di andata) = %g Nm\nCoppia motrice
media (corsa di ritorno) = %g Nm\n",Cm_medial,Cm_media2);
appendto(terminal);
printf("\ninizio calcolo per %s = %g rpm",VAR,var);
appendto(nomedata);
printf("\n\n");
risp := rhs(sol_moto[1]),rhs(sol_moto[2]),rhs(sol_moto[3]):
printf("%s",legg);
printf("\ntempo\tangolo di manovella\tvelocità angolare\tvariazione
percentuale della velocità angolare\tcoppia motrice\tresistenza
al taglio\tcoppia d'inerzia\tcoppia di Fi nel piano XY\tcoppia
di Fi nel piano XZ\tforza motrice di taglio");
printf("\n[s]\t[rad]\t[rad/s]\t[percentuale]\t[Nm]\t[N]\t[Nm]\t[Nm]\t[
Nm]\t[N]\n\n");
risoluzione := 1000;
i_incr := 1/(5*risoluzione*n)*300:
MASSIMO := (periodo)/i_incr;
for ii from 0 to MASSIMO do
printf("%+.5f\t%+.5f\t%+.5f\t%+.5f\t%+.5f\t%+.5f\t%+.5f\t%+.5f\t
%+.5f\t%+.5f\n",risp(MIN+ii*i_incr)[1],risp(MIN+ii*i_incr)
[2],risp(MIN+ii*i_incr)[3],(risp(MIN+ii*i_incr)[3]-
omega)/omega*100,Cm_0 + km*(th_pt(MIN+ii*i_incr)-
omega),eval(Res,t=MIN+ii*i_incr),J()*eval(Th_2pt,
t=MIN+ii*i_incr),eval(FI*deltaz,
t=MIN+ii*i_incr),eval(FI*deltay,
t=MIN+ii*i_incr),eval(FBX, t=MIN+ii*i_incr));
end do:
appendto(terminal);
tempo := time() - tempo:
printf("\ncalcolo concluso in %g secondi",tempo);
appendto(nomefile);
end do:
tempo_statement := (time() - tempo_inizio_statement)/60:
printf("\n\nCalcolo concluso in %g minuti",tempo_statement);
gc();
appendto(terminal);

```

## B.5 MAPLE CODE FOR THE SENSITIVITY ANALYSIS ON THE PARAMETER "I"

### # SETTINGS:

```

l := 0.197:
MM := 4:
INIZ := 1:
var := l:
VAR := convert(var, string):

```

### # DEFINITION OF THE SENSITIVITY FUNCTIONS:

```

X := subs(theta(t)=th(t), x(t)):
X_pt := subs(diff(theta(t),t)=th_pt(t),theta(t)=th(t), x_pt(t)):
Res := subs(diff(theta(t),t)=th_pt(t),theta(t)=th(t), res(t)):
X_2pt := subs(diff(theta(t),t,t)=th_2pt(t), diff(theta(t),t)=th_pt(t),
theta(t)=th(t), x_2pt(t)):
FI := m*X_2pt:

```

## Appendix B

```
Th_2pt := subs(diff(theta(t),t)=th_pt(t), theta(t)=th(t), th_2pt(t)):
CM := subs(diff(theta(t),t)=th_pt(t), Cm(t)):
FBX := subs(diff(theta(t),t)=th_pt(t), theta(t)=th(t), Fbx(t)):

# SENSITIVITY ANALYSIS CYCLE AND XLS DIAGRAM CONSTRUCTION:
appendto(nomefile);
tempo_inizio_statement := time():
for i from INIZ while i<=MM do
  l := 0.197*i;
  variabile := convert(evalf(var*1000,3), string);
  legg := cat(VAR," = ",variabile,unità);
  printf("\nVERIFICA DEI PLOT PER LE CURVE N.%d (con %s =
    %g%s)",i,VAR,var,unità);
  tempo := time():
  Cm_media := 0.1:
  Cm_0 := 0:
  printf("\nCOSTRUZIONE DEI PLOT PER LE CURVE N.%d (con %s = %g%s) -
    Calcolo in corso\n",i,VAR,var,unità);
  evalf(ciclo()):
  tempo := time() - tempo:
  printf("Calcolo riuscito in %d iterazioni (%g secondi):\nCoppia
    motrice media = %g Nm, regime medio di rotazione = %g
    rpm\n",j,tempo,Cm_0,regime_medio);
  printf("Coppia motrice media (corsa di andata) = %g Nm\nCoppia motrice
    media (corsa di ritorno) = %g Nm\n",Cm_medial,Cm_media2);
  appendto(terminal);
  printf("\ninizio calcolo per %s = %g%s",VAR,var,unità);
  appendto(nomedata);
  printf("\n\n");
  risp := rhs(sol_moto[1]),rhs(sol_moto[2]),rhs(sol_moto[3]):
  printf("%s",legg);
  printf("\ntempo\tangolo di manovella\tvelocità angolare\tvariazione
    percentuale della velocità angolare\tcoppia motrice\tresistenza
    al taglio\tcoppia d'inerzia\tcoppia di Fi nel piano XY\tcoppia
    di Fi nel piano XZ\tforza motrice di taglio");
  printf("\n[s]\t[rad]\t[rad/s]\t[Nm]\t[N]\t[Nm]\t[Nm]\t[Nm]\t[N]\n\n");
  risoluzione := 1000;
  i_incr := 1/(5*risoluzione*n)*300:
  MASSIMO := (periodo)/i_incr;
  for ii from 0 to MASSIMO do
    printf("%+.5f\t%+.5f\t%+.5f\t%+.5f\t%+.5f\t%+.5f\t%+.5f\t%+.5f\t
      %+.5f\n",risp(MIN+ii*i_incr)[1],risp(MIN+ii*i_incr)[2],risp
      (MIN+ii*i_incr)[3],Cm_0 + km*(th_pt(MIN+ii*i_incr)-
      omega),eval(Res, t=MIN+ii*i_incr),J()*eval(Th_2pt,
      t=MIN+ii*i_incr),eval(FI*
      deltaz,t=MIN+ii*i_incr),eval(FI*deltay,t=MIN+ii*i_incr),ev
      al(FBX, t=MIN+ii*i_incr));
  end do:
  tempo := time() - tempo:
  appendto(terminal);
  printf("\ncalcolo concluso in %g secondi",tempo);
  appendto(nomefile);
end do:
tempo_statement := (time() - tempo_inizio_statement)/60:
printf("\n\nCalcolo concluso in %g minuti",tempo_statement);
gc();
appendto(terminal);
```



# APPENDIX C

---



## Appendix C

### C.1 MAPLE CODE FOR THE APPLICATION OF NON CIRCULAR GEARING

Functional equation (IV.22) together with constitutive equation (IV.26) were numerically integrated to obtain the new mechanism's motion law  $\vartheta(t)$  and the gear ratio  $\tau(\vartheta)$  trend. The code for this purpose was always realized in MAPLE 9 and it is listed below together with some comments [9, 12, 19, 39, 47 and 55].

#### # NEW DATA:

```
INT := d:
Js := evalf(J(INT)*2):
E := 0:
```

#### # EQUATION OF MOTION RE-INTEGRATION WITH NEW DATA:

```
Cm_media := 0.1:
Cm_0 := 0:
tempo := time():
evalf(ciclo()):
tempo := time() - tempo:
printf("Calcolo riuscito in %d iterazioni (%g secondi):\nCoppia motrice
media = %g Nm, regime medio di rotazione = %g
rpm\n", j, tempo, Cm_0, regime_medio);
printf("Coppia motrice media (corsa di andata) = %g Nm\nCoppia motrice media
(corsa di ritorno) = %g Nm", Cm_medial, Cm_media2);
```

#### # RE-DEFINITION OF THE KNOWN FUNCTIONS IN POLYNOMIAL FORM:

```
printf("\n\nValutazione dell'andamento della soluzione in forma polinomiale
in corso"):
solp := dsolve({eq_moto, ci_moto}, numeric, output=piecewise, range=MIN-
CHI..MAX+CHI):
TH1PT := t -> convert(subs(solp, diff(theta(t), t)), float):
printf("Valutazione dell'andamento dell'Accelerazione angolare in forma
polinomiale in corso\n"):
TH2PT := t -> rhs(diff(solp[3], t)):
printf("Valutazione dell'andamento del Jerk angolare in forma polinomiale in
corso"):
TH3PT := t -> rhs(diff(solp[3], t, t)):
gc();
```

#### # FUNCTIONAL EQUATION INTEGRATING CYCLE:

```
Digits := 6:
tempo := time():
cicloRNC := proc()
global cc_RNC, eq_RNC, sol_RNC, tempo, thau, dthau, tau_medio:
cc_RNC := tau(MIN)=1.646+1/100*sigma, tau(MAX)=1.646+1/100*sigma:
eq_RNC := TH1PT(t)*(diff(tau(t), t, t)*tau(t) + (diff(tau(t), t))^2) +
3*TH2PT(t)*diff(tau(t), t)*tau(t) + TH3PT(t)*(tau(t))^2 +
(km*TH2PT(t) - J(d)*TH3PT(t))/Js=0:
printf("SOLUZIONE NUMERICA DELLA NUOVA EQUAZIONE DI MOTO (RNC) -
Calcolo in corso"):
sol_RNC := dsolve({eq_RNC, cc_RNC}, numeric, output=listprocedure,
known=[th, th_pt, TH2PT, TH3PT], method=bvp[middefer],
maxmesh=8000, continuation=sigma, interpolant=false, abserr=2e-
3):
```

```

tempo := time() - tempo:
printf("Calcolo concluso in %g minuti",tempo/60);
thau := subs(sol_RNC,tau(t)):
dthau := subs(sol_RNC,diff(tau(t),t)):
tau_medio := evalf(1/(periodo))*evalf(Int(thau(t), t=MIN..MAX, method
    = _Gquad)):
printf("\nValore medio del rapporto di trasmissione: %g\n",tau_medio);
end proc:
evalf(cicloRNC()):
odeplot(sol_RNC, [t, diff(tau(t),t)], numpoints=1000, thickness=1);
odeplot(sol_RNC, [t, tau(t)], MIN..MAX, numpoints=1000, thickness=1);

# PERIODICITY ASSIGNEMENT FOR THE GEAR RATIO
Tau := proc(k)
    num := (k-MIN)/periodo:
    numa :=floor(num):
    return thau(k-numa*(MAX-MIN)):
end proc:
Tau||1 := proc(k)
    num := (k-MIN)/periodo:
    numa :=floor(num):
    return dthau(k-numa*(MAX-MIN)):
end proc:
gc();

# PLOT OF THE NON CIRCUALR GEARING ANIMATION
tempo := time():
radius_i := t -> INT*Tau(t)/(1+Tau(t)):
radius_o := t -> INT/(1+Tau(t)):
tho := T -> Int(Tau(t)*th_pt(t), t=MIN..T, method = _Gquad):
ruote := proc(dt)
    global ruota_i,ruota_o,raggio_i,raggio_o:
    ruota_i := plot([radius_i(t)*cos(th(t+dt)),
        radius_i(t)*sin(th(t+dt)),t=MIN..MAX],scaling=constrained,color=
        blue,axes=boxed,thickness=2):
    ruota_o := plot([INT - radius_o(t)*cos(th(t+dt)),radius_o(t)*
        sin(th(t+dt)), t=MIN..MAX], scaling=constrained, color=red,
        axes=boxed,thickness=2):
    raggio_i := line([0,0], [radius_i(MIN)*cos(th(MIN+dt)), radius_i(MIN)*
        sin(th(MIN+dt))], color=blue, linestyle=1, thickness=2);
    raggio_o := line([INT,0], [INT-
        radius_o(MIN)*cos(th(MIN+dt)),radius_o(MIN)*sin(th(MIN+dt))],
        color=red, linestyle=1, thickness=2);
    display(ruota_i,ruota_o,raggio_i,raggio_o);
end:
centro_i := plot([0,0,t=MIN..MAX],color=blue,style=point,symbol=cross,
    axes=boxed):
centro_o := plot([INT,0,t=MIN..MAX],color=red,style=point,symbol=cross,
    axes=boxed):
ruote_moto := animate( ruote, [dt], dt=0..periodo, color=blue,
    scaling=constrained, frames=100 ):
display(centro_i,centro_o,ruote_moto);
tempo := time() - tempo:
printf("Costruzione dei plot conclusa in %g minuti",tempo/60);
gc();
# XLS PROFILES CONSTRUCTION:
tempo_inizio_statement := time():
appendto(nomedata);
MASSIMO := 1000:

```

## Appendix C

```
risoluzione := 1/MASSIMO:
xi := t -> radius_i(t)*cos(th(t)):
yi := t -> radius_i(t)*sin(th(t)):
xo := t -> radius_o(t)*cos(th(t)):
yo := t -> radius_o(t)*sin(th(t)):
printf("\nrisoluzione a %d punti su ciascuna primitiva",MASSIMO);
printf("\nil quadro cartesiano è centrato sull'asse di rotazione di ciascuna
ruota");
printf("\n\n");
printf("\npunto\tascissa ruota 1\tordinata ruota 1\t\tascissa ruota
2\tordinata ruota 2");
printf("\nnum.\t[m]\t[m]\t\t[m]\t[m]\n\n");
for i from 0 to MASSIMO do
    printf("%d\t%.5f\t%.5f\t\t%.5f\t%.5f\n",i,xi(MIN+i*periodo*risoluz
ione),yi(MIN+i*periodo*risoluzione),xo(MIN+i*periodo*risoluzione)
),yo(MIN+i*periodo*risoluzione));
end do:
tempo_statement := (time() - tempo_inizio_statement):
appendto(terminal);
printf("\ncalcolo concluso in %g minuti",tempo_statement/60);
gc();
```

### C.2 MAPLE CODE FOR THE NON CIRCULAR GEARING SENSITIVITY ANALYSIS

The following code regards the sensitivity analysis upon the disequilibrium torque  $T_3$  (IV.2). The first part of the code regards the comparison between its trend with and without the application of the non circular gearing solution, both analyzed in void working conditions, while the second part regards the comparison between the  $T_3$  trends with the non circular gearing application discussed in Chapter IV, but with different filling conditions, ranging from the void to the total filled condition.

The codes are always realized in MAPLE 9 and the results are shown in Paragraph IV.3, where each diagram is obtained as a sequence of points calculated with the codes and printed out in an EXCEL file.

#### # PERIODICITY ASSIGNEMENT FOR THE MOTION LAW AND DEFINITON OF THE ADDITIVE TORQUE

```
Theta := proc(k)
    num := (k-MIN)/periodo:
    numa := floor(num):
    return evalf(th(k-numa*(MAX-MIN))):
end proc:
Theta||1 := proc(k)
    num := (k-MIN)/periodo:
    numa := floor(num):
    return evalf(th_pt(k-numa*(MAX-MIN))):
end proc:
Theta||2 := proc(k)
    return evalf(subs(diff(theta(t),t)=Theta||1(k),
theta(t)=Theta(k),th2(t))):
end proc:
Theta||3 := proc(k)
```

```

        return evalf(subs(diff(theta(t),t,t)=Theta||2(k),
            diff(theta(t),t)=Theta||1(k), theta(t)=Theta(k), th3(t))):
end proc:
Cadd := t -> Js*(Tau||1(t)*Theta||1(t)+Tau(t)*Theta||2(t))*Tau(t):

# WITHOUT AND WITH NON CIRCULAR GEAR COMPARISON, VOID CONDITIONS
tempo_inizio_statement := time():
nomedata2 := "RNC_torque_cfr.xls":
appendto(nomedata2);
MASSIMO := 1000:
risoluzione := 1/MASSIMO:
printf("\nrisoluzione a %d punti",MASSIMO);
printf("\n\n");
printf("\ntime\tResistan Torque\tResistance Torque");
printf("\n \twithout ncg\twith ncg");
printf("\n[s]\t[Nm]\t[Nm]\n\n");
for i from 0 to MASSIMO do
    CM := t -> Cm_0 + km*(Theta||1(MIN+i*periodo*risoluzione)-omega):
    Cres := t -> CM(t) - J(d)*Theta||2(t):
    CresRNC := t -> CM(t) + Cadd(t) - J(d)*Theta||2(t):
    printf("%+.5f\t%+.5f\t%+.5f\n",MIN+i*periodo*risoluzione,Cres(MIN+i*pe
        riodo*risoluzione),CresRNC(MIN+i*periodo*risoluzione));
end do:
tempo_statement := (time() - tempo_inizio_statement):
appendto(terminal);
printf("\ncalcolo concluso in %g secondi",tempo_statement);
gc();

# VOID AND FILLED CONDITIONS COMPARISON
tempo := time():
nomedata3 := "RNC_filling_cfr.xls":
E := 3*10^(2):
MASSIMO := 1000:
risoluzione := 1/MASSIMO:
appendto(nomedata3);
printf("\nrisoluzione a %d punti",MASSIMO);
printf("\n\n");
printf("\ntime\tResistan Torque\tResistance Torque\tResistan
    Torque\tResistance Torque");
printf("\n \twith p=0.000\twith p=0.167\twith p=0.500\twith p=0.100");
printf("\n[s] \t[Nm]\t[Nm]\t[Nm]\t[Nm]\n\n");
for k from 1 to 4 do
    p := 0.0833*k^2-0.0833*k;
    appendto(terminal):
    Cm_media := 0.1:
    Cm_0 := 0:
    evalf(ciclo()):
    Th_2pt := subs(diff(theta(t),t)=th_pt(t), theta(t)=th(t), th_2pt(t)):
    CM := subs(diff(theta(t),t)=th_pt(t), Cm(t)):
    appendto(nomedata3):
    for i from 0 to MASSIMO do
        printf("%+.5f\t%+.5f\n",MIN+i*periodo*risoluzione,eval(CM,t=MIN+
            i*periodo*risoluzione) + Cadd(MIN+i*periodo*risoluzione) -
            J(d)*eval(Th_2pt,t=MIN+i*periodo*risoluzione));
    end do:
    printf("\n\n\n\n");
end do:
tempo := time() - tempo:
appendto(terminal);

```

## Appendix C

```
printf("\ncalcolo concluso in %g minuti",tempo/60);
gc();

# FORCING FUNCTION ANALYSIS
tempo := time():
nomedata4 := "RNC_forcing_function.xls":
MASSIMO := 1000:
risoluzione := 1/MASSIMO:
FF_J1 := t -> J(d)/Js*Theta||3(t):
FF_k := t -> -km/Js*Theta||2(t):
FF := t -> FF_J1(t) + FF_k(t):
appendto(nomedata4);
printf("\nrisoluzione a %d punti",MASSIMO);
printf("\n\n");
printf("\ntime\tnormalized time\tFORCING FUNCTION\tJ1 COMPONENT\tk
      COMPONENT");
printf("\n[s]\t\t[s-3]\t\t[s-3]\n\n");
for i from 0 to MASSIMO do
  clock := MIN+i*periodo*risoluzione:
  printf("%+.5f\t%+.5f\t%+.5f\t%+.5f\t%+.5f\n",clock, (clock-MIN) / (MAX-
      MIN),FF(clock),FF_J1(clock),FF_k(clock));
end do:
tempo := time() - tempo:
appendto(terminal);
printf("\ncalcolo concluso in %g secondi",tempo);
gc();
```



# REFERENCES

---



## References

1. Bachschmid N., S. Bruni, A. Collina, B. Pizzigoni and F. Resta. 2003. *Fondamenti di Meccanica Teorica e Applicata*. McGraw Hill.
2. Baruah D. C., and B. S. Panesar. 2005. Energy requirement model for a combine harvester, part I: development of component models. *Biosystems Engineering* 90(1): 9-25.
3. Biezeno, C. B., and R. Grammel. 1953. *Technische Dynamik*. Berlin, Germany: Springer.
4. Bloomfield, B. 1960. Noncircular gears. In *Product Engineering Special Report* 159-165.
5. Bosoi, E. S., O. V. Verniaev, I. I. Smirnov, and E. G. Sultan-Shakh. 1991. Chapter II: Cutting equipment of harvesting machines. In *Theory, Construction and Calculation of Agricultural Machines Vol. II*, 323-392. A. A. Balkema, Rotterdam, The Netherlands: Swets & Zeitlinger.
6. Brown, H. T. 1871. *Five Hundred and Seven Mechanical Movements*. New York: Brown, Coombs & Co. Cornell University Library.
7. Brown, R. H. 2000. *Handbook of Engineering Material Vol. I*. CRC Press.
8. Carena, A. 1942. Capitolo XII: Macchine per la falciatura. In *Tecnologia delle Macchine Agricole*, 333-366. Turin, Italy: UTET.
9. Carlson J. A., and J. M. Johnson. 1996. *Multivariable Mathematics with Maple*. Prentice-Hall.
10. Casini Ropa, G. 1953. Cinematica del taglio in alcune falciatrici per canapa. *M&MA* 8: 1-12.
11. Chancellor, W. J. 2000. Cutting of biological materials. In *Handbook of Engineering in Agriculture Vol. I*, 35-63. R. H. Brown, ed. Athens, Georgia: CRC Press.
12. Char, B.W., and Maplesoft. 2003. *Maple 9 Learning Guide*. Waterloo, Canada: Waterloo Maple Inc.
13. Cheli, F., G. Diana. 1993. *Dinamica e Vibrazioni dei Sistemi Meccanici Vol. I*, Turin, Italy: UTET.
14. Chen, Y., J. L. Gratton, and J. Liu. 2004. Power requirements of hemp cutting and conditioning. *Biosystems Engineering* 87: 417-424.
15. Coates W. E., and J. G. Porterfield. 1975. A compound helical cutterbar – design and field testing. *Trans. ASAE* 1: 17-19.
16. Corradi, C. 2004. La potatura meccanica della vite. *Vignevini* 31(3): 65-69.

17. Danieli, G. A. 2000. Analytical description of meshing of constant pressure angle teeth profiles on a variable radius gear and its applications. *Journal of Mechanical Design* 122:123-129. ASME.
18. Danieli, G. A., and D. Mundo. 2004. New developments in variable radius gears using constant pressure angle teeth. Article in press in *J. Mechanism and Machine Theory*.
19. Denaro, F. M. 2004. *Metodi di Calcolo Numerico per L'Ingegneria*. Napoli, Italy: Liguori Editore.
20. Dooner, D. B., and A. A. Seireg. 1995. Noncircular gears. In *The Kinematic Geometry of Gearing*, 55-62. John Wiley & Sons, Inc.
21. Dooner, D. B. 1997. Use of noncircular gears to reduce torque and speed fluctuation in rotating shafts, *J. of Mech. Design* 119: 299-306.
22. Dowgiallo, A. 2004. Cutting Force of fibrous materials. *Journal of Food Engineering*.
23. Filippi, F. 1967. *Piccola Enciclopedia di Meccanica Agraria Vol.I*. 4a ed. Rome, Italy: Esso Standard Italiana.
24. Francia, E. 1972. La potatura meccanica della piante da frutto. *Informatore Agrario* 28(16): 8725-8734.
25. Giordana, F. 2001. *Lezioni di Meccanica delle Macchine*. Milan, Italy: Edizioni Spiegel.
26. Guarnieri, A., C. Maglioni, and G. Molari. 2007. Dynamic analysis of reciprocating single blade cutter bars. Article in press in *Trans. ASAE*.
27. Gubiani, R., G. Pergher, and P. Gasparinetti. 1994. La potatura meccanica della vite nell'ambito della meccanizzazione integrale. *Informatore Agrario* 50(44): 27-30, 33-34.
28. Hansen, C. M., R. P. Larsen, and G. E. Monroe. 1968. Hedge pruning of fruit trees. *Quar. Bull. Mich. State Univ.*, 50: 331-341.
29. Harbage, R. P., and R. V. Morr. 1962. Development and design of a ten – foot mower. *Agricultural Engineering* 4: 208-219.
30. Kanafojski, C., and T. Karwowski. 1976. Cutting blade and stalk materials. In *Agricultural Machines – Theory and Construction Vol. II*, 48-120. Foreign Scientific Publications Department. Washington, D.C.: U.S. Department of Agriculture & National Science Foundation.

## References

31. Kepner, R. A. 1952. Analysis of the cutting action of a mower. *Agricultural Engineering* 33: 693-704.
32. Klenin, N. I., Popov I. F., and Sakun V. A. 1985. Chapter 21: Cutters. In *Agricultural Machines*. 294-334. New Delhi, Amerind Publishing Company.
33. Krzeminski, Z., E. Bogalecka, and Z. Kempny. 1996. Generation of variable torque in drive with error of dynamical gear ratio. *IEEE* 343-347.
34. Laczik B. 2004. *Involute Profile of Non-Circular Gears*. Unpublished.
35. Lee, H. J., and W. E. Schiesser. 2004. Chapter II: Solution of a 1 x 1 ODE System. In *Ordinary and Partial Differential Equation Routines in C, C++, Fortran, Java, Maple, and MATLAB*. Chapman & Hall/CRC.
36. Maglioni, C., and G. Molari. 2005. Analisi dinamica delle barre falcianti a semplice lama. *Atti VIII Convegno Nazionale AIIA*. Catania, Italy.
37. Manfredi, E. 1995. *Agricoltura e Tecnologia Meccanica*. Reggio, Italy: Edizioni Comer.
38. Manfredi, E., and G. Capelli. 1992. Le falciatrici per il taglio dei foraggi. *M&MA* 10: 23-27.
39. Maplesoft. 2005. *Maple User Manual*. Waterloo, Canada: Waterloo Maple, Inc.
40. McClelland, J. H., and R. E. Spielrein. 1958. A study of some design factors affecting the performance of mower knives. *Journal of Agricultural Engineering Research* 1(2): 137-145.
41. Molari, P. G., and A. Rubboli. 2002. L'impiego di ruote non circolari per ridurre l'irregolarità del moto in motori a scoppio. *Atti XXXI Convegno Nazionale AIAS*. Parma, Italy
42. Monroe, G. E., and D. L. Peterson. 1977. Oversize mower cutterbar for pruning trees. *Trans. ASAE* 20: 606-609.
43. Morris, J. R. 2000. Past, present and future of vineyard mechanization. *Proc. ASEV 50th Anniversary Annual Meeting*, Seattle, Washington.
44. Nerli, N. 1943. Capitolo I: La falciatrice. In *Macchine Agricole Vol. III*, 59-77. Turin, Italy: SEI.
45. Pellizzi, G. 1963. Confronti cinematici su macchine falciatrici. In *Memorie ed Atti del CSIA*, XVIII: 2-14. Milan, Italy: Centro di Studi per l'Ingegneria Agraria.

46. Persson, S. 1987. *Mechanics of Cutting Plant Material*. St. Joseph, Mich.: ASAE.
47. Pleym, H. 1999. Visualizing free and forced harmonic oscillations using Maple V R5\*. *Int. J. Engng Ed.* 6:437-455.
48. Pollock, J. G., E. S. Shepardson, N. J. Shaulis, and D. E. Crowe. 1977. Mechanical pruning of American hybrid grapevines. *Trans. ASAE* 20:817-821.
49. Polyanin, A. D., and V. F. Zaitsev. 2003. *Handbook of Exact Solutions for Ordinary Differential Equations*. Chapman & Hall/CRC.
50. Rappaport, S. 1960. Elliptical gears for cyclic speed variations. In *Product Engineering Special Report* 166-168.
51. Scotton, M. 1947. La velocità di taglio nella falciatrice. *M&MA* 3: 103-112.
52. Sitkei, G. 1986. Chapter 17: Cutting of agricultural materials. In *Mechanics of Agricultural Materials*. 439-457. Amsterdam, Elsevier.
53. Srivastava, A. K., C. E. Goering, and R. P. Rohrbach. 1996. Chapter 8: Hay and forage harvesting. In *Engineering Principle of Agricultural Machines*. 325-406. St. Joseph, Mich.: ASAE.
54. Stone, A. A., and H. E. Gulvin. 1967. Chapter 27: Mowers. In *Machine for Power Farming*. 387-409. New York, NY: John Wiley & Sons.
55. Tocci C., and S. Adams. 1996. *Applied Maple for Engineers and Scientists*. Norwood, MA: Artech House, Inc.
56. Wenner, H. L. 1986. Winterfutterbergung. In *Landtechnik Bauwesen*. 250-254. Munich, Germany: BLV Verlag Gesellschaft.
57. Yao, Y. A., and H. S. Yan. 2003 A new method for torque balancing of planar linkages using non-circular gears. *Proc Instn Mech. Engrs Vol 217C, J. Mechanical Engineering Science* 495-503.
58. Young, G. S. 1984. A cutter bar for summer pruning tatura trellis fruit trees. *Agricultural Engineering Australia* 13: 19-23.

